Noninvasive Brain Stimulation and Visual Field Decoding for Vision Recovery in Patients with Occipital Brain Damage

Dissertation zur Erlangung des akademischen Grades Doktoringenieur
(Dr.-Ing.)

Angenommen durch die Fakultät für Informatik der
Otto-von-Guericke-Universität Magdeburg

von M.Sc. **Jiahua Xu**
geb. am 28.12.1986 in Henan China

Gutachter:
Prof. Dr.. Andreas Nürnberger
Prof. Dr. Bernhard A. Sabel
Prof. Dr. Huiguang He

Submission date: October 23, 2021
Defense date: January 19, 2022

Jiahua Xu:
Noninvasive Brain Stimulation and Visual Field Decoding for Vision Recovery in patients with Occipital Brain Damage. Dissertation, Otto-von-Guericke- Universität Magdeburg, 2022.

Abstract

Stroke is one of the leading causes of death and disability globally. Occipital stroke often leads to visual field loss in both eyes, called homonymous hemianopia (HH), and associated problems with eye movements, attention, and visual cognition. Vision impairments are of serious concern as they significantly reduce life quality, such as orienting, identifying objects, reading, or driving. However, only few treatments exist for visual field defects after stroke, such as laborious visual training. In recent years, a new therapeutic approach has emerged: noninvasive brain micro-current stimulation, which is based on innovative brain stimulation technology that modulates brain excitability via transcranial application. Two of the most common transcranial stimulation methods are transcranial direct current stimulation (tDCS) and transcranial alternating current stimulation (tACS). They either modulate the neurons' excitability or entrain the neurons' oscillation with external frequency modulation leading to brain plasticity. This plasticity response of the brain can be assessed by graph theory, which can describe brain functional network properties by quantifying typologies of anatomical tracts or functional associations of brain networks and their changes. Machine learning has attracted much attention from neuroscience and other applications, as it allows us to gain insight into the physiological basis of high performance without predefined features.

We now combined multidisciplinary technologies such as neuropsychology, graph theory, noninvasive brain stimulation, and artificial intelligence to understand the brain network reorganization after a stroke and the possible mechanism for vision recovery. To this end, we first characterized the brain network reorganization for occipital stroke patients through the clinical trial to investigate the dynamic brain plasticity changes compared to healthy controls. Secondly, we designed a noninvasive brain stimulation intervention to investigate the underlying vision recovery mechanism of modulating the brain plasticity for stroke patients that have suffered vision loss. Finally, based on the clinical result, we propose an artificial intelligence approach to utilize the multi-model data (EEG and behavioral data) to predict the possibility of vision recovery after noninvasive brain stimulation. We also evaluated the correlation between brain oscillations and visual field defects with deep neural networks. Our result could benefit visually impaired patients after occipital stroke during the clinic's diagnostic and treatment and enhance their daily activities and quality of life.

Keywords: Stroke, EEG, Brain connectivity, Brain networks, Graph neural network, Deep learning.

Zusammenfassung

Der Schlaganfall ist weltweit eine der Hauptursachen für Tod und Behinderung. Ein okzipitaler Schlaganfall führt häufig zu einem Gesichtsfeldverlust in beiden Augen, der als homonyme Hemianopie (HH) bezeichnet wird, und den damit verbundenen Problemen mit Augenbewegungen, Aufmerksamkeit und visueller Wahrnehmung. Sehbehinderungen sind von ernsthafter Bedeutung, da sie die Lebensqualität erheblich beeinträchtigen, z.B. Orientieren, Identifizieren von Objekten, Lesen oder Fahren. Es gibt jedoch nur wenige Behandlungen für Gesichtsfelddefekte nach einem Schlaganfall, wie z.B. mühsames visuelles Training. In den letzten Jahren hat sich ein neuer therapeutischer Ansatz herausgebildet: die nichtinvasive Mikrostromstimulation des Gehirns, die auf einer innovativen Technologie zur Hirnstimulation basiert, die die Erregbarkeit des Gehirns durch transkranielle Anwendung moduliert. Um solche Netzwerke zu analysieren, hat Deep Learning in den Neurowissenschaften und anderen Anwendungen viel Aufmerksamkeit auf sich gezogen, da es uns ermöglicht, Einblicke in die physiologischen Grundlagen von Hochleistung ohne vordefinierte Merkmale zu gewinnen.

Wir haben jetzt multidisziplinäre Technologien wie Neuropsychologie, Grapietheorie, nichtinvasive Hirnstimulation und künstliche Intelligenz kombiniert, um die Reorganisation des Gehirns Netzwerks nach einem Schlaganfall und den möglichen Mechanismus zur Wiederherstellung des Sehvermögens zu verstehen. Zu diesem Zweck haben wir zunächst die Reorganisation des Hirnnetzwerks für Patienten mit okzipitalem Schlaganfall durch die klinische Studie charakterisiert, um die dynamischen Plastizitätsänderungen des Gehirns im Vergleich zu gesunden Kontrollen zu untersuchen. Zweitens haben wir eine nichtinvasive Intervention zur Hirnstimulation entwickelt, um den zugrunde liegenden Mechanismus zur Wiederherstellung des Sehvermögens bei der Modulation der Plastizität des Gehirns bei Schlaganfallpatienten mit Sehverlust zu untersuchen. Basierend auf dem klinischen Ergebnis schlagen wir einen Ansatz mit künstlicher Intelligenz vor, um die Multi-Modell-Daten (EEG- und Verhaltensdaten) zu nutzen, um die Möglichkeit einer Wiederherstellung des Sehvermögens nach nichtinvasiver Hirnstimulation vorherzusagen. Unser Ergebnis könnte sehbehinderten Patienten nach einem okzipitalen Schlaganfall während der Diagnose und Behandlung der Klinik zugute kommen und ihre täglichen Aktivitäten und ihre Lebensqualität verbessern.

Keywords: Schlaganfall, EEG, Gehirnkonnektivität, Gehirnnetzwerke, Graph Neuronales Netzwerk, Deep Learning.

Contents

List of Figures

List of Tables

List of Acronyms

TES Transcranial electric stimulation

NIBS Noninvasive brain stimulation

tACS Transcranial Alternating Current Stimulation

tDCS Transcranial Direct-Current Stimulation

DBS Deep brain stimulation

tRNS Transcranial random noise stimulation

US Ultrasound stimulation

LGN Lateral Geniculate Nucleus

HH Homonymous Hemianopia

DTI Diffusion Tensor Magnetic Resonance Imaging

CNN Convolutional Neural Network

BOLD-fMRI Blood-Oxygen-Level-Dependent Imaging-Functional Magnetic Resonance Imaging

EEG Electroencephalogram

MEG Magnetoencephalography

DNN Deep Neural Network

AI Artificial Intelligence

ML Machine Learning

DL Deep Learning

SL Supervised Learning

UL Unsupervised Learning

LSTM Long-short Term Memory

MLP Multilayer Perceptron

SGD Stochastic Gradient Descent

Adam Adaptive Moment Estimation

MSE Mean Squared Errors

MAE Mean Absolute Error

VGG16 Visual Geometry Group 16

RPN Region Proposal Network

GNN Graph Neural Network

RNN Recurrent Neural Network

ReLU Rectified Linear Unit

ResNet Residual Neural Network

AM Adjacency Matrix

SVM Support Vector Machine

ROIs Regions Of Interests

AE Autoencoder

ICA Independent Component Analysis

AAL Automatic Anatomical Labeling

FCN Functional Connectivity Network

HRP High Resolution Perimetry

CNN Convolutional Neural Networks

2DCNN TwoDimension Convolutional Neural Networks

3DCNN ThreeDimension Convolutional Neural Networks

CONV CONVolutional layer

CCNN Channel-wiseConvolutional Neural Networks

BCI Brain Computer Interface

SAE Stacked Auto Encoders

LT Left Temporal Lobe

RT Right Temporal Lobe

LF Left Frontal Lobe

RF Right Frontal Lobe

LO Left Occipital Lobe

RO Right Occipital Lobe

LP Left Parietal Lobe

RP Right Parietal Lobe

PRE Before treatment

POST After 10 days treatment

FU Follow Up after two months

ANOVA Analysis Of Variance

ELU Exponential LinearUnit

CV Cross Validation

LH Lesion Hemisphere

IH Intact Hemisphere

1 Motivation

1.1 Motivation

This chapter describes the research questions and motivation.

In order to obtain a better insight into the functional consequences of occipital strokes and the underlying mechanisms and to find ways of vision rehabilitation and restoration, we initiated a detailed exploration of the brain´s physiological underpinnings in chronic stroke survivors. This was guided by the proposal that vision loss following stroke is not only the result of the local, primary loss of nerve cells in the brain but that the local lesion has more widespread, remote effects on the brain network. While magnetic resonance imaging (MRI) evidence suggests that activation changes can be observed in stroke patients (Pineiro et al., 2001), the electrophysiological basis of vision loss is still considered to be only a function of the size of the local brain lesion. To better understand the physiological underpinnings of hemianopia, it is therefore desirable to find out if and how a local occipital lesion may affect the global brain network organization and reorganization. The idea that visual system lesions lead unexpected consequences on visual field than previously thought is supported by prior observations showing that (i) patients with visual field loss have reaction time deficits in the "intact" visual field of the non-damaged hemisphere (Bola et al., 2013), and (ii) even patients with "peripheral" optic nerve damage show "central" breakdown of synchronization in brain networks which can be improved by non-invasive brain current stimulation which correlates with behavioral recovery (Bola et al., 2014; Sabel et al., 2011b). Therefore, a better understanding of brain network organization and reorganization is mandated.

Our understanding of brain networks after occipital stroke is essential for identifying the disrupted communication between occipital and other brain regions. There is ample evidence already of brain network reorganization in different neurological disorders such as glaucoma (Wang et al., 2016b), stroke (Carmichael et al., 2001; Crofts et al., 2011; Goodin et al., 2018; Nelles et al., 2007), Alzheimer disease (Dickerson and Sperling, 2009; Li et al., 2013; Sulaimany et al., 2017), depression (Beard et al., 2016; Dusi et al., 2015; Gong and He, 2015; Wu et al., 2017), or traumatic brain damage (Gilbert et al., 2018; Hou et al., 2019; Medaglia, 2017; San Lucas et al., 2018). Thus, brain network analyses provide an important window into the pathology of the human brain of patients and healthy subjects (Husain and Schmidt, 2014).

Indeed, there is already evidence for the role of global functional connectivity network (FCN) reorganization, which was obtained in patients with (peripheral) optic nerve damage: they suffer deficits in upstream visual pathways with associated brain FCN dysfunctions in the alpha-band, and when FCN are resynchronized again with alternating current stimulation, this leads to partial recovery of vision (Bola et al., 2014). These observations support the "theory of activating residual vision" (Sabel et al., 2011b) and suggest that brain network plasticity and reorganization plays an important role not only in normal and abnormal vision but also in recovery (Dundon et al., 2015; Sabel et al., 2011a; Sabel and Kasten, 2000a).

This study involved the approach of noninvasive transcranial electrical stimulation (TES) on patients after an occipital stroke. It aimed to better understand the neuronal

mechanisms of brain plasticity after visual field loss (homogeneous hemianopia: HH). The outcomes of the modulation effect of neuron synchronization within the cortical networks will help find appropriate protocols to restore vision in stroke patients using noninvasive brain stimulation.

Though numerous studies support the critical role of FCN in different neurological functions and dysfunctions, including those after optic nerve damage, none have explored the relationship between global neurophysiological resting-state network organization and reorganization and how they relate to visual performance in hemianopia after stroke. To fill this gap, we now compared electroencephalography (EEG) recordings of hemianopia occipital stroke patients with age-matched controls and used graph theory to analyze network parameters and their correlation with visually elicited responses. We firstly excluded the possible existence of differences in the left and right hemispheres of the control group and calculated the reorganization in the lesion hemisphere and intact hemisphere. The brain of control subjects from the left and right hemispheres was averaged as a single half hemisphere. The statistic was performed to reveal the brain network changes between single half hemispheres of the control subject (Control), lesion hemisphere of the patients (Lesion/LH), and intact hemisphere of the patients (Intact/IH). Because of the size and location of the lesion are thought to bring the diversification of post-stroke neuroplasticity reorganization (Xu et al., 2015), here we also investigate the location influence for the brain network reorganization. The small-world network was determined to show the network changes globally. Finally, we evaluated the correlated relationship between the brain network measures with the high-resolution perimetry data.

A general protocol of transcranial direct current stimulation (tDCS) for balanced interaction between two hemispheres after unilateral stroke was proposed for this study: cathodal tDCS over visual cortex of the intact hemisphere to reduce the inhibition of damaged hemisphere with anodal electrode placed on Fpz (Gall et al., 2015). It is a challenge to design the sham condition in order to respond to phosphenes in Transcranial alternating current stimulation (tACS) and cutaneous sensations in tDCS. In the tDCS/tACS condition, cathodal tDCS was applied immediately prior to tACS to compare the possible difference with Sham/tACS group.

It was hypothesized that the combined stimulation using tACS/tDCS and tACS alone significantly improve visual functions compared to sham stimulation, both tACS/tDCS and tACS strengthened the related brain connectivity measures and modulated the brain networks synchronization. Furthermore, we considered that tACS/tDCS induces stronger improvement compared to the tACS stimulation alone. Overall, the target of this study was to find an evidence-based brain stimulation protocol for clinic use with vision loss after occipital stroke. This study was also the first definitive trial, a large-scale consortium on non-invasive brain stimulation for a stroke patient with vision loss combining tDCS and tACS.

Machine learning techniques have drawn considerable attention and outperformed the traditional methods in analyzing the brain connectome in recent years. This thesis proposed three chapters to reveal the relationship between resting-state EEG brain network measures and visual performance. For example, electrode-level brain connectivity predicts stroke patients' visual field distribution using a convolutional neural network in the time and frequency domain, which tried to help neuroscientist and clinicians understand the

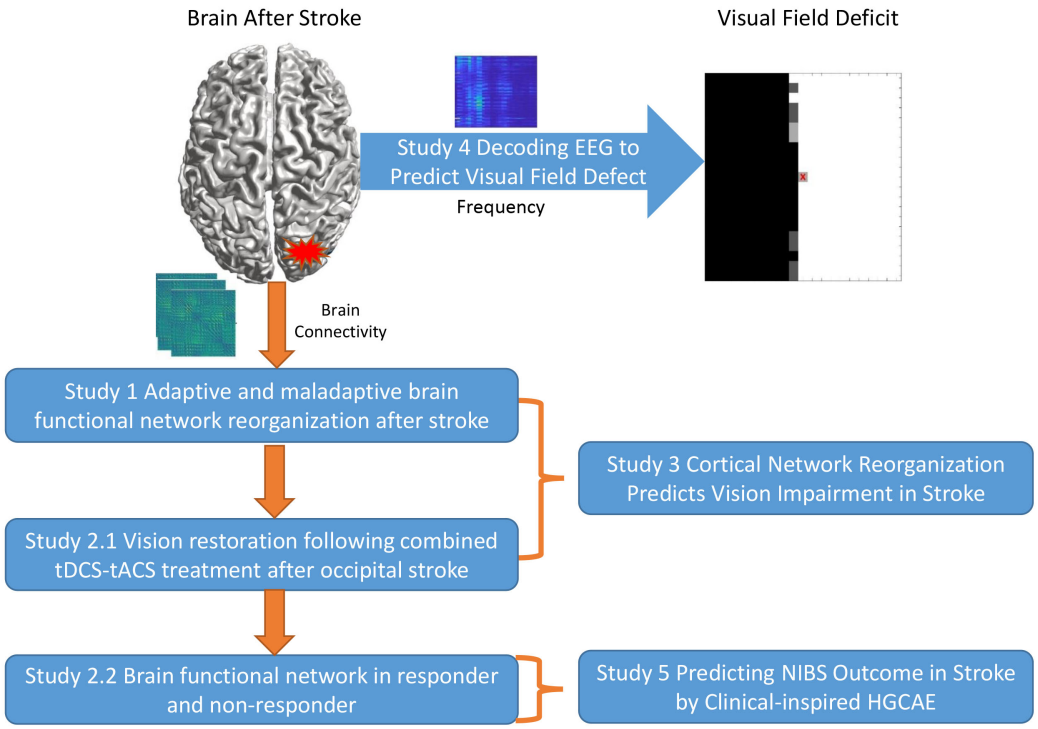

Figure 1: Research framework

possible correspondence between the visual field and brain oscillation. The results will be very beneficial for the clinical diagnostic and understanding of brain plasticity after stroke. A clinical system for visual neglect diagnostic after brain damage could be developed with a more robust pre-trained model, allowing doctors and patients to get the potential awareness of this symptom as early as possible in the future. Furthermore, graph neural network model's prediction could help the neurologist and rehabilitation specialist decide whether the stroke patients can restore vision after noninvasive brain stimulation treatment. In the future, the prospect of this thesis could be producing an integrated clinical system that benefits both patients and medical experts.

1.2 Research questions

Generally, this thesis tried to find the answers to the following questions(See Fig. 1):

1. *What is the role of local and global brain network in stroke patients, adaptive or maladaptive?*

   Hemianopia following occipital stroke is thought to be mainly due to local damage at or near the lesion site. Nevertheless, MRI studies suggest functional connectivity network (FCN) reorganization also in distant brain regions. Because it is unclear if reorganization is adaptive or maladaptive, compensating or aggravating vision loss, we characterized FCNs electrophysiologically to explore the role of local and global brain plasticity and correlated reorganization with visual performance (Study 1).

2. *What is the brain network modulation effect by noninvasive brain stimulation in a random-controlled and sham study?*

The rehabilitation of patients with partial vision loss after occipital stroke remains unknown in the clinic, and only few treatments exist for partial vision loss recovery. Therefore, this study aimed to apply randomized and sham-controlled noninvasive brain stimulation protocols to modulate brain networks and validate their clinical practice potential for vision recovery (Study 2.1).

3. *What is the underlying mechanism of brain network which can contrast the for responders and non-responders?*

   Most patients with residual structures and functions spared by the damage have some shade of grey in their visual filed where function is neither completely lost nor normal (Sabel et al., 2018). This pattern follows the idea of 'areas of residual vision' (Sabel and Gudlin, 2014). The improvement of reaction time in the white and grey grids during the Follow-up demonstrated that the visual acuity was enhanced in the responder group compared to the baseline. Furthermore, the responder group has a significantly higher vision (Field of vision: FOV) field than the non-responder group, both after treatment and Follow-up. This raised a question: How does the responder group local and global brain network differ from the non-responder group after TES ? Through this question, we may get some insight to optimize the noninvasive brain stimulation paradigm design accurately and efficiently, targeting the brain network reorganization toward the neuron rehabilitation purpose(Study 2.2).

4. *Could we identify the vision loss patients with a stroke by the disrupted brain connectivity network?*

   Graph theory has been widely applied to investigate brain network alteration for different kinds of neurological diseases. Brain connectivity and network measure have been highlighted recently in clinical diagnostic as prediction biomarkers. Some methodologies, such as fluid and tissue analysis, can enhance diagnostic precision and guide clinical practice treatment for stroke patients. However, a biomarker that predicts stroke patients' brain network state is rare for vision loss patients in stroke. This study characterized the brain network state utilizing a deep neural network given multiscale brain network and corresponding it with the physiological patterns(Study 3).

5. *Could we map the EEG frequency domain or connectivity domain to visual field deficit distribution with deep learning technology?*

   Decoding resting-state electroencephalography (EEG) to predict patients' visual field distribution could be an essential reference for a better understanding of the compensation of visual functions after a stroke. In addition, the result could be beneficial for clinical diagnostics and treatment. This study proposed a frequency spectrum-based 2D convolutional neural network (CNN) and brain connectivity-based 3DCNN model to predict the visual field defect (Study 4).

6. *Could we find a biomarker to predict the responder or non-responder after noninvasive brain stimulation for vision recovery after stroke, inspired by the clinical result ?*

   Noninvasive brain stimulation (NIBS) has gained lots of attention from both academics and clinical usage. Its curative effect shows positive feedback in kinds of

neurological disorders and brain damage. Stroke is one of them that could benefit from this new technology. However, the unknown underlying mechanism of brain stimulation helping brain recovery after stroke hinders our further exploration of brain functions. Studies on the prediction of possible recovery rates with brain network features are pretty rare. This study proposed a hybrid graph convolutional autoencoder (HGCAE) to predict the stroke recovery potential after brain electrical stimulation therapy. Twenty-four occipital stroke patients have been randomized, divided into three groups, and received the specific NIBS interventions. After two months, we identified the responders based on the visual performance (Study 5).

2 Fundamentals and structure

2.1 The visual system of the brain

The visual system is the most critical human sensory system. One-third of the human cerebral cortex is related to vision information processing that humans receive from the outside world (Grill-Spector and Malach, 2004). Moreover, it can strongly influence humans' cognition performance, decision-making, emotions, and so on. In addition, the visual system collectes information from the eye and recognizes the low-level feature information, such as movement, depth, color, direction, and form, as well as the high-level meaning of visual objects (Felleman and Van Essen, 1991).

The central (neural) part of the visual system consists of central nervous system tissue including photoreceptor cells and neurons in the retina, optic nerves, optic tract, visual cortex and visual association areas (see Fig. 2 and Fig. 3).

The visual cortex is the primary cortical area of the brain that is used to receive, integrate and process visual information from the retina (Huff et al., 2020). It is located in the occipital lobe at the back of the brain. The visual cortex is made of five different areas (V1 - V5) according to function and structure (Luck et al., 1997). The light information is first captured by the eye (retina) and then passes to the first area of the primary visual cortex (V1). From there, it creates a bottom-up saliency map of the visual field to guide attention or eye gaze to salient visual locations (Li, 2002), The information processed by the visual cortex is transmitted to other brain areas for reprocessing. Therefore, the visual cortex acts as a fundamental logical unit for external behavior or response to external stimuli. The visual cortex plays a vital role in daily human life.

The visual system is one of the most extensively studied sensory systems so far. As the nervous system's primary function is to obtain, process, and output information, the visual cortex occupies a large proportion of all external information obtained by organisms, especially for higher animals. As the main center of information reception and processing, if the visual cortex is damaged, it will impact the entire brain, for example after stroke.

2.2 Vision loss caused by stroke

The main clinical manifestations of a stroke is cerebral ischemia and hemorrhagic injury, see Fig. 4, which has very high mortality and disability rate. Hemorrhagic stroke and ischemic stroke are two most common categories. Stroke has a rapid onset and high fatality rate. There are over 13.7 million new stroke cases per year. Almost 60% of all of the patients with stroke are under 70 years (Benjamin et al., 2017; Feigin et al., 2017). Many stroke survivors have various symptoms such as visual and movement impairments (Rowe et al., 2009; Rowe, 2017; Xu et al., 2015). If the stroke occurs in the occipital lobe of the visual cortex, it will lead to vision loss, for which there are only few options for effective treatment (Gall et al., 2015). The most common type of vision loss is homonymous hemianopia (HH), in which the same half of the visual field in both eyes is lost (Zhang et al., 2006a). This happens in about 40% of stroke cases when occipital lobe is damaged (See Fig. 3, the visual cortex as 7 in the right hemisphere), 30% at the parietal lobe (Pambakian and Kennard, 1997). The functional life ability and life quality of patients

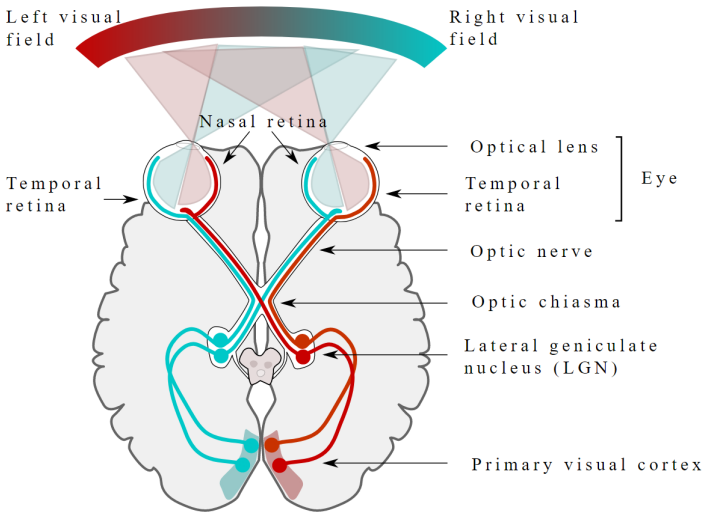

Figure 2: Vision pathway (Image source@Miquel Perello Nieto)

with HH are seriously impacted (Gall et al., 2010b). Patients with visual field defects have a risk of falling, impaired ability to read, and might develop depression (Gall et al., 2010b; Jones and Shinton, 2006; Ramrattan et al., 2001; Ribeiro et al., 2015a). Many patients may not be aware of the visual defects or may not consider their symptoms of HH (Gall et al., 2015).

The cause of HH relayed to different brain areas of the visual pathway, which was damaged, 40% of HH patients were due to the lesions in the occipital lobe (Pambakian and Kennard, 1997; Zhang et al., 2006a). But specific visual field defects do not always indicate specific lesion locations (Zhang et al., 2006a). The diagnoses of visual impairments and treatment after vision loss was therefor needed for stroke survivors (Rowe et al., 2009, 2013). Perimetry index is currently the most common visual deficit measurement standard, such as high-resolution perimetry (HRP) developed by (Sabel et al., 1997) or Oculus twinfield, both of which measure the visual field.

2.3 Therapy for vision recovery after stroke

2.3.1 Intravenous injection

Traditionally, intravenous thrombolytic treatment (TPA) is used to restore perfusion in the hyperacute phase of ischemia, which had only relieved for HH when the neuronal tissue damage developed impermanent by ischemia (Strbian et al., 2012b,a). After the hyperacute phase, the brain automatically tries to compensate for the loss of functions. This compensation is incomplete and even a barrier for brain functional recovery, as the hyperactivities of the intact hemisphere inhibit neuron activities in lesion area (Corbetta et al., 2005). Some scientists proclaimed that visual training can improve vision, such as visual stimulation paradigms to improve vision recovery after many years after damage (Kasten et al., 1998; Poggel et al., 2004; Sahraie et al., 2006). However, the HH is still considered somewhat permanent damage to neurons in the visual cortex and resilient to rehabilitation (Zhang et al., 2006b). Except for intravenous thrombolysis (Strbian et al., 2012b), brain modulation was also highlighted recently because vision loss in the blind

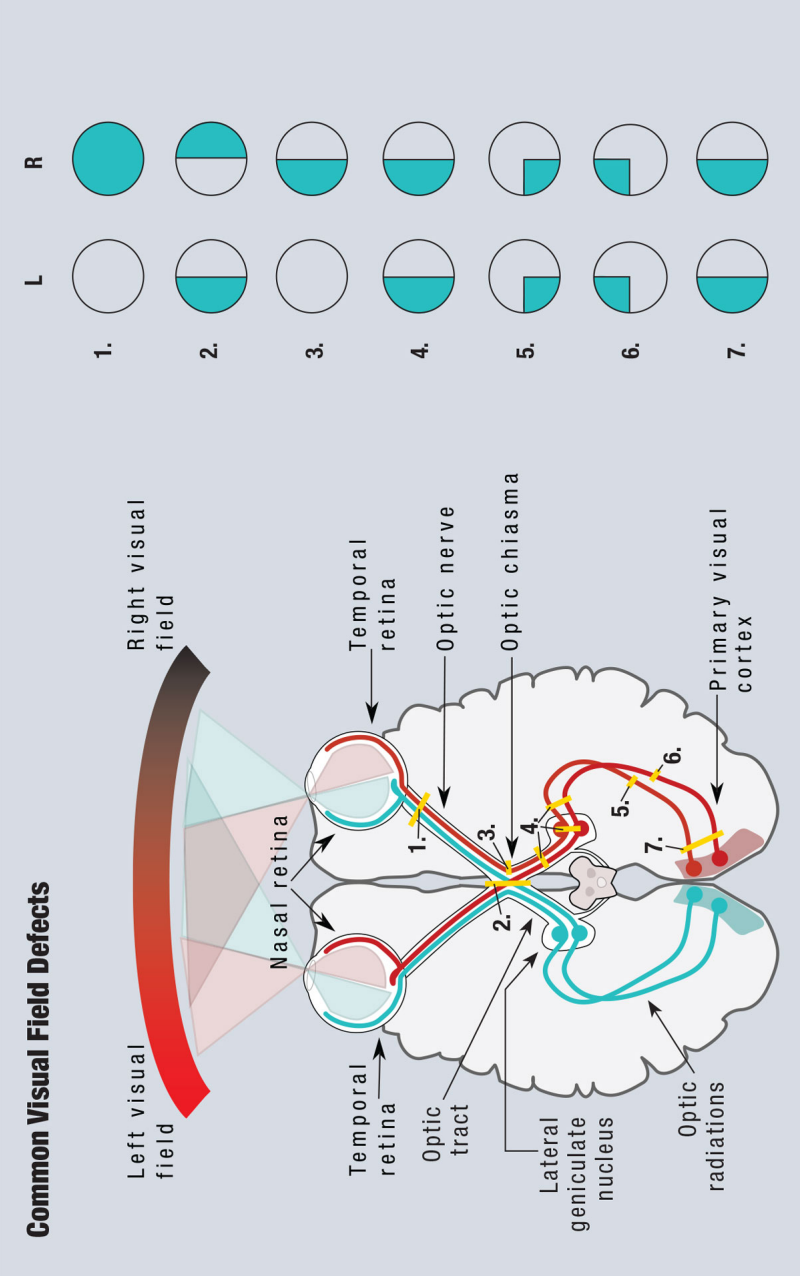

Figure 3: Vision system deficit (Image source@Miquel Perello Nieto)

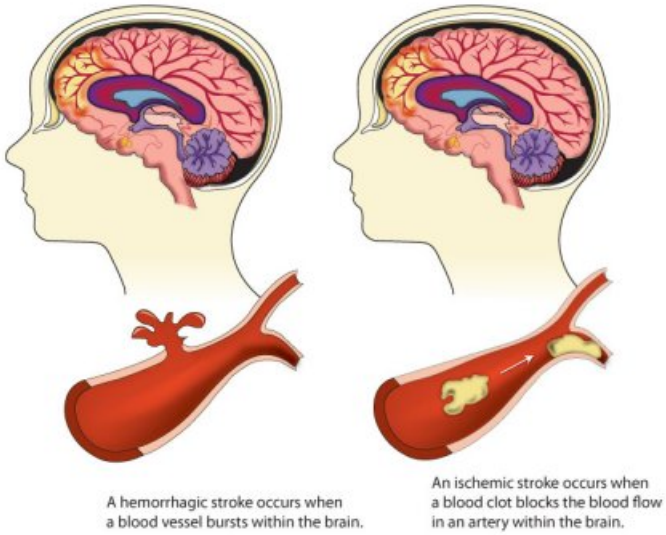

Figure 4: stroke type (image source@cdc.org)

induces not only by primary tissue damage but also can be interpreted by a breakdown of synchronization in brain networks (Bola et al., 2014; Sabel et al., 2011b).

2.3.2 Residual vision activation theory

'Residual vision activation theory 'was first proposed by Sabel et al. (Sabel et al., 2011b) on how visual functions can be reactivated and restored after retinal or cerebral visual injury. This "residual vision activation theory" considered the following observations and potential mechanisms that might help explain recovery:

- (i) Areas of partial damage at the visual field border: this area is in the transition area between the normal visual field and the completely damaged visual field. Although this does not match the lesion location of the brain area, it is still an area worthy of our attention because it has the highest probability of being recovered;
- (ii) "Islands" surviving tissue within the blind area: there are some surviving neurons in the blind zone which possibly benefit from external intervention and treatment;
- (iii) Extrastriate pathways unaffected by the damage;
- (iv) Downstream, higher-level neuronal networks: human vision is not only controlled by the visual cortex but is the result of the synchronization and coordination of multiple brain regions. Therefore, after visual impairment, adjusting the downstream brain network may also stimulate the performance of rehabilitation.

The author also stated that the residual vision is subject to the following points: (i) fewer live neurons, (ii) lack of sufficient attentional resources, (iii) the lesioned hemisphere is inhibited by the dominant intact hemisphere, and (iv) disturbance in their temporal processing. For these reasons, the residual part cannot perform its normal function and may even be inhibited. Therefore, for the residual visual field, our Lab believes that based on its more than 20 years of scientific research (Sabel et al., 2020a), the following two methods could be the most promising tools for vision recovery: (i) visual training and

(ii) noninvasive electrical brain current stimulation. Such methods will strengthen the synaptic transmission and network plasticity (Sabel et al., 2011b), which can help vision restoration. Here we consider this theory would also fit for the treatment of vision loss after the stroke. The goal of this thesis is to evaluate the potential of repetitive noninvasive brain stimulation for vision recovery in stroke patients.

2.3.3 Brain stimulation

The transmembrane potential of neurons or occurrence of action potentials could be affected by the neuron itself or external intervention (Anastassiou et al., 2010). Deep brain stimulation (DBS) and noninvasive brain stimulation (NIBS) through the scalp could locally or globally modulate the brain plasticity and potentially improve the treatment performance of brain disease (Priori, 2003).

For invasive brain stimulation, deep brain stimulation (DBS) is the most common treatment technique that involves the use of implanted electrodes to measure pathological brain activity and deliver adjustable electrical current to selected brain structures (Perlmutter and Mink, 2006; Breit et al., 2004; Kringelbach et al., 2007). In addition, it has been proved to be effective at reducing symptoms of Parkinson's disease, essential tremor, and dystonia, and depression (Lozano et al., 2019). However, DBS needs high-risk surgery to open the skull and implant the electrode into the specific brain area. During this process, unpredicted damage to the brain could occur, which make it not suitable for most of patients. Up to now, it is not popular in clinical usages also for its-complexity. However, it has a promising future in the treatment of other(non-visual) brain diseases such as Parkinson's disease.

Noninvasive brain stimulation was the most widely used for the treatment of the kind of neurological disease in clinic (Antal and Herrmann, 2016). it modulates the neuron's membrane for neurological and psychiatric rehabilitation without any medical surgery, see Fig. 5. The plasticity of neuron correlation could be induced with the specific treatment protocol with electrodes superimposed on the scalp (Huang et al., 2017), and NIBS have been considered the most promising tool to explore the human brain currently. In the last few years, the NIBS has been used in rehabilitation for stroke (Elsner et al., 2017), Alzheimer (Benussi et al., 2021), and other diseases.

Generally, NIBS could be categorized into different approaches:

Transcranial direct current stimulation (tDCS) is one of noninvasive brain stimulation method used to modulate cortical excitability (Nitsche and Paulus, 2000; Priori et al., 1998). A constant, low-intensity current is passed though through two electrodes (from anodal to cathodal) placed the head, which modulates neuronal activity (Purpura and McMurtry, 1965). Anodal stimulation acts to excite neuronal activity, while cathodal stimulation inhibits or reduces neuronal activity (Antal and Herrmann, 2016). The main effect of tDCS on neurons is the transition of the resting membrane potential for depolarization or hyperpolarization below the threshold, which depends on the current direction relative to the axon orientation (Bindman et al., 1964; Purpura and McMurtry, 1965; Gorman, 1966). tDCs has been proved effective in many neurological disease such as pain (Klein et al., 2015; Attal et al., 2016), prkinson (Ferrucci et al., 2016; Kaski et al., 2014), motor stroke (Allman et al., 2016; Rossi et al., 2013), multiple sclerosis (Ayache et al., 2016; Tecchio et al., 2015), epilepsy (Tekturk et al., 2016; Fregni et al., 2006), Alzheimer's

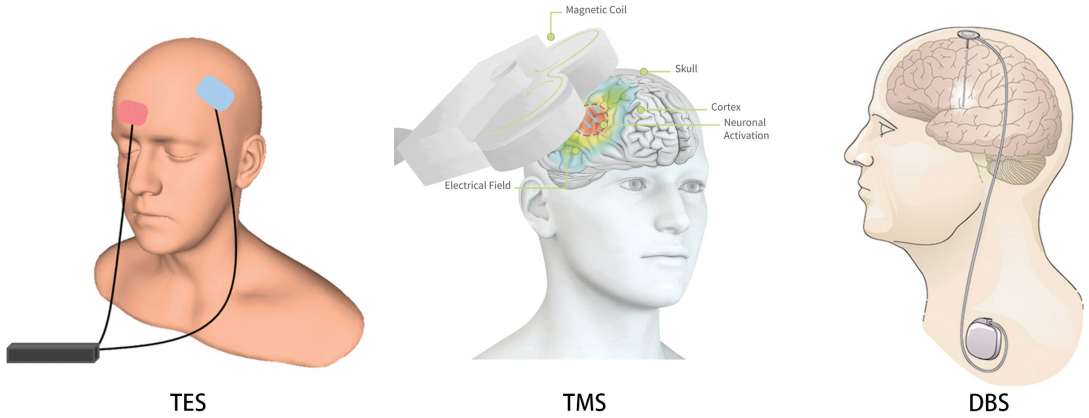

Figure 5: Transcranial electric stimulation (Dayan et al., 2013), Transcranial Magnetic Stimulation@image source: Neuroncare, Deep brain stimulation@image source: nih.gov

disease (Ferrucci et al., 2008; Bystad et al., 2016) and so on.

Transcranial Alternating Current Stimulation (tACS) is expected to synchronize or desynchronize cortical oscillations (Antal and Paulus, 2013). It is believed that the tACS mainly entraines or synchronizes ongoing oscillatory brain activity (Antal and Herrmann, 2016). Compared with tDCS, the major difference could rely on the frequency, the intensity, and the phase of the stimulation, and the frequency of AC stimulation can be matched to the frequency of the brain's internal oscillation in the closed-loop mode (Moliadze et al., 2010). tACS is a low-intensity sinusoid current across an active electrode placed on the head while the reference electrode could be settled with a specific protocol design. The low-intensity electric field across a targeted brain region entraines oscillations and neurons, making tACS a powerful tool to modulate brain plasticity. The long-lasting effect was observed in many clinical trials (Neuling et al., 2013b; Clancy et al., 2018). The unique capabilities altering the brain and behavior provided by tACS have been hypothesized (Antal and Paulus, 2013; Antal and Herrmann, 2016). In the treatment of many kinds of brain diseases, the results have been confirmed by various stimulation protocols, such as Parkinson's disease (Del Felice et al., 2019; Krause et al., 2014), stroke (Bao et al., 2020; Wischnewski et al., 2019), Alzheimer disease (Buss et al., 2019; Chang et al., 2018).

Transcranial Random Noise Stimulation (tRNS) was firstly applied in humans in 2008 (Terney et al., 2008). Instead of constant direct current delivery, tRNS stimulation differs from tDCS in that current levels are randomly delivered. The alternating current with random amplitude and frequency (commonly 0.1 - 640 Hz) in healthy subjects, increased the motor cortex excitability (i.e., increased MEP) after 10 minutes of stimulation. Later research shows that the high-frequency band (hf-tRNS, from 100-640 Hz) has shown to be the most effective in increasing neural excitability (Moret et al., 2019). The tRNS induced robust changes in cortical excitability could be related to the repeated opening of sodium channels or modulation of neuronal networks with a increased sensitivity (Remedios et al., 2019; Terney et al., 2008). tRNS has shown some promising results in motor learning (Contemori et al., 2019), multiple sclerosis (Palm et al., 2016a), or Parkinson (Stephani et al., 2011).

Transcranial Magnetic Stimulation(TMS) is a neuromodulatory technique that applies a magnetic field carrying short-lasting electrical current pulse to the brain via

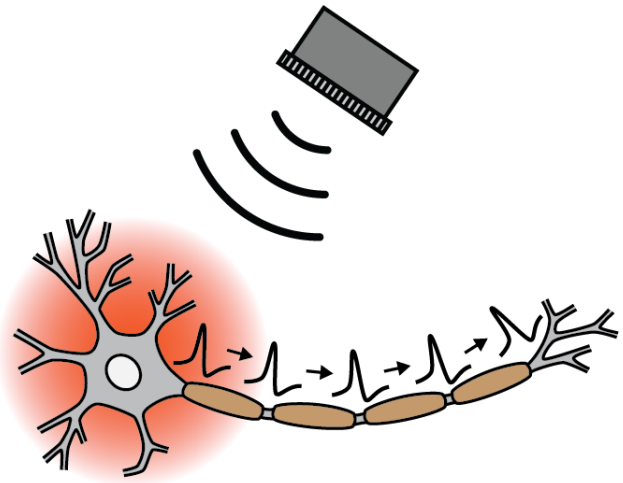

Figure 6: Ultrasound Neuromodulation@image source:epfl.ch

a 'coil' (Barker et al., 1985), see Fig. 5. Different coil types allows different magnetic field patterns, and using more focal points can elicit a deeper magnetic field for deeper cortical layers (Ziemann, 2011). A high-intensity TMS pulse induces a synchronized high-frequency burst of discharge in a large group of neurons (Siebner et al., 2009). The external interfered synchronization followed by inhibition effectively modulates brain motor cortex (Barker et al., 1985), vision perceptual, and cognitive processing (Strafella and Paus, 2000). TMS is a very critical tool that can be used in the clinic to study the function and dysfunction of the human brain in a non-invasive and painless way (Ziemann, 2011). The TMS applications have been combined simultaneously with other neurophysiology or neuroimaging techniques such as EEG (Conde et al., 2019), or fMRI (Peters et al., 2020). Although its exact mechanism of action is still unknown, current evidence suggests its role in inhibition and excitement of neurons could be used for the treatment of psychosis and neuropathy disease (Chail et al., 2018).

Transcranial Ultrasound Stimulation (TUS) is a emerging technique that can noninvasively excite or inhibit neuron's state in specific brain regions by emitting pulsed ultrasonic waves (Tufail et al., 2011), see Fig. 6. Compared with magnetic or electrical non-invasive brain stimulation, this technology has higher spatial resolution and can reach deep structures (di Biase et al., 2019). There are several studies trying to reveal the mechanism of the TUS, most of them agrees that TUS can modify the membrane gating kinetics through the action on ion channels or neurotransmitter receptors (Tufail et al., 2010). In addition, the mechanical energy of US leads to periodic expansions and contractions of the membrane (Krasovitski et al., 2011).

Above-mentioned neuromodulation technology is known to be able to change brain networks. Therefore, the question is how to quantify changes in the brain, a very important issue. We used graph theory to study this question, for it is widely used to quantify the dynamic changes of brain networks. In the next paragraph, we will describe related brain network quantification and machine learning methods

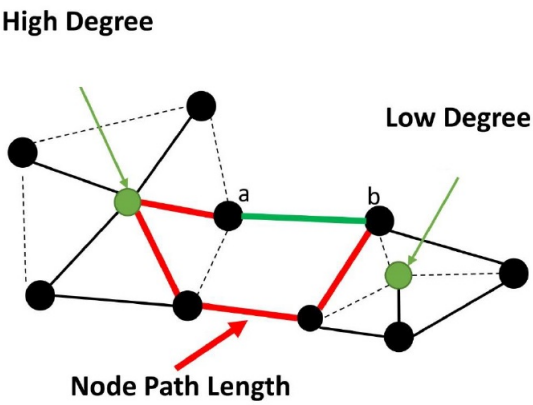

Figure 7: Graph theory, CC: Clustering Coefficient. From a to b: short node path (green line); long node path (red line)

2.4 Graph theory and machine learning

2.4.1 Brain connectome and graph theory

The brain networks (connectome) means the explicitly defined anatomical and functional connections on the same map of brain regions, which quite help explore functional connectivity relationships (Zhou et al., 2006). The graph theory describes important properties of brain networks by quantifying typologies of their respective network measures by anatomical tracts or by functional associations (Newman, 2004). According to this theory, brain areas correspond to nodes or vertices, and edges are the connections between the nodes, see Fig. 7. Node degree is the number of links connected to a center node, and strength is the sum weights of links connected to the center node. The clustering coefficient is the fraction of triangles around the center node (Rubinov and Sporns, 2010). Node betweenness centrality is the value of all shortest paths that pass though a given node. Nodes with high values of centrality involved in a large number of shortest paths. If the network structure has a high cluster coefficient and a short path length, the network structure is called a "small world" which is a fraction between ordered and random networks. Patterns of anatomical connectivity in neuronal networks are sometimes characterized by high clustering and a small path length (Watts and Strogatz, 1998).

A single network measurement can characterize one or several aspects of large-scale brain connections. For example, there are various measures to examine various aspects of functional integration and separation, quantify the role of specific brain regions, characterize the patterns of local anatomical circuits, and test the network's ability to recover from insults (Rubinov and Sporns, 2010).

Metrics for specific network elements (for example: nodes or links) often quantify the connections associated with these nodes or links, reflecting how these nodes or links are embedded in the network. In addition to these different representations, network metrics can be described as binary and weighted, directed and undirected variants. The undirected binary variant is usually a generalization of a weighted and directed metric (Rubinov and Sporns, 2010).

Characteristic path length. The shortest path length is the short distance from

one node to another node, which are related to network efficiency and information transfer rate in graph theory. The characteristic path length is the average shortest path length of all nodes in the network with a definition:

$$L = \frac{1}{n}\sum_{i \in N} L_i \tag{1}$$

where L_i the average path length between node i and all other nodes

Clustering coefficient. The "small world" combines the presence of functional modules with robust intermodular links (Rubinov and Sporns, 2010), networks are more clustered than the random network and have approximately the same characteristic path length (Watts and Strogatz, 1998). The clustering coefficient is the fraction of triangles around a center node with the following definition:

$$C = \frac{1}{n}\sum_{i \in N} C_i = \frac{1}{n}\sum_{i \in N} \frac{2t_i}{k_i\,(k_i - 1)'} \tag{2}$$

Modularity Modularity is a statistic measure that quantifies the degree to which the network may be subdivided into such delineated groups (Newman, 2004). A higher value of modularity shows that nodes in a nonoverlapping group maximizes the number of within-group edges and minimizes the number of between-group edges (Rubinov and Sporns, 2010).

$$Q = \sum_{u \in M} [e_{uv} - (\sum_{v \in M} e_{uv})^2] \tag{3}$$

where the network is fully divided into non-overlapping modules M, and e_{uv} is the proportions of all links that connect nodes in module u with nodes in module $.v$

Betweenness centrality. Node betweenness centrality is the value of all shortest paths in the network that pass though a given node. Nodes with high values of betweenness centrality involve a large number of shortest paths (Rubinov and Sporns, 2010; Freeman, 1978)

$$b_i = \frac{1}{(n-1)(n-2)} \sum_{h,j \in N \; h \neq i, h \neq j, j \neq i} \frac{p^i_{hj}}{p_{hj}} \tag{4}$$

where p_{hj} is the short path length between node p and j,p^i_{hj} is the number of shortest path length that pass the node i

These brain network attributes can help us to better understand the exchange and flow of mutual information between brain nodes, and they are widely used in the field of brain science. For the subjects of our research, these measurement methods can also help us to better understand the relationship between visual field damage and brain network changes in stroke patients. In the next paragraph, we will focus on the methods that reveal changes in brain network of patients with visual field deficit.

After a stroke on the occipital lobe, the brain network analysis for HH patients was essential for identifying the disrupted communication between the occipital and other brain regions. The "residual vision activation theory" was proposed for vision restoration after brain and retina damage (Sabel et al., 2011b). In theory, the brain plasticity of patients could be modulated or reorganized by vision training or electronic brain stimulation (Dundon et al., 2015; Sabel et al., 2011a; Sabel and Kasten, 2000a). However, Considering

the unclear mechanism of brain network reorganization in neurological disorders, many studies focus on the pathology to investigate the brain lesions in HH patients (Brandt et al., 1998; Nissa et al., 2016; Pambakian et al., 2000; Sawaya et al., 2014; Stayman et al., 2013). Very few studies have been done on the functional brain connectivity and dynamic network changes with HH patients in the resting state EEG. Brain functional connectivity and network are the critical window in revealing disrupted brain oscillation in brain activity between patients and healthy subjects (Husain and Schmidt, 2014).

One study reported that HH patients with damage on the left primary visual cortex had less activities than healthy subjects; patients showed greater activation on other lobes in the lesioned hemisphere and the intact hemisphere in the associative visual cortex (Wang et al., 2010). Another study reported that the connectivity was enhanced by new forming connections. Compensatory connections mainly originated from the infarction area and targeted contralesional frontal, central, and parietal cortices (Guo et al., 2014). In the temporal lobe, the disturbed neural synchronization in vision loss patients indicated disrupted communication within the visual pathway (Bola and Sabel, 2015). Thus the state of synchronization or desynchronization of brain networks plays a vital role in visual cortex functional signal preprocessing and transferring. Therefore, disturbed synchronization in patients with vision loss might aggravate the functional consequences of reduced visual input (Bola et al., 2014). The related phenomena after stroke in the left or right hemisphere have been reported in many types of research (Forss et al., 1999; Kalénine et al., 2010; Vallar and Perani, 1986).

In summary, graph theory could help us illustrate the brain network properties with nodes and links in a brain connectivity matrix. We will discuss graph neural networks more detail in next chapter.

2.4.2 Machine learning and graph neural network

Machine learning refers to a subarea of artificial intelligence that automatically learns the patterns based on the dataset and predicts the new instance label without being explicitly programmed. The traditional algorithms could be considered to solve the two problems classification or regression, such as decision tree, support vector machines (SVM), and linear discriminant analysis (LDA), linear regression. There have been many applications for these algorithms and they achieved an remarkable performance—the feature and dataset size and the logic of the algorithm influence the performance strongly. In the last few years, based on the multiple linear perceptions, Yann LeCun (LeCun et al., 2015) had proposed a convolutional neural network that performs end-to-end feature extraction and ROI pooling in imaging processing. Furthermore, the LSTM and other more complex modes had been proposed to handle the time serial data and natural language preprocessing (Hochreiter and Schmidhuber, 1997). This paper will focus on the deep learning technologies to handle the sensor level and source-level brain connectivity matrix.

Convolutional neural network: Convolutional Neural Networks (CNN) is a type of feed-forward neural network that includes convolution, non-linear and pooling operations in deep layers. It is one of the most representative algorithms of deep learning (LeCun et al., 2015). The eruption of deep learning is also based on the outstanding performance of convolutional neural networks in image recognition (Krizhevsky et al., 2012). 2DCNN and 3DCNN can effectively reduce the dimensionality of a large amount of data into a

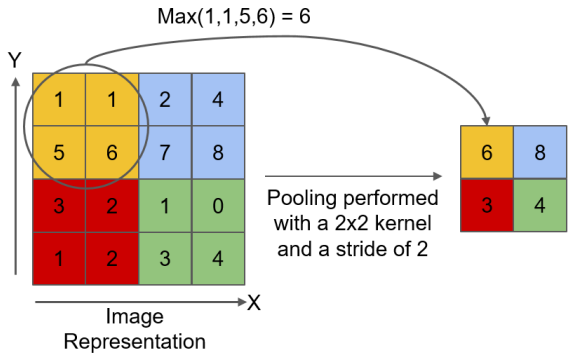

Figure 8: A example of convolution operation

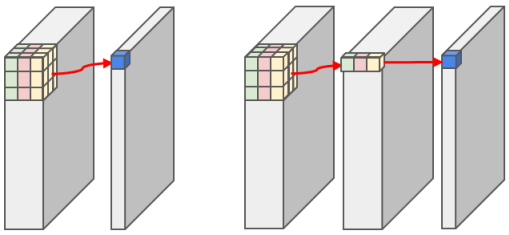

Figure 9: An general concept of 3DCNN

small amount of data and retain the feature patterns of the image, see Fig. 8 and 9 . Many researchers believe that the human vision system inspires the CNN structure, but some considered it was only the merits of mathematics and the expansion of computational abilities nowadays.

There are many variants of convolutional neural networks. They have achieved great performance compared with traditional ones in some specific fields, such as the Resnet (He et al., 2016), Densenet (Iandola et al., 2014), YOLO (Redmon et al., 2016), Fast-RCNN (Ren et al., 2015), and Faster-RCNN (Ren et al., 2016). In computer vision problems, the current state of art network structure is based mostly on attention mechanism (Vaswani et al., 2017). For example, vision transformer (Dosovitskiy et al., 2020), which divides the whole image into sub-regions and applies multi-head attention gates, achieves excellent performance in object detection and segmentation tasks. Another highlighted method in medical imaging is Unet (Ronneberger et al., 2015) which was firstly proposed in the blood vessel segmentation task and had been extended to various medical applications. At present, most imaging solutions in deep learning for medical imaging are based on Unet architectures.

Recurrent neural network: In contrast to the remarkable achievements of convolutional neural networks in image processing, the recurrent neural networks (RNN) is unique in time series data such as natural language processing and medical signal processing and have received significant attention from researchers. The most famous one is the long short term memory (LSTM) algorithm (Hochreiter and Schmidhuber, 1997), which combined various gates and the previous hidden state, see Fig. 10. For example, in machine translation problems, this algorithm effectively combines the context to obtain global weights.

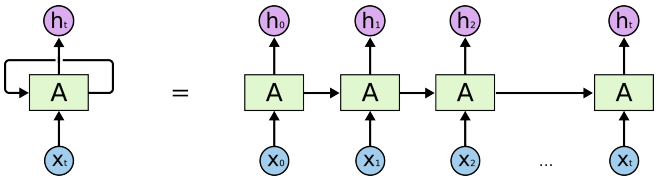

Figure 10: An unrolled recurrent neural network@images source:colah's blog (Cohen, 2015)

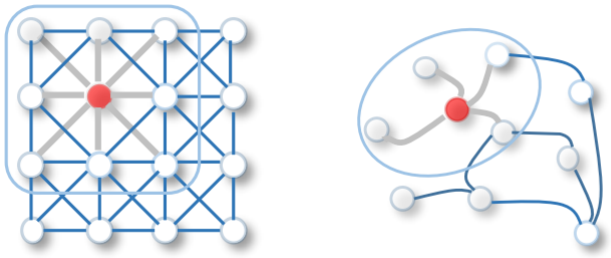

Figure 11: 2D convolution (Euclidean space) vs. Graph convolution (Non-Euclidean space) (Wu et al., 2020)

Although the later self-attention mechanism completely outperforms the recurrent neural network (Vaswani et al., 2017), its inner core still draws on the idea from RNN. Another particular LSTM structure: Bidirectional LSTM gained our attention (Graves and Schmidhuber, 2005). This structure feeds the data into the LSTM layer from different directions and could obtain integrated features. The variant of this structure has been extended in language understanding successfully, such as (BERT) (Devlin et al., 2018). Moreover, considering its mechanism and interhemispheric brain, it may have excellent potential usage in brain network applications.

Graph neural network: Deep learning definitely could effectively learn the hidden features from the Euclidean data such as image, video, and text. However, there is an increasing demand for a new methodology to handle the non-Euclidean data, such as recommendation systems in e-commerce, molecular chemistry, and brain connectivity in neuroscience where the graph was made of the nodes and edges. The nodes can be directly connected to all the nodes in the graph or partially connected with neighbor nodes. The edges between two nodes could be binary and weighted, the numbers of nodes and links could be various for individual subjects. These data structures in graphs demonstrated a complex relationship and inter-dependency presentation, which imposed a significant challenge on existing deep learning technology, see Fig. 11.

The early study in GNN was tracked back to 1997, Sperduti et al. (Sperduti and Starita, 1997) proposed a neural network to handle the acyclic graphs, and Gori et al. (Gori et al., 2005) firstly referred to the neural network as graph neural network in 2005 and extended by Scarselli et al. (Scarselli et al., 2008). Then, inspired by the excellent performance of CNN on images, Braun et al. (Bruna et al., 2013) proposed a spectral-based convolutional graph neural network (spectral GCN) which has a solid theoretical foundation in signal processing. However, spatial GCN attracted more attention than the Spectral GCN for higher lower efficiencies, higher generality, and more flexibility compared with spectral GCN, which was firstly proposed by Micheli et al. (Micheli, 2009). In sum,

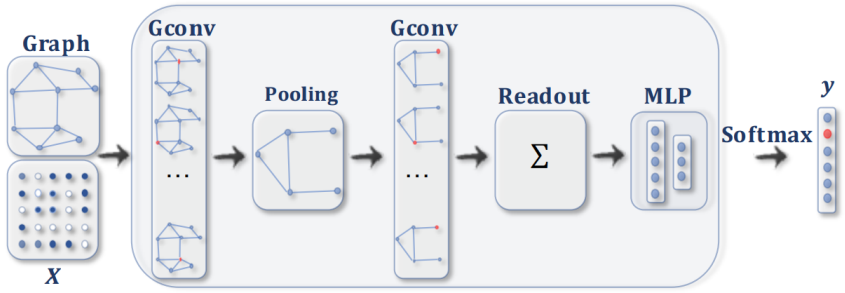

Figure 12: A convGNN with pooling and readout layers for graph classification (Defferrard et al., 2016)

spectral GCN has to calculate the eigenvector and Fourier basis while spatial GCN could directly operate convolution in the whole graph. Another thing, spectral GCN requited the directed graph while the spatial GCN is more flexible to handle multiple source graphs.

Graph network embedding targets to present the graph with lower-dimensional nodes, both persevering the topology structure and node information, see Fig.12. Traditional algorithms could perform directly on node levels for classification, clustering, or prediction. CNN is more likely a group of neural networks, which is designed for an end-to-end classification task. GNNS could address the graph network embedding problem with the autoencoder structure while the graph network embedding contains non-deep learning ways to extract features. Graph autoencoder (GAES) maps the nodes into high-level features with deep learning structures, primarily used for latent feature (network embedding) and new graphs generation. The iconic work from Wang et al. (Wang et al., 2016a) presented a stacked autoencoder to preserve the nodes in the first ordered and second ordered proximity jointly by minimizing the distance from the center node and its neighbors.

After GNN generates the latent features, the graph may have redundant nodes that require high computations. Therefore, a downsampling strategy referred to as GCN pooling was performed to reduce the numbers of the node. Max/Mean/Sum are the most common ways to do pooling, depending on the target in specified network design. Recently, a differentiate pooling method (Ying et al., 2018) was proposed to generate a hierarchical structure of a graph, which instead of simply clustering the nodes in a graph, tried to keep the graph structure topology and node information when doing the node assignment. For example, in neuroscience, the clustering is pre-defined by brain regions. In a word, graph pooling is an important step to reduce the graph size and prevent over-fitting, while achieving this target is still an open question.

2.5 Structure of thesis

To be better to classify our contributions and results in revealing the mechanism of brain network reorganization and neuron modulation effect for vision recovery, this thesis has the following chapters to evaluate these key points: Chapter 3 and Chapter 4 focus on the understanding of the brain network reorganization after a stroke and intervention with brain stimulation; Chapters 5, 6, 7 reveal the relationship between vision loss and behaviour data with deep learning technology. The structure of the thesis is listed as follows:

- Chapter 1 and Chapter 2 addressed the motivation, research background, and related methodology.

- Chapter 3 demonstrates that stroke brains showed altered FCNs in the alpha- and beta-band in numerous occipital, temporal and frontal brain structures. FCN had a less efficient network organization globally, while node networks reorganized on the local level, especially in the intact hemisphere. Here, the occipital network was 58% more rigid (with a more "regular" network structure) while the temporal network was 32% more efficient (showing greater "small-worldness"), both of which correlate with worse or better visual processing, respectively.

- Chapter 4 demonstrates that real tDCS/ real tACS (ACDC) enhanced the lesion hemisphere's alpha band strength in the superior occipital lobe during the follow-up. The sham tDCS/ real tACS (AC) and sham tDCS/ sham tACS (Sham) group maintained the baseline level. A negative correlation (r=-0.80, p=0.017) appeared between the intact visual field and characteristic path length after treatment in the ACDC group. The alpha band centrality of intact middle occipital decreased after treatment in ACDC. The ACDC protocol significantly decreased the delta band coherence between the lesion and the intact occipital lobe. Meanwhile, we found an enhancement of coherence between the intact occipital lobe and intact temporal lobe. The responder group has significantly higher strength than the non-responder group, in both hemispheres at lingual, calcarine, and on the lesion side of superior occipital in the low alpha band during the follow-up. The responder group has lower coherence between intact occipital and lesion frontal. The FOV negatively correlated with the ipsilesional frontal strength of the NonResponder group in the high alpha band.

- Chapter 5 explores multiscale brain network and deep neural network to evaluate brain network patterns for identifying vision impairment patients after occipital stroke. The prediction model and statistical analysis result indicate that the low and high alpha band under specific density could be a predictor to characterize brain network reorganization. The Bi-LSTM achieved a balanced performance between sensitivity and specificity, which could prove valuable for applications in brain feature extraction later. Further investigation was needed to extend this algorithm with more data samples and an optimized network structure. These results may bring insight for clinical diagnostics and interventions in the future.

- Chapter 6 proposes a frequency spectrum-based 2D convolutional neural network and a connectivity-based 3D convolutional neural network to decode the relationship between the brain oscillation and the visual field defect caused by a unilateral occipital stroke. The spectrum-based 2DCNN model demonstrated better visual field location prediction than the connectivity-based 3DCNN model, while the visual field percentage was not predictable in our evaluation. The visualization of EEG characteristics and feature maps help make results more explainable. But more samples

and optimized network structure are needed in further studies.

- Chapter 7 discusses the possibility of predicting the noninvasive brain electrical stimulation therapy effect with the alpha band brain functional network in visual loss patients after occipital stroke. We emphasized the dynamic changes with graph theory and proposed a hybrid graph convolutional network for NIBS outcome prediction. The results show the HGCN achieved an overall accuracy of 74% and 91% sensitivity on recovery potential prediction after NIBS intervention. Although this is still far away from proper clinical usage, this predictable outcome could be an incentive for future development in the clinical application of noninvasive brain stimulation.

- Chapter 8 summarized all the contributions in this study and proposed further studies.

3 Study 1: Adaptive and maladaptive brain functional network reorganization after stroke

*(**This work has been published by Brain connectivity**)*

3.1 Background

Hemianopia following unilateral occipital stroke creates problems in everyday visual tasks such as reading, navigating, or driving (Ribeiro et al., 2015a). While the scotoma is thought to be a "local" problem of retinotopic, cortical cell death at or near the lesion site, it also creates global problems caused by remote deafferentation or network disturbances throughout the brain (Catani et al., 2012), including cross-hemispheric influences.

Based on prior studies, we expected that brain network plasticity could be both adaptive or maladaptive (Nava and Röder, 2011). Whereas adaptive changes could compensate or improve the function (i.e., restoration of visual function), maladaptive changes would interfere, reduce or disrupt the functional state (Li et al., 2016; Woolf, 1989) depending on the pathophysiological condition (Dalise et al., 2014). Both are expected to be caused by or associated with structural or functional modifications of brain networks (Naro et al., 2016; Pascual-Leone et al., 2005). Examples of adaptive and maladaptive neuroplasticity were reported in various studies of pain (Li et al., 2016), stroke (Altman et al., 2019), focal dystonia (Quartarone et al., 2006) or tremor (Lee et al., 2014), to name but a few.

Our understanding of brain networks after occipital stroke is essential for identifying the disrupted communication between occipital and other brain regions. There is ample evidence already of brain network reorganization in different neurological disorders such as glaucoma (Wang et al., 2016b), stroke (Carmichael et al., 2001; Crofts et al., 2011; Goodin et al., 2018; Nelles et al., 2007), Alzheimer disease (Dickerson and Sperling, 2009; Li et al., 2013; Sulaimany et al., 2017), depression (Beard et al., 2016; Dusi et al., 2015; Gong and He, 2015; Wu et al., 2017), traumatic brain damage (Gilbert et al., 2018; Hou et al., 2019; Medaglia, 2017; San Lucas et al., 2018). Thus, Brain network analyses provide an important window into the pathology of the human brain of patients and healthy subjects (Husain and Schmidt, 2014).

Such studies rely typically on MRI, which measures the oxygenation state (blood flow), a rather indirect measure of brain network organization and reorganization, and brain functional connectivity. Nevertheless, they provide a first approximation of spatially distributed networks and their temporal synchronization and reorganization after stroke. For example, one study of HH patients with primary visual cortex lesions revealed fewer brain activities than healthy subjects and greater activation of other lobes in the lesioned and the intact hemisphere in the associative visual cortex (Wang et al., 2010). Nelles et al. (Nelles et al., 2002) carried out hemifield stimulation in hemianopia patients and compared activation patterns to those in normal subjects. In controls, the most significant activation was found in the contralateral visual cortex (area 17) and bilaterally in the extrastriate cortex (areas 18 and 19) . In patients, these areas were also activated during visual stimulation of the patients' intact hemifield. Because visual stimulation of the hemianopia visual field provoked stronger ipsilateral activation of the extrastriate visual cortex, the authors concluded extensive neuronal plasticity. Others reported that vision training in hemianopia alters the activation changes in different brain regions (Vanni et al., 2001).

While MRI informs us about the general activation state of different brain regions, its low temporal resolution does not allow conclusions about the synchronization state of the electrophysiological networks, which the EEG can measure. On the other hand, with its high time resolution, the EEG comprises a much more direct measure of functional

synchronization states in the brain and network dynamics. As a result, there is a growing number of investigators that used EEG to characterize brain functional connectivity and their dynamics (Rossini et al., 2019).

Brain FCN reorganization is well established using MRI techniques in different neural disorders such as early blindness (Striem-Amit et al., 2015), glaucoma (Wang et al., 2016b), stroke (Wang et al., 2010), Alzheimer disease (Dennis and Thompson, 2014), schizophrenia and depression (Wu et al., 2017), traumatic brain injury (Sharp et al., 2014), or following occipital damage (Pedersini et al., 2020). Yet, the functional role of FCN reorganization in hemianopia is rather unclear. On the one hand, widespread FCN changes might be "maladaptive", because hemianopia patients have slowed reaction times and perceptual deficits in their intact hemifield (Bola et al., 2013; Cavézian et al., 2015; Chokron et al., 2008). On the other hand, FCN reorganization might be "adaptive," as shown in patients with optic nerve damage, where neuromodulation-induced FCN reorganization can strengthen occipital-frontal interactions, which correlates with visual field improvements (Bola et al., 2014)

Indeed, there is already evidence for the role of global FCN reorganization, which was obtained in patients with (peripheral) optic nerve damage: they suffer deficits in upstream visual pathways with associated brain FCN dysfunctions in the alpha-band, and when FCN are resynchronized again with alternating current stimulation, this leads to partial recovery of vision (Bola et al., 2014). These observations support the "theory of activating residual vision" (Sabel et al., 2011b)and suggest that brain network plasticity and reorganization plays an important role not only in normal and abnormal vision but also in recovery (Dundon et al., 2015; Sabel et al., 2011a; Sabel and Kasten, 2000a).

To characterize adaptive or maladaptive plasticity, we recorded EEG in the resting state of hemianopia patients. Unlike MRI, an indirect biomarker of neural activity using oxygenation as a surrogate of neural activity, the EEG is a direct neurophysiological biomarker with excellent time resolution. Therefore, we recorded resting-state EEG in stroke patients with hemianopia. We described brain FCN properties by quantifying topologies of functional associations and their changes using well-known graph theory metrics "clustering coefficient" (fraction of triangles around a node) and node "betweenness centrality" (hereafter referred to as "Centrality"). A network´s clustering coefficient and path length define "small worldness" (SW), which represents the network´s degree of orderly (regular) vs. random connections. In this manner, we could collect information on neuronal synchronization and FCN dynamics independent of energy consumption (Rossini et al., 2019) intending to clarify the functional role of local and global network reorganization. Specifically, we hypothesized that FCNs graph metrics significantly differ between healthy controls and patients with stroke. We hoped to learn which FCN plasticity features are adaptive or maladaptive by correlating them with a visual performance.

3.2 Method

3.2.1 Experimental setting

We recruited hemianopic patients with occipital ischemic stroke (n=24; age: 58.4±10.9 yrs., mean±SD, lesion age>6 months, 21male/3female) and age-matched healthy controls (n=24, age: 57.4±10.5 yrs., 18 male/6 female) as shown in Tab 1. Of note, some patients

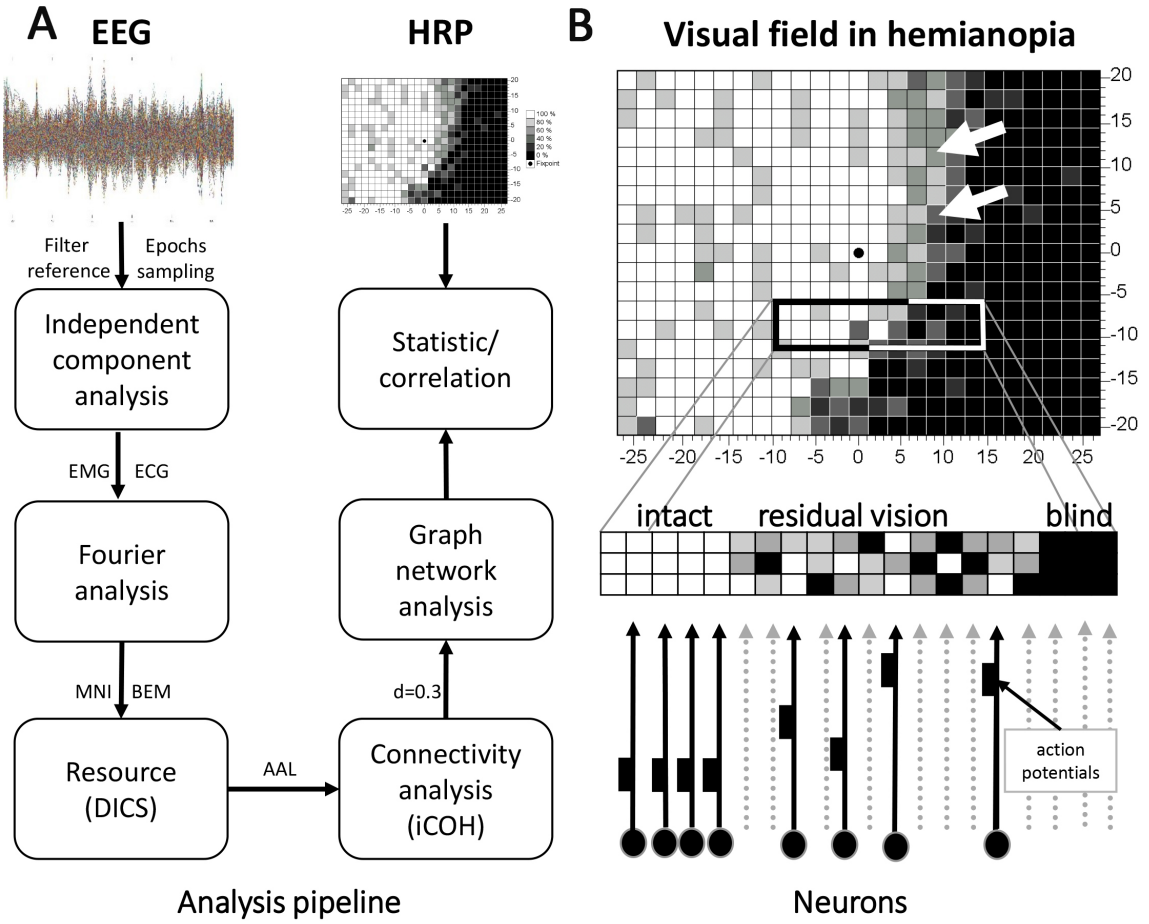

Figure 13: Left panel (A): Analysis pipeline ECG: electrocardiogram; EMG: electromyography; MNI: standard brains template from the Montreal Neurological Institute; BEM: Boundary Element Method; AAL: Automatic Anatomical Labeling, the adjacent matrix was thresholded with density=0.3. Right panel (B): Visual field plot in hemianopia as assessed by high resolution perimetry (HRP). White regions show the intact visual fields, grey regions represent visual field sectors where patients' response accuracy was inconsistent and with only partial vision ("areas of residual vision", ARVs, shown by arrows), and black regions showed no responses ("blind"). Partial function in ARVs is supported by partial cell survival of cells, which are not sufficiently synchronized to fire action potentials.

had middle cerebral artery (MCI) territory and brainstem strokes, a possible source of heterogeneity and FCN variability. Inclusion criteria were as follows: homonymous visual field defects (after middle or posterior artery stroke), stable visual field defect (spontaneous recovery completed), lesion age >6 months, age of patients >18 and <75 years.

Exclusion criteria were published previously in our lab (see (Gall et al., 2015; Li, 2016)), here we listed some important information from above mentioned publications: complete blindness, visual hemineglect, electrical or metal implants (e.g., heart pacemakers), any kind of epilepsy or photosensitivity, autoimmune diseases at an acute stage, psychiatric disorders (schizophrenia, etc.), severe substance abuse, diabetic retinopathy or diabetes mellitus with average blood glucose level >seven mmol/l, high blood pressure >160/100mmHg, instable or high level of intraocular pressure (>27mmHg), retinitis pigmentosa, pathological nystagmus, any severe ophthalmological disorders with a high probability of ongoing vision loss, pregnancy, atrial fibrillation, the risk for vascular thrombosis, arteriosclerosis with more than 75% stenosis, myocardial infarction with high cardioembolic risk level, coronary severe heart disease including unstable angina pectoris, any operation targeting the heart, head or vascular system during the past three months.

The measurement method was described before by (Li, 2016), we also listed some of the important information here from above mentioned publications: Binocular visual fields were tested using a particular high-resolution computer-based campimetric test (HRP) as previously described (Kasten et al., 1998). The patients were seated in a darkened room in front of a 17-in. monitor. Patients were instructed to keep looking at the fixation point and to press the space bar on the computer keyboard whenever either a target stimulus or an isoluminant change in the colour of the fixation point was detected. Simultaneous control of eye movements was carried out utilizing an eye-tracker. Stimulus detection, as well as reaction times, were measured by the program at all stimulus positions (Li, 2016). For each patient, three measurements were performed. The visual field areas were categorized as intact shown in white (three correctly detected stimuli per location), partially damaged regions shown in grey (one or two stimuli detected), and impaired (blind) areas shown in black (no stimulus detection).

EEG acquisition, preprocessing and analysis High dense array EEG was recorded using a HydroCell GSN 128-channel net and a Net Amps 300 amplifier (EGI Inc., Eugene, Oregon, USA) (sample frequency: 500 Hz; impedance <50 kΩ). Five-minute long resting-state EEG per subject was recorded under eye-closed and no-task conditions. A digital 1-145 Hz band-pass filter and a 50 Hz notch filter were applied. Data were down-sampled to 250 Hz and referenced with the common average reference method. Bad channels of controls (4.08±1.31, mean±SD) and patients (4.67±1.43) were removed following visual inspection, and six neighboring electrodes were averaged to represent the removed channels. Five-minute-long EEG recordings were segmented into 2-sec epochs overlapping 0.5 s, with comparable clean trials count for controls (123.6±20.1) and patients (120.1±21.2). Components of eye-blinks or cardiac activity of controls (3.7±1.4) and patients (5.9±3.1) were removed by independent component analysis (ICA); The signal was then decomposed to Delta (1-3Hz), Theta (4-7Hz), Alpha1 (8-10Hz), Alpha2 (11-13Hz), Beta1 (13-21Hz), Beta2 (22-30Hz) and the total alpha (8-13Hz) frequency bands. The analysis pipeline is displayed in Fig. 13A.

Fourier analysis with multitapers and discrete prolate spheroidal sequences (DPSS) ta-

per was used to reduce spectral leakage and achieve frequency smoothing. In our frequency analysis, sensor level Fourier spectra were computed to obtain cross-spectral density per frequency bin, and all trials were kept. To locate the origin of neural activity, we used the standard Boundary Element Method volume conduction model of the head (Oostenveld et al., 2003) and a standard 3D volumetric source model in 8 mm resolution with Montreal Neurological Institute (MNI) coordinates for EEG forward and inverse computations. Generally, the forward model was calculated using the symmetric boundary element method (BEM) (Fuchs et al., 2001). In contrast, the inverse model was calculated with a beamforming method using the partial canonical correlation (PCC) method (Rao, 1969), which implemented the Dynamical Imaging of Coherent Sources (DICS) algorithm for computing the spatial filters for each dipole location in the volumetric source model (Gross et al., 2001). This was subsequently used for connectivity analysis. Finally, the original neural activities were resourced within dipoles from 1-30 Hz according to frequency bands, and the frequency bins were summed and weight averaged into six frequency bands for statistical analysis. We applied the volumetric automatic anatomical labeling (AAL)-VOIs atlas (Tzourio-Mazoyer and Landeau, 2002) which is constructed based on a single subject, high-resolution T1-MRI (Collins et al., 1998), and defines 120 structures, of which we analyzed 90.

We first compared FCN in the left and right hemispheres of age-matched controls (CH) and, after averaging them, with lesioned (LH) and intact hemispheres (IH) of patients using the small-world network as a parameter of global network states.

3.2.2 Estimating functional connectivity

FCNs are defined by statistical synchronization of resting-state EEG patterns, which allows quantification of interaction between different pairs of brain regions (Pereda et al., 2005) with the imaginary part of coherence (Nolte, 2003), a method insensitive to false connectives arising from volume conduction.

$$icoh_{(f,t)} = |im\left(\frac{\sum_{n=1}^{N} S_1^n(f,t)S_2^{n*}(f,t)}{\sqrt{\sum_{n=1}^{N}|S_1^n(f,t)^2|\sum_{n=1}^{N}|S_2^n(f,t)^2|}}\right)| \tag{5}$$

where $S_1^n(f,t)$ and $S_2^{n*}(f,t)$ are the frequency-decomposed EEG data from two specific regions,for every subject and condition the coherence matrix are 128(channel) $\times$ 128(channel)for all pairs at sensor level, the coherence was segmented into short and long range, the short range coherence was within each lobes of interest

$$RT, RF, RP, RO, LT, LF, LP, LO$$

, the long range coherence was between([RO] to

$$RT, RF, RP, LT, LF, LP, LO$$

and [LO] to

$$RT, RF, RP, RO, LT, LF, LP$$

, at source level, between all pairs of dipoles on source data was calculated with imaginary part of coherence, for each one subject per band,

To reduce the dimensionality in the connectivity matrix, we adopt a parcellation

scheme with the AAL atlas and combine the connectivity values between sets of dipole pairs that belong to a given pair of parcels; the parcellated connectivity matrix (116×116) was generated to further complex network analysis.

Graph theory describes the properties of brain networks by quantifying typologies of anatomical tracts or functional associations of brain networks and their changes. Key graph metrics are "clustering coefficient" (fraction of triangles around a node) and node "betweenness centrality" (hereafter referred to as "Centrality"), the fraction of all shortest paths of a given node. A network´s clustering coefficient and short path length define the "small worldness" (SW). It represents the network´s degree of orderly (regular) vs. random connections. In our study, nodes represent brain regions and edges represent the synchronization between two regions at the anatomical level as defined by the AAL atlas (Rubinov and Sporns, 2010).

We calculated the global efficiency (GE), global clustering coefficient (GCC), and global characteristic path length (GCPL) per density to evaluate the stabilization and robustness of network patterns in the alpha band. In this case, we could retain the non-arbitrary and stabilized network pattern and also removed the weak and noisy connectivity (see Fig. 14A, D). Briefly, the density of a connectivity matrix was limited to those with a threshold of 0.3; only 30% of the strongest weight edges were considered to ascertain that the densities (proportion of existing edges out of all possible edges) were equal for each graph and subject (Bola and Sabel, 2015). Generally, fixing the probability for the existence of an edge excludes criteria of Erdős-Rényi random networks for group analysis (van den Heuvel and Hulshoff Pol, 2010). We then calculated the following graph measures: node strength, node degree, node betweenness centrality, and node clustering coefficient; degree and strength represent the sum of links and their weight in a node, centrality demonstrates how many shortest path length pass a node, and the clustering coefficient describes the network around the node. In addition, we assessed the global characteristic path length and clustering coefficient to identify long-range functional connectivity between ROIs.

The EEG was preprocessed and resourced in Fieldtrip (Oostenveld et al.) with Matlab 2017a (MATLAB, 2017) to visualize long connectivity by BrainNetViewer (Xia et al., 2013). Firstly, Mann-Whitney U-test was used to compare the FCN measures between the PCAI and Non-PCAI groups to exclude the effects with Non-PCAI individual lesions. We then compared control subjects with the lesioned and non-lesioned (intact) hemisphere of stroke patients (per frequency*per node). In controls, the FCN metrics were averaged for both hemispheres and compared with intact and the lesioned hemispheres of patients. Significant differences between them were then calculated with a one-way Kruskal-Wallis test for three independent samples. In the post-hoc pairwise comparison with Mann-Whitney U-test ($p<0.05$), the p-value was corrected with family-wise error rate adjusted by the Bonferroni method to consider the multiple comparison problem. Pearson correlations were calculated between FCN metrics and visual performance (detection ability, reaction time) as measured by high-resolution perimetry (HRP) in normal (shown in white in Fig. 13B), impaired (grey) or blind (black) visual field regions.

3.2.3 Ethic and trials

Standard Protocol Approvals, Registrations, and Patient Consents: This study complied with the ethical standards of the Declaration of Helsinki (1964) and was approved

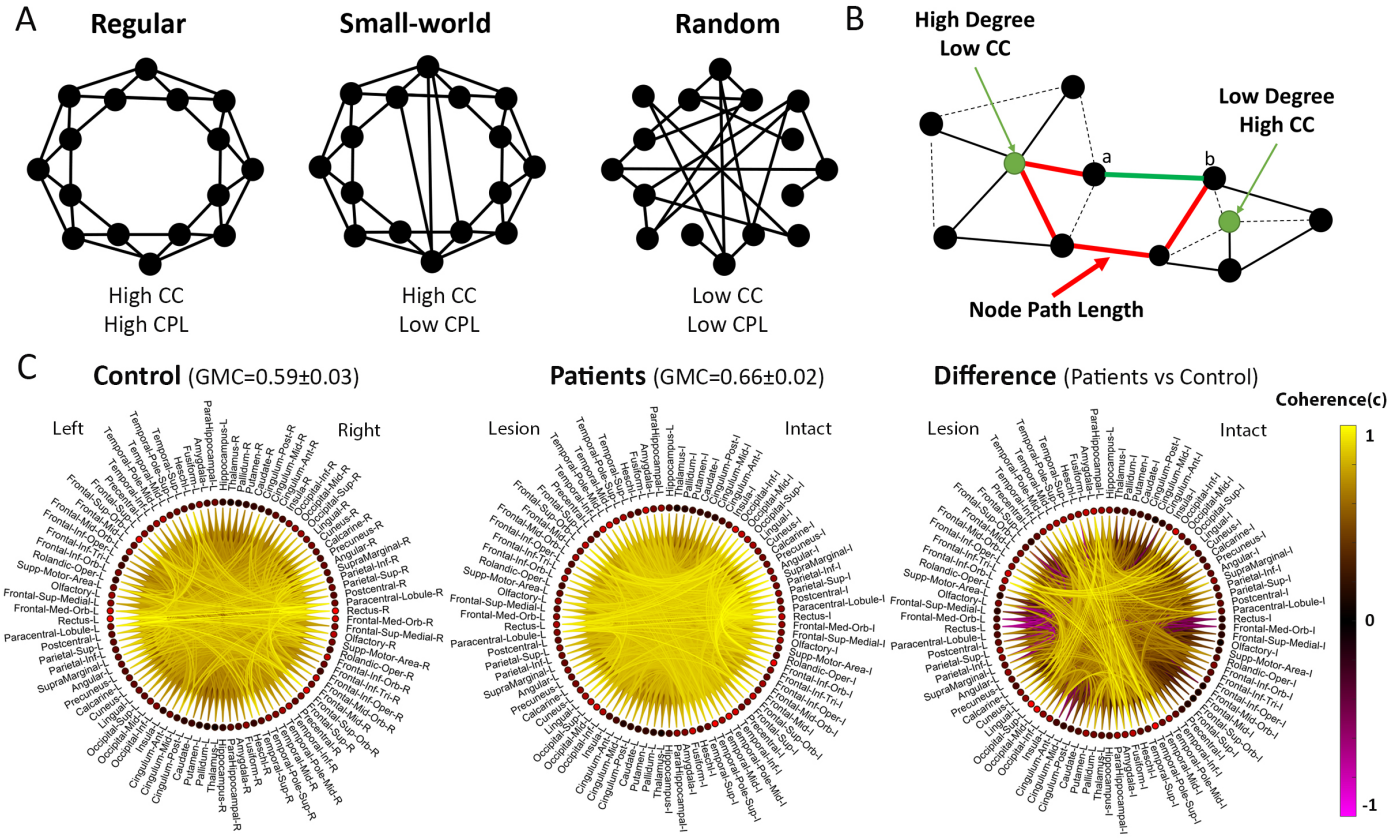

Figure 14: Part A: Neural networks of the brain, like any other network in nature, have two extremes structures: On one end of the extremes is the "regular" structure: here, nodes are connected only with their immediate neighbors. Regular structures score high on the graph metrics clustering coefficient (cc), characteristic path length (CPL), centrality, degree, and or strength, and such networks are considered to be stable (rigid) and inflexible, and low on efficiency and adaptability. On the other end of the extremes are "random" structures which score low on the above metrics. They are highly instable and flexible, but unpredictable and also inefficient. For networks– including neural network – to be efficient yet predictable, they structures are in between the two extremes in a state of "small-worldness" (SW) which combines regularity with flexibility for stability and plasticity (adapted from Stam et al. 2007). Part B: Cartoon illustrating three measures: "centrality", CPL and CC: when neural information travels from a to b, the red path (longer CPL) is less efficient than the green one. Part C: Cycle brain network plot showing normalized global mean coherence (GMC) between regions for controls and stroke patients in the alpha band. Patients had a more diffuse FCN pattern due to a greater number of connections. Increased CC and CPL suggests a loss of "small-worldness" which is interpreted as a sign of overall less efficient global network organization.

as a clinical trial by the local ethics committee (University of Magdeburg, Medical Faculty, Magdeburg/Germany; no.173/13) and national regulatory bodies (ClinicalTrials.gov-Identifier: NCT04008589). The study started on 14. Jan 2014 and ended 16. March 2015; 24 patients were finally recruited (all patients signed consent forms). Data Availability Statement: Data not published with GDPR protection in the EU. However, anonymized data are available to appropriately qualified investigators upon request.

3.3 Result

Graph theory features betweenness centrality, clustering coefficient, and characteristic path lengths (Fig. 14A, B) were used to describe FCN organization. "Centrality" represents how many shortest path length pass this brain region (node), while the "clustering coefficient" explains the network around the node. Thus, global FCN structures are represented by "characteristic path length" and "clustering coefficient". The mean connectivity matrix of control subjects and stroke patients (Fig. 14C) shows the dominant functional connections between ROIs. Whereas normal subjects had more clearly defined FCN with few regions interconnecting, the FCN pattern was more diffuse in patients, with many different functional connections. Because there was no significant left/right hemispheric difference in local FCN metrics in controls, both were pooled because Non-PCAI (n=8) and PCAI patients (n=16) were comparable in the alpha band (Fig. 15B), both were also pooled.

3.3.1 FCN graph metrics in intact and lesion hemispheres

Tab 2 summarizes graph analysis results for regions with the most critical differences in the alpha band, namely the FCN metrics in occipital, parietal and temporal brain regions. No significance was found in the frontal areas.

Network Centrality: The parameter "centrality" (also called "betweenness centrality") is the most relevant and sensitive graph metric in all ROIs compared to other graph measures. It represents how many times the shortest path length passes through one node. A node with high centrality has considerable influence within a network by controlling the information processing of other nodes. By comparing EEGs between patients and controls, we studied how nodes react to the occipital stroke and how they communicate with other nodes´ "centrality" (Fig. 16A, C). Post-hoc testing revealed that centrality in the LH of precuneus was significantly higher than in the CH ($p<0.05$) by 44.8%; the centrality in the IH of Occipital_Sup was significantly higher than in the CH ($p<0.01$) by 58.7%, and the IH centrality of the Occipital_Mid was 27.3% higher than the LH ($p<0.05$). Thus, the visual cortex of the intact hemisphere had higher centrality than the lesioned hemisphere. Group differences were also found for the middle temporal (Temporal_Mid) ($F(2,69)=10.52$, $p=0.005$) and inferior temporal gyrus (Temporal_Inf) ($F(2,69)=9.13$, $p=0.01$). Post-hoc analysis showed that the centrality of Temporal_Mid ($p<0.005$) and Temporal_Inf ($p<0.05$) of the IH was significantly lower than the CH (-32.6% and -30.7%, respectively).

Clustering Coefficient: The clustering coefficient (CC) describes the network clustering capacity of the local nodes. When it is high, the node is considered to be less flexible (stable), having a "regular" FCN structure. Post-hoc analysis indicates that LH clustering

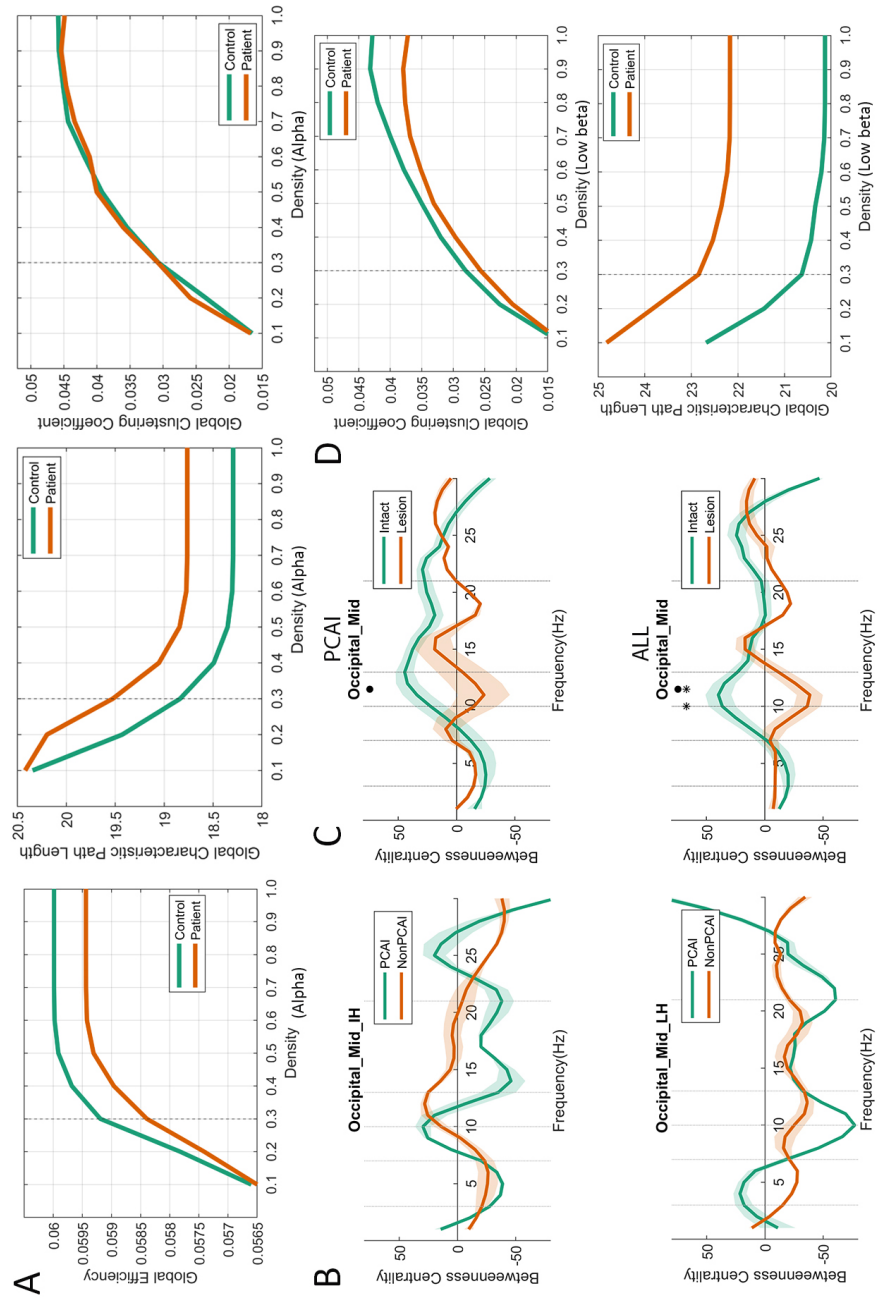

Figure 15: Part A: The patterns of the functional connectivity network per density in the alpha band for controls and patients. The dotted, vertical line indicates a threshold of d=0.3. As the density increases toward 1.0, the difference between patients and control network parameters GE, GCPL, and GCC remained stable; Thus, d=0.3 is a reasonable threshold value to represent such patterns. Part B: centrality pattern of Non-PCAI and PCAI patients in occipital regions are not significant. The zero-line is the value of the control group, and the vertical lines inside the graph represent the different frequency domains: delta, theta, low and high alpha, low and high beta. Tests of significance are based on the total values for each frequency band domain. Part C: Centrality of a lesioned and intact hemisphere is comparable when all patients or only PCAI patients are considered. Thus, the pooling of both patient groups for subsequent analyses is justified. Part D: The GCC and GCPL distribution between controls and patients confirms that the conclusion about the small-worldness dynamic change in the low beta band was stabilized.

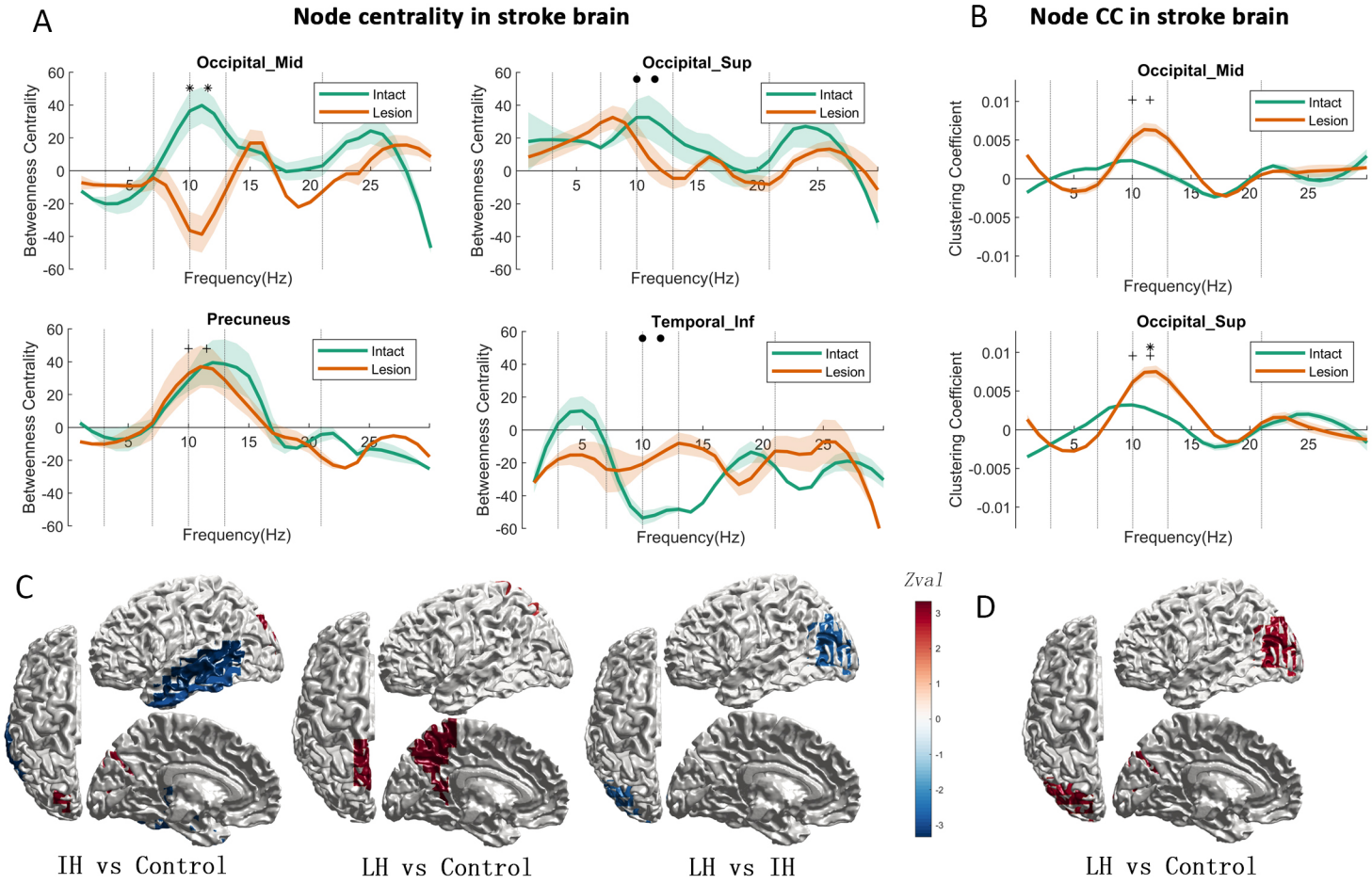

Figure 16: Node centrality (A) and clustering coefficient (B) visualization for control hemisphere, intact (IH), and lesion hemisphere (LH). The horizontal zero-line represents the control baseline. Upper graphs: brain network measures across different frequency bands. Occipital_Mid centrality was significantly enhanced in the intact hemisphere and reduced in the lesioned hemisphere. Lower graph(C and D): Only significant z-value are shown in the half hemisphere surface plots. Negative Z-values are shown in blue and positive Z-values in red. The clustering Coefficient (D) of the occipital lobe was enhanced in both hemispheres, but to a larger extent so in the lesioned than the intact hemisphere. "+"= significant difference between lesion and control hemisphere; *= significance between the lesion and intact hemisphere; =significance between intact and control hemisphere

coefficients in Occipital_Sup ($p<0.05$) and Occipital_Mid ($p<0.05$) were higher than in controls by +22.2% and +20.7%, respectively (Fig. 16B, D). This is a sign that the network at or near the lesion site has more stability (=less flexibility), i.e., a more "regular" FCN structure, with fewer global interactions due to structural or functional disconnection.

Network degree and strength: Degree: The number of local node connections (degree) showed significant differences in Post-hoc analysis (Fig. 17A): IH degree was significantly lower in controls in Temporal_Mid ($p<0.05$) by -20.3%, in Temporal_Sup ($p<0.01$) by -17.6%, and in Temporal_Inf ($p=0.005$) by -19.4%. Furthermore, degree in Temporal_Mid of IH was 26.1% lower than LH ($p<0.05$) and 31.6% or 21.3% higher in IH Occipital_Sup ($p<0.05$) and Occipital_Mid ($p<0.005$) above controls, respectively. This shows FCN-degree enhancement of intact middle occipital and superior occipital lobes, while the degree of the intact temporal ITG was lower, which matches the centrality results above. Strength: (Fig. 17B). Post-hoc analysis showed that local network strength was lower in IH of patients than controls in Temporal_Sup ($p<0.05$) by -12.4% and Temporal_Inf ($p<0.05$) by -15.5%, but higher in LH Temporal_Mid ($p<0.05$) and Temporal_Inf ($p<0.05$) by 20.0 and 22.2%. And we observed increased strength of Cuneus ($p<0.05$) and Occipital_Sup ($p<0.05$) in the IH compared to controls by 33.2% and 42.5%. In contrast, intact temporal regions had reduced degree and strength. Thus, local node strength and degree were significantly enhanced in the occipital lobe of IH above control levels (intact>lesion>control), while a significant reduction was noted in the temporal lobe (control>lesion>intact). In the LH, FCN reorganization was less pronounced occipitally and unaffected in temporal structures. FCN reorganization included an increased number of links and sum of weights in the intact occipital lobe while being reduced in the intact temporal lobe to levels beyond those of the lesioned hemisphere. Clustering also increased, but only in the LH.

3.3.2 Reorganization of inter-cortical connectivity in left and right stroke patients

Because visual processing may differ in both hemispheres (Cavézian et al., 2015), we compared FCNs in left vs. right-sided damage in the alpha-band (8-13Hz). Reorganization of long-range connectivity was enhanced in patients compared to controls. Still, the change differed between left vs. right hemispheric strokes. In left stroke, long-range connectivity (coherence) was significantly enhanced between left occipital (LO) and left frontal lobe (LF) in the alpha2 band ($z=3.118$, $p=0.012$) and the right frontal regions ($z=2.62$, $p=0.031$) (Fig. 18). In contrast, in right hemispheric strokes, coherence was higher than controls in the left occipital and right parietal lobe (RP) ($z=2.70$, $p=0.031$). In left hemispheric stroke patients, only a trend of enhanced alpha2 band connectivity between the right occipital and right frontal lobe ($z=2.58$, $p=0.06$). Thus, regardless of side, the intact visual cortex had a pronounced elevation in node centrality (Fig. 18B).

3.3.3 Global small-world network

Global characteristic path length (CPL) and Clustering Coefficient (CC) describe "small-worldness" patterns of the global brain network (Fig. 18C, D). Mann-Whitney U-test revealed that in the low beta band patients had a significantly higher CPL ($z=2.6$, $p=0.009$) and lower CC than controls ($z=2.3$, $p=0.02$) which resulted in an overall lower small-world network pattern in stroke; the stabilization of this network pattern was also

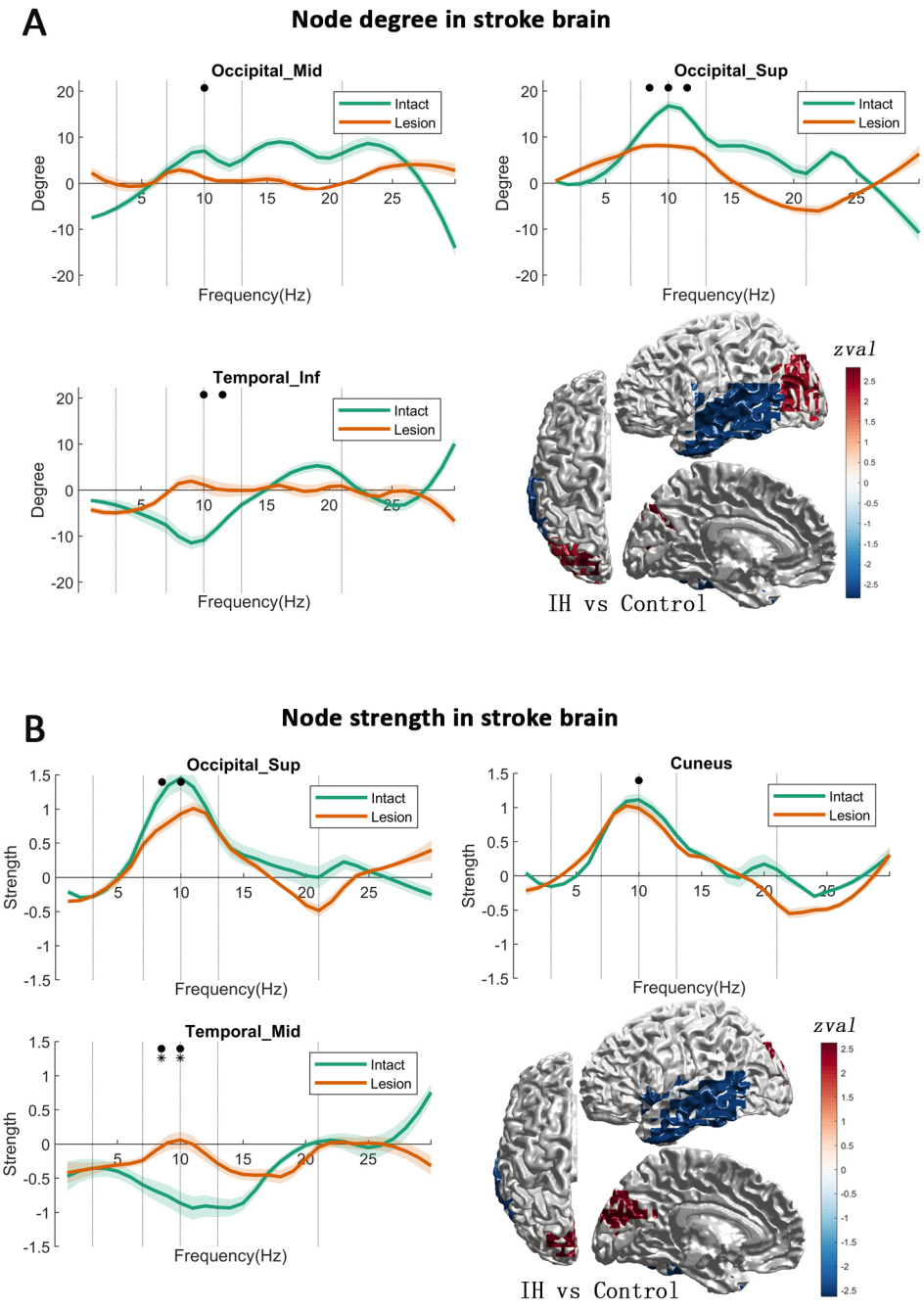

Figure 17: Part A: Node degree visualization for CH, LH, and IH. Lower right: areas with significant z-value are shown in a single hemisphere surface plot. Negative Z-values showed in blue and positive values in red. Part B: Node strength was enhanced in Occipital_Sup and cuneus, but it was inhibited in the intact temporal lobe. The significant difference symbols: "+"=LH vs. CH; *= LH vs. IH; = CH vs. IH. The x-axis frequency band differences are compared to the control-zero-baseline); Y-axis: distribution of the brain network measures ($p<0.05$, FDR-corrected).

evaluated cross multiscale thresholding (Fig. 15D).

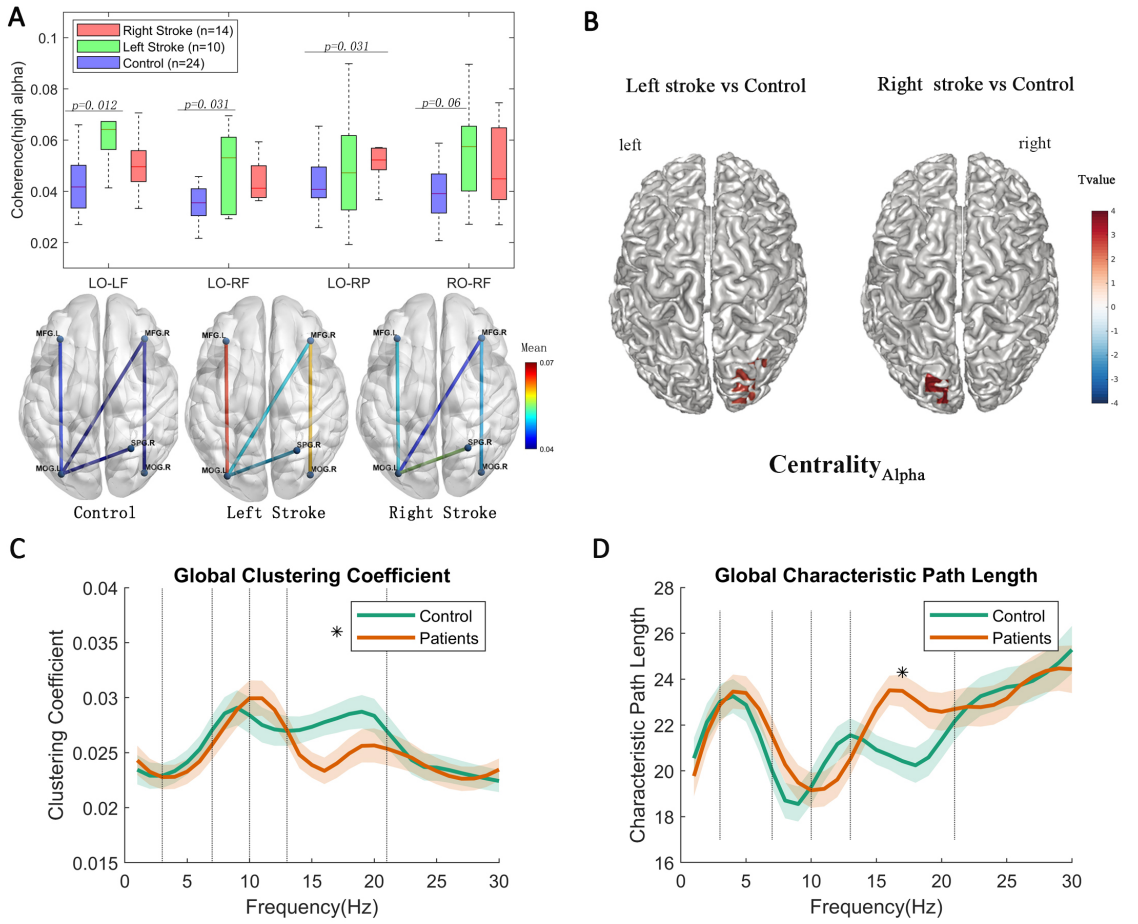

Figure 18: Part A: Visualization of long-range connectivity with 0.3 sparsity (high alpha-band); box plots show significant changes (p-value, FDR-corrected). Frontal_Mid.L/R: Middle frontal gyrus of the left or right hemisphere, Occipital_Mid.L/R: Middle occipital lobe of the left or right hemisphere. Parietal_Sup.R: Superior parietal gyrus of the right hemisphere. LO/RO: left/right occipital lobe. LF/RF: Left/Right frontal lobe. RP: Right parietal lobe. Part B: Centrality difference between left vs. right-stroke vs. control. Both show in the contralateral hemisphere more alpha-band connectivities. Part C and D: Global CPL network comparison shows that patients had high CPL in the Beta1 band and a lower global CC network. A trend was observed in the Alpha2 band with a higher CC in the patient group. Here, the small-world network was observed with higher CPL and lower CC in patients. *=significance between control and patients.

3.3.4 Correlations between network measures and vision

Correlating FCN parameters with visual performance outside the scotoma (i.e., in "intact" visual field sectors) (white regions in the HRP chart displayed in Fig. 13): The (intact) visual field (FV) size includes regions normal detection in the intact hemifield as well as any residual vision on the scotoma side. VF size was positively correlated with centrality in the IH Occipital_Sup (r=0.526, n=24, p=0.008) in the alpha-band and negatively with the clustering coefficient (CC) in the Occipital_Inf of the IH (r=-0.463, p=0.023). Both, node centrality (r=0.478, p=0.018) and CC (r=0.417, p=0.043) of LH Temporal_Pole_Mid were significantly correlated with normal vision size (Fig. 19). And the node centrality of IH supplementary motor area (SMA) correlated negatively with normal vision size (r=-0.414, p=0.044) in the alpha band (Fig. 19). Furthermore, node CC

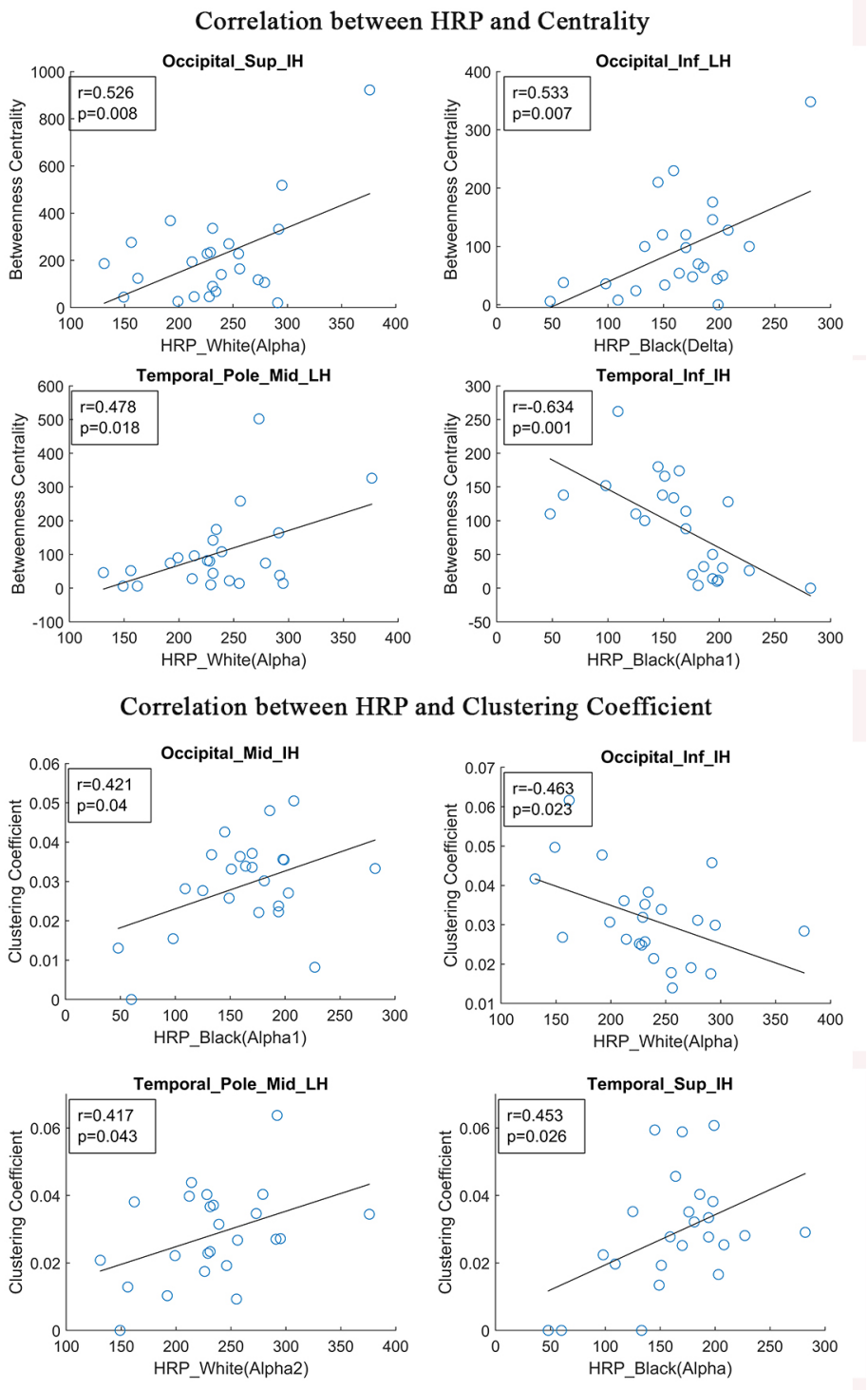

Figure 19: Pearson correlation between visual detection accuracy in HRP and local network measures (Centrality, Clustering Coefficient) in the intact and lesioned hemisphere. Note: x-axis shows vision performance for white, grey, and black areas. No significant correlation was observed with global CPL or CC measures and visual functions (data not shown here).

of SMA in both hemispheres correlated positively with the VF size (IH: r=0.424, p=0.039; LH: r=0.524, p=0.009) and the centrality of IH frontal_Inf_Orb positively correlated with the normal vision size (r=0.509, p=0.011) in the alpha band.

A correlation heat map (Fig. 20) shows how visual functions relate to FCN graph measures in the alpha band of patients. Greater visual detection ability was associated with larger values in degree and strength in occipital and temporal regions and more clustering in temporal and frontal lobe structures of LH (Fig. 20A). The IH showed a reverse pattern: detection was associated with lower coherence in occipital and temporal regions and lower degree and strength in occipital, temporal and frontal regions. While VF-size is a spatial attribute, reaction time probes temporal visual processing (Fig. 20B). Because smaller values represent faster reaction times, negative correlations indicate that better temporal processing was associated with greater "small-worldness." Interestingly, a negative (moderate) correlation pattern was observed for alpha band clustering in most brain regions in both hemispheres. Thus, we conclude that global alpha-band clustering benefits temporal processing. Other overall correlation patterns were only found in the intact hemisphere (occipital, temporal, frontal), where a greater degree and strength was associated with poor temporal processing.

3.4 Discussion

This is the first systematic study of FCN reorganization using EEG-tracking in chronic, occipital stroke patients. Similar to other functional systems (Rossini et al., 2003; Vecchio et al., 2019), we found FCNs reorganization in visual system structures both locally (at or near the lesion site) and globally, i.e., via long-range FCN changes, where different structures showed either strengthening or weakening of FCN patterns (Tab 2). We observed increased centrality, degree, and strength in occipital regions, which were moderate in the lesioned (11%-36%) but massive (31%-58%) in the intact hemisphere. This more "regular" (rigid) FCN pattern suggests less flexibility and less efficiency. The opposite was encountered in the temporal lobe, where FCN values dropped markedly in the intact hemisphere (-12% to -32%) (Greater "small-worldness"), indicating greater flexibility and efficiency in neural processing. In contrast, FCNs remained unchanged on the lesion side.

What is the functional consequence of this network plasticity? Higher FCN values in centrality, degree, strength, and clustering signify greater rigidity/stability and less flexibility, signs of a more "structured" network (Fig. 14A), where nodes are more tightly connected with immediate neighbors. In contrast, lower values suggest less clustering and shorter path length, believed to support greater functional integration and processing efficiency ("small-worldness"). This is thought to signify increased functional (neurocognitive) relevance for a given function or action (Bassett and Bullmore, 2017; Douw et al., 2011). Our stroke patients demonstrate massive FCN changes with both "adaptive" and "maladaptive" signs of reorganization.

In the intact hemisphere, occipital brain areas (including visual cortex) show a more "regular" FCN-structure, suggesting a functional disturbance, having less flexible and less efficient FNC ("maladaptive" plasticity). But temporal regions show increased small-worldness, i.e., more network efficiency and global integration ("adaptive" plasticity). "Maladaptive" plasticity in the intact visual cortex may be triggered by a loss of cross-hemispheric inhibition following occipital lesions, leading to hyperactivation and desyn-

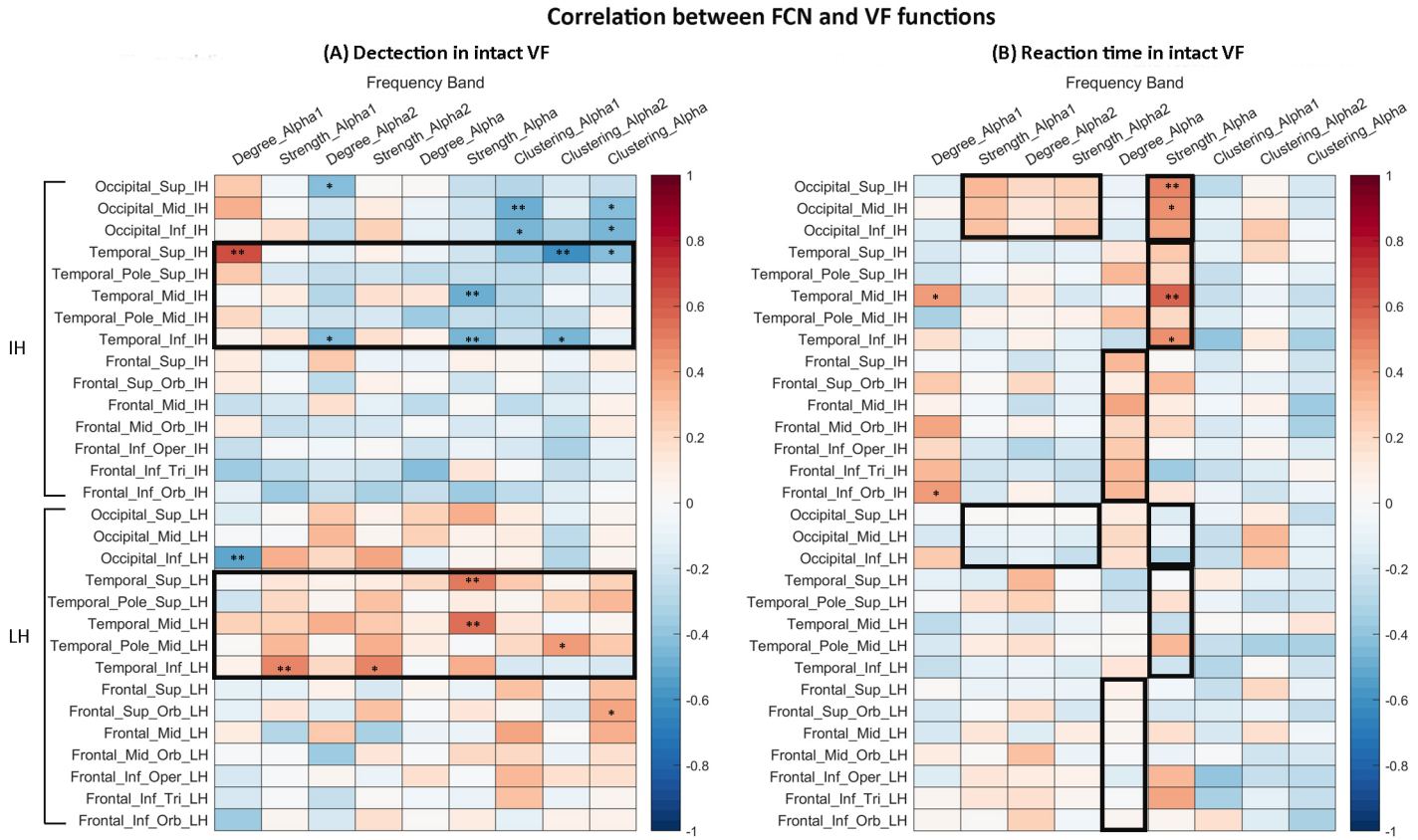

Figure 20: Heat map summary of correlations between functional connectivity (FCN) graph measures in the alpha band and visual function (detection ability in HRP) of stroke patients. When FCN metrics (degree, strength, clustering) score high, this indicates greater rigidity/stability and less flexibility (=low "small-worldness"). In contrast, low FCN metrics indicate less rigidity/stability and more flexibility (= greater "small-worldness"). Black frames show common patterns of positive (red) or negative (blue) correlations in different structures of the occipital, temporal, and frontal lobes in the intact (IH) or lesioned (LH) hemisphere. For the interpretation of our results, we considered both significant values (*p<0.05, **p<0.01) and non-significant patterns of correlation polarities as they are also informative. Part A: Correlations between FCN metrics and intact visual field (VF) size (detection ability) show which FCN state is associated with smaller or larger VFs (i.e., size of residual vision). Part B: Correlations between FCN metrics and reaction time (RT), a measure of temporal processing independent of VF size.

chronization of visual signal processing. In contrast, greater FCN efficiency and integration in the intact temporal lobe indicate an adaptive role of temporal regions. Thus, EEG-tracking with subsequent FCN graph analysis unveiled signs of both "adaptive" and "maladaptive" FCN plasticity which MRI-imaged oxygenation changes cannot observe. Thus, EEG tracking markedly, and more precisely, extends our understanding of post-stroke brain network reorganization. Furthermore, the observation we collected in our patients is largely compatible with the current state of the art.

3.4.1 Maladaptive FCN reorganization in the intact visual cortex

Using MRI, Wang et al. report that brain activity is lower in the damaged regions but above normal values in the intact hemisphere (Wang et al., 2010). Nelles et al. stimulated the intact hemifield of hemianopic patients with visual stimuli, comparing BOLT activation patterns with normal subjects (Nelles et al., 2007), more activation was observed in the intact visual cortex (area 17) and bilaterally in the extrastriate cortex (areas 18/19). But when stimulating the hemianopic side, this led to bilateral activation of the extrastriate cortex, which was stronger in the intact hemisphere, suggesting that the intact hemisphere was compensating by over-activation.

Our findings are compatible with the proposal of plasticity of the intact visual cortex. But because, unlike the evidence of MRI overactivation, the EEG captures frequency-specific electrophysiological network changes even when there is no change in energy consumption (oxygenation), offering a more detailed understanding of the neurophysiology consequences of unilateral stroke. Most prominently, our EEG analyses revealed a rather massive reorganization of the intact hemisphere node-centrality, -degree and –strength, yet no change in the clustering coefficient (Tab 2). Furthermore, patients´ intact occipital regions were much less flexible and less efficient (involved in a lower small-worldness) than control (up to 58%), suggesting that the intact cortex is not only hemodynamically more active (as shown by MRI), but, processing neural information less efficiently, with less signal and more noise in visual cortical regions.

Over-activation of the intact hemisphere should not be all that surprising. After all, in everyday life, heminaopic patients have to process visual information with only one visual cortex, not two. However, this challenge could impact the physiology and function of the visual system in various ways: (i) functionally, the intact visual cortex can no longer share the task of analyzing the visual world with its "buddy"-hemisphere. (ii) When only one visual cortex has to manage tasks such as object tracking, synchronizing the right and left side of space ("perceptual crowding"), controlling perception-action interactions, and so on. (iii) Physiologically, unilateral lesions lead to transcallosal anatomical/functional deafferentation caused by the loss of interhemispheric inhibition (the "Sprague-effect")(Sprague, 1966), creating an interhemispheric imbalance which could explain why (iv) the contralateral "intact" hemifield has subtle perceptual deficits (Bola et al., 2013). In addition, (v) eye movement coordination is a problem because compensatory eye movements towards the hemianopic side complicates temporal integration of visual stimuli (Dundon et al., 2015), and (vi) the function and coordination of microsaccades are impaired– tiny eye movements which are critical for high resolution vision (Gao et al., 2018).

Given this conglomerate of challenges, the intact visual cortex has a neural processing

load that is way above normal levels. While greater metabolic activity (observed with MRI) seems to signify adaptive compensation, our EEG-tracking suggests the contrary: less "small-worldness" with lower efficiency of neuronal synchronization in space and time. Therefore, a reduced (neural network) efficiency in combination with a (metabolic) cell hyperactivation may signify less signal and more noise in the intact occipital lobe. Perhaps this is the price the brain has to pay when only one occipital cortex represents a "bilateral" visual world. We, therefore, propose that FCN reorganization in the intact visual cortex is "maladaptive," creating more "noise" (less signal) in an overwhelmed visual cortex. But how can "maladaptive" occipital and "adaptive" temporal FCN plasticity be explained? In a speculative spirit, we propose that the loss of cross-hemispheric inhibition leads to an FCN disturbance and over-activation of the intact region. Indeed, hemianopia patients suffer perceptual impairments in the presumably "intact" visual field sector.

Such deficits include accuracy and response time deficits when detecting or categorizing natural scenes (Cavézian et al., 2010), reduced detection ability, and temporal processing (slowed reaction time) (Bola et al., 2013), pathological completion of simple figures (Paramei et al., 2017), reduced detection of contours composed of non-contiguous Gabor patches embedded in a random patch array (Paramei and Sabel, 2008), and Gestalt perception impairment with associated alterations of the gamma-band EEG activity (Schadow et al., 2009). Furthermore, late blind individuals have less dynamic low-frequency fluctuations (lower flexibility) of visual thalamocortical activity.

3.4.2 Adaptive FCN reorganization of intact temporal lobe

In contrast to the intact occipital lobe, temporal regions showed marked reduction of node-centrality, -degree, and –strength which were up to -32% of control values. This change towards FCN structures of greater "small-worldness" signifies more flexibility and greater efficiency. Surprisingly, temporal brain regions remained at normal (control) levels. Temporal lobe alterations in stroke patients were also reported by others, but the results are mixed. Vanni et al. (Vanni et al., 2001) recorded MRI alternations in a hemianopia patient with right posterior cortical damage who had undergone significant vision rehabilitation training. They found longer-latency responses in the damaged (right) superior temporal cortex, which was interpreted as a sign of compensation of the brain to produce synchronized population responses in the early visual processing of the cortex (Vanni et al., 2001).

On the other hand, when a hemianopia patient was trained with flicker stimulation (Henriksson et al., 2007), functional MRI revealed that information from both hemifields was processed in the intact hemisphere. This was true not only in visual areas V1, V2, V3, and V3a but also in the visual motion-sensitive area V5 in the superior temporal gyrus. This finding is compatible with our EEG-tracking results, and both are compatible with the hypothesis of "adaptive" plasticity in temporal structures. It is debatable if greater oxygenation (activation) in MRI is good or bad for vision. Although increased oxygenation might well signify that more neurons fire action potentials, it does not teach us this creates more synchrony in neural signaling, i.e., more signal improving vision or more noise, reducing vision.

The greater small-worldness of occipital-temporal, intra-hemispheric adaptations are behaviourally meaningful if one considers the role of the temporal gyrus in normal vision

as investigated in monkeys. The monkey brain is homologous to the human brain (Kolster et al., 2010). Similar to humans, the temporal lobe processes motion perception with its motion-sensitive middle temporal (MT)/V5+ complex with four regions: the MT/V5 proper, the ventral part of the medial superior temporal area, the fundus of the superior temporal area, and the transition of V4, each representing the complete contralateral visual hemifield. They are sensitive to three-dimensional structures from motion and for the perception of a static stimulus and movement perception. Together with some nearby regions, the V5+ complex supports about 70% of the motion localizer activation. The middle temporal (MT)/V5+ complex is unaffected by occipital cortex lesions, as it receives is afferent input directly from the retina through the extrastriate route. This would explain why the temporal lobe FCN was unaffected on the lesioned hemisphere and why it can support "blindsight" hemianopic patients, who can correctly identify visual stimuli inside the hemianopic field without being aware of it (Stoerig and Cowey, 1997).

Our stroke patients had a sharp rise of "small-worldness" in the middle temporal gyrus (+32.6%) and this was correlated with improved temporal processing (faster reaction times). We propose that this FCN change is "adaptive" FCN, possibly supporting better movement perception of the intact hemifield and thus help the (overwhelmed) intact visual cortex to manage everyday activities, increase visual sensitivity and better temporal processing. This interpretation is compatible with reports that training with moving stimuli can improve perception in hemianopia (Huxlin et al., 2009; Jobke et al., 2009), that blindsight training improves visual field sensitivity (Sahraie et al., 2006), and it may explain why "compensatory" eye movement training improves daily activities and visual fields (Kerkhoff et al., 1992).

3.4.3 The dominant role of alpha-band oscillations

Our FCN changes were mainly found in the alpha and low beta1 frequency bands, confirming their well-known role in visual processing. Especially alpha oscillations are believed to increase signal-to-noise ratio by inducing a balance of inhibitory and excitatory influences in the brain (Sourav et al., 2018), where alpha regulates the bottom-up influences (Schepers et al., 2012) and controls the top-down attentional sampling of visual perception at around 10 Hz. Van Rullen (VanRullen, 2016) suggested that brain functions, including vision, are sustained by oscillations of neuronal aggregates with firing rates at various frequencies, which ascertains perception and cognition to operate periodically. Therefore, different oscillations (frequency bands) require synchronization across space and time to transiently bind/unbind different sensory modalities, tasks, and cognitive states. We believe our FCN graph analysis is a valuable tool to help understand how multiple periodic functions are orchestrated or synchronized after stroke, so that internal sampling rhythms can be coordinated for the expression of overt behavior by way of short- (local) and long-distance (global) functional connections. As in normal vision, alpha-band oscillations play an important role in the damaged brain, and FCNs in the alpha band are critically altered in stroke-induced vision loss, both with adaptive and maladaptive consequences.

3.4.4 Reorganization in the damaged hemisphere

Compared to the intact hemisphere, the damaged hemisphere actually had less pronounced FCN plasticity. Specifically, the Occipital_Mid and Occipital_Sup had a clustering coefficient which was higher than the intact and control hemisphere (Lesion>Intact Control), ie. Showing involvement in lower small-worldness (more stability, less flexibility). We interpret this to signify greater local activity and/or less long-range neural interactions in the lesion and/or its surround (Crofts et al., 2011; Wang et al., 2010). Specifically, the lack of impairment in the damaged hemisphere could be explained as follows: firstly, the (MT)/V5+ complex receives direct retinofugal fibers through the extra-striate route which supports eye movement control and movement perception. It is one of two main pathways mediating blindsight (Stoerig and Cowey, 1997; Cowey and Stoerig, 1991), the other being residual tissue of incomplete cortical damage (Wüst et al., 2002). Under normal conditions, the extra-striate pathway interacts with V1 projections so to integrate retinotopy and eye movements. However, because this extra-striate pathway bypasses V1, it can still support movement perception and eye movement control. Hence, FCNs are largely unaltered.

3.4.5 Global small-world network reorganization

The 'small-world' is characterized by a high clustering coefficient (CC) and low characteristic path length (CPL) (Rubinov and Sporns, 2010; Watts and Strogatz, 1998) (Fig. 14), showing if nodes are tightly connected with their nearest neighbours (high cc and high CPL) or not (low cc and low CPL). FCNs can be either highly stable and inflexible, or they are instable and highly flexible. Because neurological functions require both stability and flexibility to support stable and/or transient operations, the brain´s FCN can adopt different states of "small-worldness" which lies inbetween both extremes.

Patients had lower beta band CC compared to controls, i.e. global FCN synchronization was impaired, reducing neural processing efficiency (low small-worldness). Fig. 14C shows the more diffuse FCN pattern in patients due to a greater number of connections with increased CC and CPL suggests a loss of "small-worldness", i.e. a less efficient network organization.

FCN reorganization between remote regions after stroke is well known and indicates local and global effects in different functional systems (Grefkes and Ward, 2014; Vecchio et al., 2019; Wang et al., 2012). Our own observations of a loss of occipito-frontal functional connectivity in patients with optic nerve damage (Bola et al., 2014) are in line with our current finding that stroke patients have greater coherence between the occipital lobe and ipsilateral frontal lobe both in the damaged and in the intact hemisphere. However, patients´ left and right hemisphere differed: left stroke patients had enhanced coherence between the lesioned occipital lobe and the intact frontal lobe, but right hemispheric stroke group had greater coherence between the intact occipital and parietal lobe of the damaged hemisphere. This brain network (re-)organization may explain the known left/right differences in visual processing (Cavézian et al., 2015; Chokron et al., 2008).

3.4.6 Brain network correlation with behavioral data

We correlated graph measures in the alpha band with visual function to interpret our findings on a functional level. Fig. 20 is a correlation heatmap, where high scores in FCN degree, strength, and clustering indicate greater "regularity" of the network. Greater network regularity in occipital, temporal, and frontal regions of the lesioned hemisphere was associated with larger visual field size, which is found in patients with incomplete hemianopia. This suggests that residual vision on the hemianopic side interferes with the overall network structure (lower "small-worldness"). However, negative correlations were found in the intact hemisphere of the occipital, temporal and frontal lobes. Fig. 20B shows correlations between FCN metrics and reaction time, a marker of temporal processing of residual vision, which is independent of visual field size. In the intact hemisphere, greater "regularity" (strength, degree) of the alpha band network was associated with longer reaction times in occipital, temporal, and frontal regions. Therefore, greater "small-worldness" correlates with faster temporal processing, i.e., more efficient visual processing in the temporal and frontal lobes. Because temporal lobe gain of "small-worldness" (=loss of regularity, Tab 2) matches the reaction time gain, this indicates "adaptive" FCN-plasticity.

3.5 Limitations

Because FCN analyses were based on a standard head model, this might obscure subtle FCN changes caused by individual lesion sizes/locations. But this would create a bias against the hypothesis of finding group differences. Secondly, some patients had Non-PCAI lesions, but this did not affect our results. Thirdly, we cannot solve the cause-effect problem because we do not know if FCN alterations result from chronic stroke or if persons with such FCNs are at greater risk of suffering stroke. Indeed, personality and stress resilience are known risk factors for CNS diseases such as stroke and glaucoma (Sabel et al., 2018).

3.6 Conclusions

Graph measures of FCN based on EEG-tracking are a valuable tool to unravel the role of electrophysiological oscillations in brain network reorganization. As we showed, the stroke brain shows both local and global FCN reorganization in the high alpha and low beta band, which can be both "maladaptive" or "adaptive" in different brain regions. To be clear, we do not believe that a given subject has either whole-brain "adaptive" or "maladaptive" FCN plasticity. Still, we propose that FCN reorganization may be "adaptive" in some brain regions but "maladaptive" in other regions of the same individual. Specifically, the stroke FCN changes towards a more "regular" pattern that is maladaptive in the intact occipital region, possibly creating perceptual deficits causing temporal and spatial visual impairments in the "intact" but crowded visual field. But FCN can also be "adaptive," enabling temporal gyrus structures to compensate for vision loss. Thus, exploring the complex architecture of the brain´s FCN using EEG-tracking adds critical temporal dimensions to our understanding of brain reorganization to better explain the normal and abnormal (low) vision. In addition, brain FCN graph analysis might inspire new approaches for the diagnosis and rehabilitation of low vision loss and other neurode-

generative disorders.

Patients							Controls	
ID	**Gender**	**Age**	**Lesion age (Months)**	**Type**	**Lesion side**	**Etiology**	**Gender**	**Age**
1	M	25	45	Ischaemia	Left	PCAI	M	24
2	M	46	61	Ischaemia	Left	PCAI	M	44
3	M	66	20	Ischaemia	Left	PCAI	M	55
4	M	74	19	Ischaemia	Left	PCAI	F	75
5	M	63	28	Ischaemia	Left	PCAI	M	65
6	M	53	29	Ischaemia	Right	PCAI	M	53
7	M	63	25	Ischaemia	Left	PCAI	M	61
8	M	55	156	Ischaemia	Left	PCAI	M	56
9	M	71	21	Ischaemia	Right	PCAI	M	68
10	M	50	11	Ischaemia	Right	PCAI	M	51
11	M	67	49	Hemorrhage	Right	PCAI\MCAI	M	66
12	M	61	25	Ischaemia	Right	PCAI	M	62
13	M	46	43	Ischaemia	Right	PCAI	F	48
14	F	55	106	Ischaemia	Right	PCAI	F	55
15	F	61	7	Hemorrhage	Right	PCAI	F	60
16	M	52	10	Ischaemia	Right	PCAI	M	50
17	M	69	45	Ischaemia	Right	OLS	M	68
18	F	53	117	Ischaemia	Right	OLS	F	54
19	M	73	19	Ischaemia	Right	OLS	M	67
20	M	54	93	Hemorrhage	Left	OLS	M	53
21	M	59	6	Ischaemia	Left	OLS	M	59
22	M	59	27	Hemorrhage	Right	POIH	M	57
23	M	71	12	Hemorrhage	Left	POIH	F	72
24	M	55	9	Ischaemia	Right	BSI	M	54
Total	21M/3F			5 Hemorrhagic 19Ischaemic	10 left 14 righ	16 PCAI 1PCAI and MCAI 5 OLS 2POIH 1 BSI	18 M/6F	
Mean		58.37	40.95					57.37
(SD)		(10.87)	(39.21)					(10.56)

Table 1: Demographics of patients and age-matched controls. PCAI: posterior cerebral artery infarcts, MCAI: Middle cerebral artery infarct, OLS: occipital lateral superior stroke, and POIH: parieto-occipital intracerebral hemorrhage. Gender: M-male, F-Female, Lesion age in months since time of stroke (Note: 25 patients were recruited, one patient dropped out), totally 5 Hemorrhagic, 19 Ischaemic.

Region of interest		FCN measures	Control	Intact hemi.	Lesioned hemi.	Percent difference		
			mean±SE	mean±SE	mean±SE	IH/CH	LH/CH	LH/IH
Occipital	superior occipital gyrus (SOG)	Centrality	91.3 ± 38.7	144.9 ± 66.7	124.7 ± 63.8	58.7%**	36.6%	-13.9%
		Degree	34.5 ± 9.4	45.4 ± 12.2	38.4 ± 8.5	31.6%**	11.3%	-15.4%
		Strength	2.8 ± 0.9	3.99 ± 1.5	3.3 ± 1.0	42.5%*	17.9%	-17.3%
		Clustering coeffcient	0.027 ± 0.006	0.028 ± 0.006	0.033 ± 0.008	3.7%	22.2%*	17.9%
	middle occipital gyrus (MOG)	Centrality	113.7 ± 39.6	150.0 ± 59.4	109.0 ± 49.0	31.9 %(*)	-4.1%	-27.3%*
		Degree	36.2 ± 8.8	43.9 ± 12.6	38.1 ± 7.3	21.3%*	5.2%	-13.2%
		Clustering coeffcient	0.029 ± 0.006	0.0295 ± 0.007	0.035 ± 0.008	1.7%	20.7%*	18.6%
	Cuneus (CUN)	Strength	2.8 ± 1.0	3.73 ± 1.3	3.5 ± 1.2	33.2%*	25.0%	-6.2%
Parietal	Precuneus (PCUN)	Centrality	105.1 ± 47.1	138.9 ± 62.7	152.2 ± 73.9	32.2%	44.8%**	9.6%
Temporal	superior temporal gyrus (STG)	Degree	37.4 ± 5.9	30.8 ± 10.7	34.8 ± 11.1	-17.6%*	-7.0%	13.0%
	middle temporal gyrus (MTG)	Centrality	135.1 ± 39.7	91.1 ± 43.6	144.4 ± 92.2	-32.6%**	6.9%	58.5%**
		Degree	38.0 ± 6.4	30.3 ± 12.1	38.2 ± 10.7	-20.3%*	0.5%	26.1%*
		Strength	2.9 ± 0.7	2.54 ± 1.7	3.1 ± 1.0	-12.4%*	6.9%	20.0%*
	inferior temporal gyrus (ITG)	Centrality	136.6 ± 51.1	94.7 ± 55.5	124.2 ± 57.6	-30.7%**	-9.1%	31.2%
		Degree	37.1 ± 7.2	29.9 ± 10.8	36.5 ± 12.7	-19.4%*	-1.6%	22.1%
		Strength	2.9 ± 0.7	2.45 ± 1.5	3 .0 ± 1.3	-15.5%*	3.4%	22.4%*

Table 2: The FCN measures' change (mean±SE) in occipital, temporal and parietal lobe of Control (CH), Intact (IH) and Lesion hemisphere (LH); IHCH: the percent changes of intact hemisphere with control hemisphere as the baseline ((Intact hem. - control hem.)control hem.), LHCH: the percent changes of lesion hemisphere with control hemisphere as the baseline ((Lesion hem-control hem.)control hem.), LHIH: the percent changes of lesion hemisphere with intact hemisphere as the baseline ((Lesion hem-Intact hem.)intact hem.); Positive or negative (green/yellow) values which are a statistical trend or significant ((*)p<0.10, *p<0.05, **p <0.01), or their value is >10%.

4 Study 2: Reorganization of brain functional connectivity network and vision restoration following combined tDCS-tACS treatment after occipital stroke

(This work has been published by Frontiers of Neurology 2021)

4.1 Background

The potential to restore visual fields following central visual system damage has attracted some attention in the last two decades (Kasten et al., 1997; Sabel and Kasten, 2000a; Sabel et al., 2004; Dundon et al., 2015; Fedorov et al., 2011; Sabel et al., 2020a; Tharaldsen et al., 2020), Occipital stroke, for example, leads to homonymous hemianopia (HH) whereby a quarter or the same half of the visual field in both eyes is lost (Zhang et al., 2006a). This impairs visual functional abilities and quality of life (Gall et al., 2010b), which puts patients at risk to fall or have difficulties in reading, and to develop secondary neuropsychological deficits such as depression and social isolation (Ramrattan et al., 2001; Jones and Shinton, 2006; Gall et al., 2010b; Ribeiro et al., 2015a). While visual training can improve visual fields (Sabel and Kasten, 2000b; Cavanaugh and Huxlin, 2017), it is time-consuming, and progress of recovery takes many months of daily exercises.

To overcome this limitation, efforts were made to use non-invasive brain stimulation (NIBS) as a new therapeutic approach. NIBS has already been applied in the rehabilitation of different neurological diseases affecting the motor system, memory, language, or cognition (Antal et al., 2017). They include low-intensity NIBS such as alternating or direct current stimulation (tACS, tDCS), which are believed to alter brain excitability (Woods et al., 2016). Especially tDCS was often used to treat various neurological and neuropsychiatric dysfunctions (Palm et al., 2016b; Ciechanski and Kirton, 2017). Here, current flows from the anodal to the cathodal electrode, where the anode is thought to enhance (excite) and the cathode reduce (inhibit) neuronal activities (Nitsche and Paulus, 2000; Nitsche et al., 2003). In contrast, the direction of current flow in tACS alternates between both electrodes and thus is able to modulate periodic oscillations (Woods et al., 2016). This can, in turn, entrain endogenous brain oscillation in a frequency and phase-specific manner (Ali et al., 2013; Herrmann et al., 2013). With tACS, it is, therefore, possible to enhance the power, shift the peak, and change the EEG oscillations phase by applying the ACS at a frequency identical or close to those oscillations (Zaehle et al., 2010). tACS was already shown to increase parieto-occipital alpha activity and to synchronize cortical oscillations with entrainment of specific frequencies (Helfrich et al., 2014), and this impacts the endogenous alpha oscillation with long-lasting "after-effects" (Neuling et al., 2013a). When stimulating the brain in the alpha frequency range, for example, this increased alpha power, reflecting neuroplasticity changes rather than induced entrainment (Vossen et al., 2015a). NIBS can also be used to purposely modulate neuron excitation and inhibition in many neurological diseases with a potential to induce recovery of function (Lefaucheur et al., 2017).

tACS has also been shown to enhance recovery following visual cortex or optic nerve damage (Sabel et al., 2011a; Gall et al., 2011, 2013, 2016). A 10-day treatment course achieved improvements in visual fields, reduced reaction time, and visual acuity. The proposed mechanism of action is to modulate the synchronization of neuronal networks firing of partially damaged "areas of residual vision" that survived the injury, possibly involving the strengthening of synaptic transmission along with various parts of the visual pathway and enhancing blood flow (Sabel et al., 2020a). Indeed, tACS-induced visual improvements significantly correlated with neuronal synchronization changes (Gall et al., 2010a; Fedorov et al., 2011; Gall et al., 2016), and enhanced alpha-band activity or power citeSchmidt.2013 (Vossen et al., 2015b). Considering tDCS, several previous studies sug-

gest that visual cortex damage leads to hyperactivity of the intact hemisphere, presumably inhibiting the lesioned side (Corbetta et al., 2005; Oliveri et al., 1999), and a dual-mode tDCS can reduce visual neglect symptoms (Sunwoo et al., 2013).

That tDCS can modulate visual functions was shown in normal subjects and patients with visual system damage. For example, Plow et al. combined tDCS with visual training which improved hemianopic visual fields (Plow et al., 2012). In healthy subjects, anodal tDCS of the occipital poles significantly reduces psychophysical surround suppression (Spiegel et al., 2012) and enhanced occipital blood flow (Sabel et al., 2020b) However, little is known about possible frequency-specific neural-plastic mechanisms for vision recovery after occipital stroke. Only a few studies explored the potential of NIBS to induce recovery of visual functions in patients suffering from a unilateral occipital stroke (Gall et al., 2015). Therefore, a better understanding of the neurophysiological mechanism of tACS and tDCS is needed to understand and eventually maximize their potential to improve visual fields after unilateral occipital stroke.

We now used both protocols alone or in combination to learn more about the mechanisms and effects of tACS and tDCS in occipital strokes. Specifically, we hypothesized that cathodal tDCS might inhibit the intact visual cortex, reduce its hyperactivity and thus lower the associated cross-hemispheric inhibition. Treatment with tACS, on the other hand, might induce endogenous neuronal oscillations of the whole brain. Therefore, we now studied both methods alone as well as in combination. We expected that a "double-punch" approach of combined tACS/tDCS would be most effective, as it would simultaneously reduce cross-hemispheric inhibition and enhance the excitability of the tissue at or near the lesion site. We already reported our vision recovery and fMRI-activation results elsewhere. In the present paper, we characterize brain neurophysiological changes focusing on brain network reorganization and plasticity and studied how this correlates with visual parameters in our stroke patients.

4.2 Materials and Method

4.2.1 Demographics

Unilateral occipital stroke patients (n= 24) suffering from hemianopia were recruited as previously described (Gall et al., 2015) and randomly assigned to one of three groups (see Fig. 21A):): tDCS/tACS group (ACDC, n=8, age: Mean ± SD=53.45±14.18); Sham tDCS/tACS group (AC, n=8, age: Mean ± SD =58.25±9.54); sham tDCS/Sham tACS group (SHAM, n=8, age: Mean ± SD=63.87±5.38). Their EEG results were compared to 24 healthy subjects (age: Mean ± SD =57.4±10.5) (see Tab 3 and Tab 1). The study was conducted with the guidelines of the International Conference on Harmonization of Good Clinical Practice (ICH-GCP) and the applicable national legislation requiring all participants to sign a consent form in agreement with the declaration of Helsinki. The study was approved by the institutional review board of the University of Magdeburg. The patient's group identity was only known to the experimenter who performed the stimulation. The participants were informed about their stimulation protocol after completion of follow-up diagnostics at eight weeks(Gall et al., 2015).

Patients' cause of hemianopia was ischemic (n=19) or hemorrhagic (n=5) stroke, and their age range was 18-75 years. Lesion age was at least six months, and diagnostic results

ID	Group	HRP_PRE			HRP_POST			HRP_FU			RT_PRE		RT_POST		RT_FU		Field of vison		
		Black	Grey	White	Black	Grey	White	Black	Grey	White	Grey	White	Grey	White	Grey	White	PRE	POST	FU
1	2	181	29	231	182	28	231	180	33	228	0.4967	0.4280	0.4929	0.4260	0.5250	0.4203	24	25	25
2	2	109	41	291	112	36	293	117	23	301	0.5193	0.4137	0.5179	0.4306	0.4272	0.4228	26	26	25
3	0	60	5	376	56	14	371	55	13	373	0.4381	0.3469	0.3796	0.3403	0.4201	0.3493	26	26	26
4	0	145	65	231	123	92	226	122	85	234	0.4688	0.4217	0.5209	0.4626	0.5182	0.4604	21	20	20
5	1	208	71	162	214	69	158	205	60	176	0.5519	0.4829	0.5459	0.4756	0.6027	0.4827	26	26	26
6	2	125	24	292	115	33	293	110	33	298	0.4987	0.3893	0.4858	0.3886	0.5022	0.3837	28	27	28
7	1	194	8	239	188	16	237	191	23	227	0.4884	0.3878	0.5180	0.3931	0.4845	0.4260	28	28	27
8	1	98	48	295	103	51	287	92	79	270	0.4900	0.4014	0.4820	0.4163	0.5030	0.4346	27	27	27
9	0	149	13	279	150	13	278	149	19	273	0.5038	0.3818	0.5317	0.3780	0.4619	0.3780	27	27	27
10	1	176	19	246	176	15	250	177	16	248	0.5062	0.4167	0.4874	0.4144	0.5000	0.4173	24	27	27
11	1	133	109	199	133	117	191	157	73	211	0.4810	0.4276	0.5274	0.4048	0.5414	0.4094	23	23	24
12	2	198	14	229	198	7	236	193	18	230	0.5329	0.4801	0.5323	0.4783	0.5333	0.4873	27	28	29
13	0	170	79	192	179	39	223	180	56	205	0.4460	0.3927	0.5099	0.4140	0.5377	0.4533	23	27	27
14	0	164	128	149	138	141	162	162	123	156	0.5510	0.4409	0.5439	0.4498	0.5303	0.4524	26	25	25
15	2	186	21	234	176	31	234	177	27	237	0.5096	0.3729	0.5029	0.3632	0.5079	0.3685	28	29	29
16	2	151	34	256	133	45	263	145	32	264	0.6036	0.4588	0.5436	0.4329	0.5665	0.4443	24	24	24
17	0	48	120	273	16	91	334	47	76	318	0.4994	0.4165	0.5011	0.4094	0.5596	0.4262	26	29	26
18	1	199	30	212	202	21	218	200	27	214	0.5334	0.3602	0.4795	0.3551	0.4963	0.3622	21	23	25
19	2	170	16	255	170	6	265	172	4	265	0.5240	0.4413	0.4936	0.3820	0.5779	0.3927	25	27	27
20	1	282	28	131	283	26	132	287	25	129	0.5225	0.4678	0.5580	0.4826	0.5637	0.4855	26	26	26
21	0	194	19	228	191	14	236	193	19	229	0.6211	0.5256	0.6314	0.5571	0.6296	0.5385	22	24	24
22	1	203	12	226	199	10	232	206	9	226	0.5488	0.4455	0.6010	0.4537	0.5678	0.4795	29	29	27
23	0	227	58	156	246	59	136	248	54	139	0.6599	0.6471	0.7353	0.7153	0.7472	0.7151	26	25	24
24	2	159	68	214	177	88	176	160	88	193	0.5498	0.4221	0.5443	0.4331	0.5411	0.4302	27	28	28
Total	Group 0 Sham/Sham 1 Sham /rtACS 2 rtDCS/rtACS																		
Mean (SD)		163.70 (51.68)	44.12 (35.92)	233.16 (54.46)	160.83 (57.55)	44.25 (37.25)	235.91 (58.64)	163.54 (54.59)	42.29 (30.98)	235.16 (56.31)	0.5145 (0.0515)	0.4219 (0.0619)	0.5194 (0.0644)	0.4211 (0.0763)	0.5318 (0.0668)	0.4282 (0.0737)	25.41 (2.22)	26.08 (2.18)	25.95 (1.96)

Table 3: Patient information, Etiology: PCAI: posterior cerebral artery infarcts, MCAI: Middle cerebral artery (MCA) infarct, OLS: occipital Lateral Superior, PICAI: Posterior inferior cerebellar artery infarct, BSI: Brain Stem Infarction, POIH: parieto-occipital intracerebral hemorrhage, Sex: M-male, F-Female, Lesion age: the months since stroke happened, Side of vision loss: left part of vision, right part of vision

showed stable visual field defects across repeated baseline measurements. Subjects with spontaneous fluctuations and recovery of vision were not entered in the trial. Moreover, all patients had corrected visual acuity of at least 0.4 (20/50 Snellen) or better. The presence of residual vision and detectable gradual transition between the intact and the blind part of the visual field was confirmed according to the clinician's evaluation. Patients were excluded if they had at least one of the following symptoms: malignant brain tumor, eye or other central nervous system diseases, electric or metallic implants in the eyes or head, expected low compliance, history of epileptic seizures within the last ten years, or use of antiepileptic or sedative drugs during the recruiting process. Before admission to our study, A neurologist checked the medical history. A comprehensive examination of visual dysfunction, was carried out. The confirmation of further involved in this study depended on the preliminary investigation results. The patients must demonstrate some residual visual performance, which could be identified by a gradual transition between the blind area and the visual field's intact area.

4.2.2 Experiment design

tDCS/tACS: The tACS and cathodal tDCS stimulation was delivered with conductive-rubber electrodes placed in saline-soaked sponges and connected with a NeuroConn MC8 stimulator. The tACS stimulation electrode (5 × 7 cm) and a reference electrode (10 × 10 cm) were placed at Fpz and the right upper arm, respectively, according to 10–20-system EEG recordings. Stimulation started with a 5 Hz burst, and then frequency increased in steps of 1 Hz up to 30 Hz using a 48 second-long "rtACS block." The tACS stimulation was given for 20 min per day with a maximum current of 1.5 mA (peak-to-peak), which was well above the phosphene threshold (Schutter and Hortensius, 2010). Then, the block was repeated for 20 minutes. In the tDCS condition, the cathode was positioned above the intact hemisphere, and stimulation was done for 10 min immediately before rtACS and set at one mA using one electrode placed at either O1 or O2 position (3 × 3 cm) with anode at Fpz. The impedance was kept below 10 kΩ.

Sham design: Sham patients had identical electrode montage and stimulation duration. The tACS sham-condition was designed so to induce (short-lasting) phosphenes that patients could notice (Schutter and Hortensius, 2010), i.e., it was a minimal stimulation. In addition, occasional current bursts were given to create short but presumably therapeutically ineffective phosphenes (Gall et al., 2015) involving one 5 Hz burst/min with individual amplitude for phosphene perception as used in a previous study where none of the subjects could tell to which group they belonged (Gall et al., 2015). In contrast, the tDCS sham condition was designed to elicit only cutaneous sensations that gradually disappear because of habituation (Dundas et al., 2007). Here, the current was ramped up for 30 sec, then stopped, and at the end of the session, ramped down for another 30s as shown in Fig. 21A. Through this design, we ensured that all patients' felt their skin comparable in degree and duration with the active tDCS. The combined tDCS / tACS stimulation was designed to indicate whether prior cathodal tDCS on the intact hemisphere (a kind of conditioning) could enhance rtACS effects compared to sham-stimulation and rtACS without preceding tDCS (Gall et al., 2015). Here, cathodal tDCS was applied to reduce the interhemispheric imbalance by inhibiting the visual cortex of the intact hemisphere Fig. 21B. All sham patients had been offered to receive stimulation treatment after the final follow-up evaluation. The stimulation parameters were kept unchanged for 20-30

minutes per day during the two weeks' treatment ((Fig. 21C). Of note: for all stimulation condition the default-setting of the neuroConn stimulator gives short pulse of 50Hz at 0.5 µAmp every two seconds to monitor the skin resistance.

Safety aspects of the applied electrical current stimulation: The relatively large surface area of electrodes during stimulation limited the maximum threshold of current densities compared with other studies. The maximum current density was 42 µA/cm2 below AC stimulating electrodes and 15 µA/cm2 below the reference electrode. In the case of tDCS, it was 111 µA/cm2 below the stimulating electrodes, which corresponded to a total charge density lower than 0.1 C/cm2, which was below the safety limits as described in the previous study (Nitsche et al., 2003). Safety guidelines for direct current applied to the human brain were reported (Nitsche et al., 2003; Iyer et al., 2005; Antal et al., 2017). The following undesirable symptoms had been observed immediately after stimulation and the following day before the next stimulation: dizziness, headache, blurred vision immediately after stimulation, skin sensation, fatigue/drowsiness, and others.

4.2.3 EEG recording and preprocessing

High dense array EEG was recorded using a HydroCell GSN 128channel net and Net Amps 300 amplifier (EGI Inc., Eugene, Oregon, USA) with a sampled frequency of 500 Hz. Impedance was ascertained to be below 50 kΩ throughout the recording. The patient's resting-state EEG was recorded at three time points (before treatment: PRE, after ten days of treatment: POST; follow-up after two months: FU). During the recording, patients were instructed to keep relaxed, with their eyes closed, for at least 5 minutes. There was no significant difference in patient's age in three groups after a Kruskal-Wallis test ($p>0.05$), ACDC (Mean ± SD=53.45±14.18), AC (Mean ± SD =58.25±9.54), Sham (Mean ± SD=63.87±5.38).

EEG signals were analyzed with Matlab version 2019a and Fieldtrip (Oostenveld et al., 2011). A digital 1-145 Hz band pass filter was applied as well as a 50 Hz notch filter, and the data was down-sampled to 250 Hz and then referenced by the common average reference method. Five minutes long EEG recordings for both groups were segmented into 2 seconds long epochs with 0.5 s overlapping. Components of eye-blinks and cardiac activity were removed by an independent component analysis (ICA) algorithm. The frequency was decomposed as seven frequency bands: Delta ($1 \sim 3$Hz), Theta ($4 \sim 7$ Hz), Alpha1 ($8 \sim 10$Hz), Alpha2 ($11 \sim 13$Hz), Beta1 ($14 \sim 21$ Hz), Beta2 ($22 \sim 30$ Hz) and the whole Alpha band as ($8 \sim 13$Hz).

4.2.4 Source construction and functional connectivity estimation

See previous description(see Chapter 3).

4.2.5 Visual field diagnostic

Visual field parameters (Visual field: FOV, High-resolution Perimetry: HRP) were assessed in patients to quantify the visual impairment in different phase. The contralateral eye's FOV was measured by OCULUS Twinfield®[2]. HRP demonstrates the visual field charts generated by high-resolution computer-based Perimetry developed by the Sabel laboratory (Sabel et al., 1997).

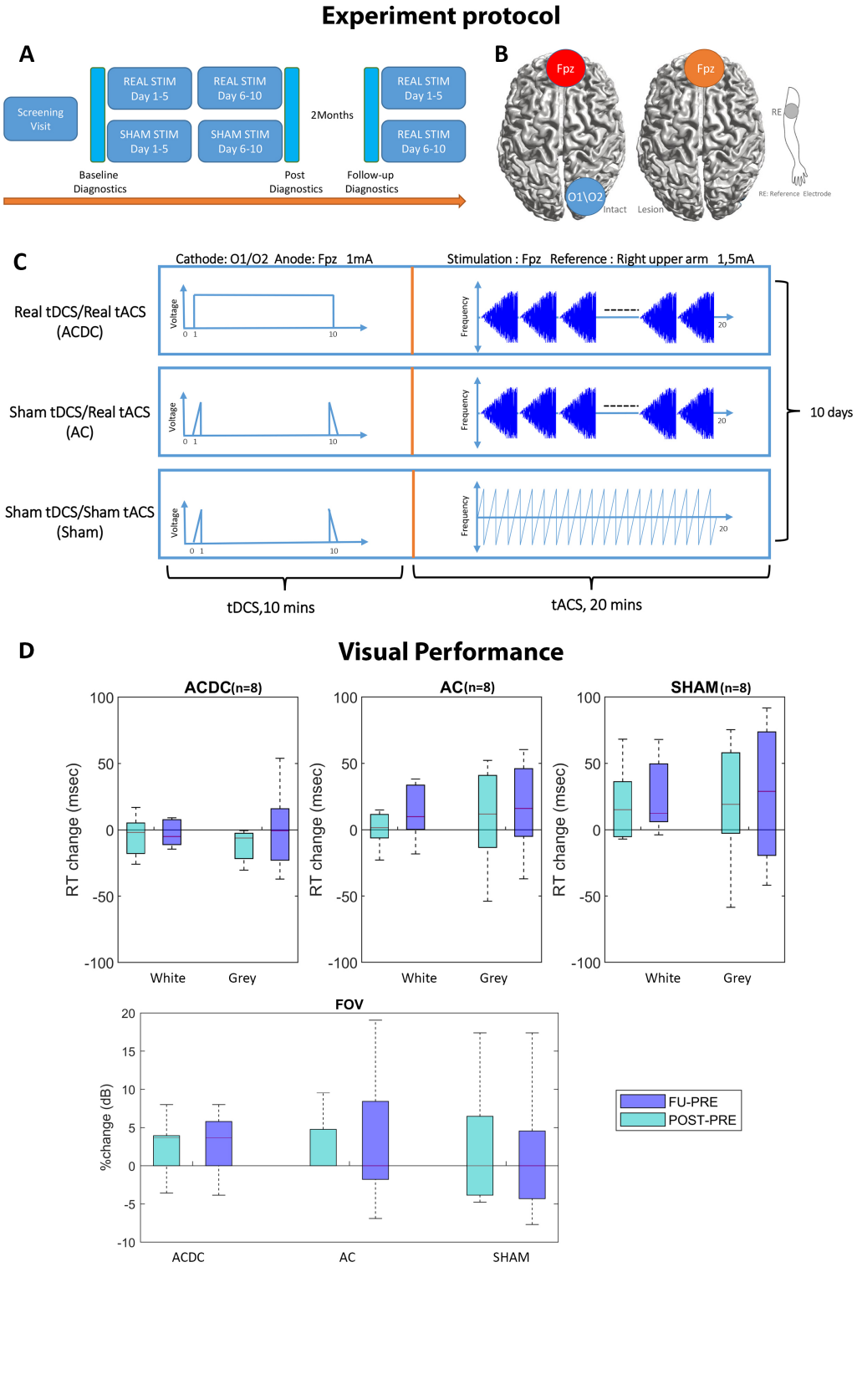
Experiment protocol
A
Screening Visit
REAL STIM Day 1-5
REAL STIM Day 6-10
SHAM STIM Day 1-5
SHAM STIM Day 6-10
2Months
REAL STIM Day 1-5
REAL STIM Day 6-10
Baseline Diagnostics
Post Diagnostics
Follow-up Diagnostics
B
Fpz
O1\O2
Intact
Lesion
RE
RE: Reference Electrode
C
Cathode: O1/O2 Anode: Fpz 1mA
Stimulation : Fpz Reference : Right upper arm 1,5mA
Real tDCS/Real tACS (ACDC)
Sham tDCS/Real tACS (AC)
Sham tDCS/Sham tACS (Sham)
Voltage
Frequency
10 days
tDCS,10 mins
tACS, 20 mins
D
Visual Performance
ACDC(n=8)
AC(n=8)
SHAM(n=8)
RT change (msec)
White
Grey
FOV
%change (dB)
ACDC
AC
SHAM
FU-PRE
POST-PRE

Figure 21: A). The pipeline for experiment time schedule and post-diagnostic, five mins-rsEEG, and Visual parameters were recorded before the experiment as a baseline, after ten days of stimulation, and two months later in Follow-up. Moreover, all sham patients were offered to receive stimulation treatment after the final evaluation. B and C). Therefore, three treatment groups were organized: Real tDCS/Real tACS (ACDC), Sham tDCS/Real tACS (AC), Sham tDCS/Sham tACS (SHAM). The primary purpose of this design was to decrease the activity in the intact occipital to balance the interhemispheric interaction and modulate the brain oscillation with tACS, especially in the lesioned hemisphere. Study design protocol: 10 minutes-tDCS was firstly applied on Cathode: O1 or O2 and Anode: Fpz over the intact hemisphere; then, immediately, 20 minutes-tACS was applied on an active electrode: Fpz and reference electrode: right upper arm. 1mA current in Real tDCS for all the stimulation period and Sham tDCS current was being ramped up for 30 s then stopped and at the end of the session ramped down for another 30s. Max current 1.5mA in Real tACS for all the stimulation period and only one 5 Hz burst per minute for sham tACS stimulation. D) The boxplot of White and grey areas' reaction time, ACDC has faster reaction time than before treatment as well as other two groups. This may indicate that the ACDC's visual functionality has been enhanced with more probability than the other two groups. RT: reaction time, Unit: millisecond. In the bottom part, the FOV percentage changes in each group, the median of percentage changes of ACDC was observed positive both in POST and FU. In contrast, AC and SHAM group remains zero. From both HRP and FOV, the ACDC group shows a more promising visual performance improvement than the other two groups. FOV: Field of Vision. Unit: dB.

4.2.6 Data analysis and software

Data analysis was conducted with Matlab 2017a (MATLAB, 2017). EEG was pre-processed and resourced in Fieldtrip (Oostenveld et al., 2011), the functional connectivity measures were calculated by the brain connectivity toolbox (Rubinov et al., 2009), and the long coherence was visualized by BrainNetViewer (Xia et al., 2013). Pearson correlation was performed between the behavior data and brain network measures at each frequency band. Because our study was explorative, no adjustment was made for multiple-comparison (Rubin, 2017).

Visual fields were analyzed with respect to absolute change in HRP and percentage change in FOV after non-invasive brain stimulation per group. A repeated measure ANOVA test was performed (three groups: ACDC, AC, SHAM, and two-time: Post-Pre and Fu-Pre). P-value was corrected by the Tukey-Kramer test in the posthoc analysis.

4.3 Results

4.3.1 Visual field recovery

A detailed description of visual field recovery is published elsewhere. However, to explore the functional meaning of brain network changes, here we report detection performance in the visual fields and the reaction times.

Visual field: There was no significant main effect ($F(1, 21) = 0.002$, $p=0.9$) and no interaction effect ($F(2, 21) = 0.46$, $p=0.63$) in visual field detection performance. However, as shown in Fig. 21D, the ACDC group's FOV increased after treatment, and this was maintained at follow-up. In contrast, the other two groups' median FOV remained unchanged after treatment and at follow-up. This suggests that the visual functionality of the ACDC group had a trend of an enhancement at a group level compared with a baseline which was not observed in the other two groups.

Reaction time: No significant interaction effect was observed ($F(2, 21) = 1.49$, $p=0.24$) on white and grey RT percentage shown in Fig. 21D. However, there was a trend of ACDC reaction time decrease (which is an improvement) in both POST and FU in the intact

sector of the visual field. In contrast, both AC and SHAM groups' reaction time increased in POST and FU compared with baseline. As for the grey area, there was no significant interaction (F (2, 21) = 0.006, p=0.99) nor a main effect for the group interactions (F (1, 21) = 0.84, p=0.37). However, RT of ACDC decreased while the RT of AC and SHAM increased comparing with baseline in POST and FU. This indicates the ACDC group has a greater visual acuity percentage change than the other two groups.

4.3.2 Brain network after brain stimulation

We performed a two-way 3 (Stimulation group: ACDC, AC, and Sham) x 3(Time: PRE, POST, and FU) mixed-design ANOVA with repeated measures on the time variable of local node strength and long coherence (see Fig. 22A). A compound symmetry assumption was checked before statistical analysis was performed. The regular p-value calculations in the repeated measures were reported if the theoretical distribution of the response variables was of the same variance if provided the compound symmetry assumption was not true. P-value calculations were corrected with Greenhouse-Geisser approximation. The post-hoc test was estimated with a significant sign ($p<0.05$) after a mixed-design ANOVA test, and the family-wise error rate was controlled by the Tukey-Kramer test after estimating homogeneity of variances. To explore the role of brain functional network reorganization as potential mechanisms of recovery, we calculated the two global parameters "characteristic path length" and "global clustering coefficient" using a 30% threshold of the connectivity matrix (Bola and Sabel, 2015).

4.3.3 Between-group analysis:

There is no significant interaction effect on the occipital lobe in the alpha band.

4.3.4 Within-group analysis

A significant main effect of strength was observed in the ACDC group with repeated time measures on occipital_sup (O1, MNI index: 49 50) of the lesioned hemisphere (F (2, 42) =5.31, p=0.009). We tested whether the assumption of sphericity was not violated (W=0.97, p=0.74). Thus, in the ACDC group, the strength of three treatment time points on occipital_ sup_LH differed significantly. Post-hoc analysis showed that FU strength on occipital_sup_LH was significantly higher than PRE (MD±SEM=0.84±0.32, p=0.044). The significant main effect of strength in SHAM group was observed with repeated time measures on occipital_mid (O2, MNI index: 51 52) of the lesioned hemisphere (F (2, 42) =4.486, p=0.017) and occipital_sup (O1, MNI index: 49 50) of lesioned hemisphere (F (2, 42) =5.31, p=0.009). The assumption of sphericity was not violated (W=0.99, p=0.98 and W=0.97, p=0.74, respectively). This shows that if we only consider the sham group's treatment, the strength of three-time points on occipital_mid_LH, and occipital_sup_LH significantly differed. Post-hoc analysis showed that the node strength of occipital_mid_LHafter SHAM treatment was significantly higher than before treatment (MD±SEM=1.01±0.42, p=0.050) and follow-up (MD±SEM=1.35±0.39 p=0.007). Moreover, the occipital_sup_LH node strength after SHAM treatment was also observed to be significantly lower than follow-up (MD±SEM=1.30±0.41, p=0.011) (see Fig. 22A right part).

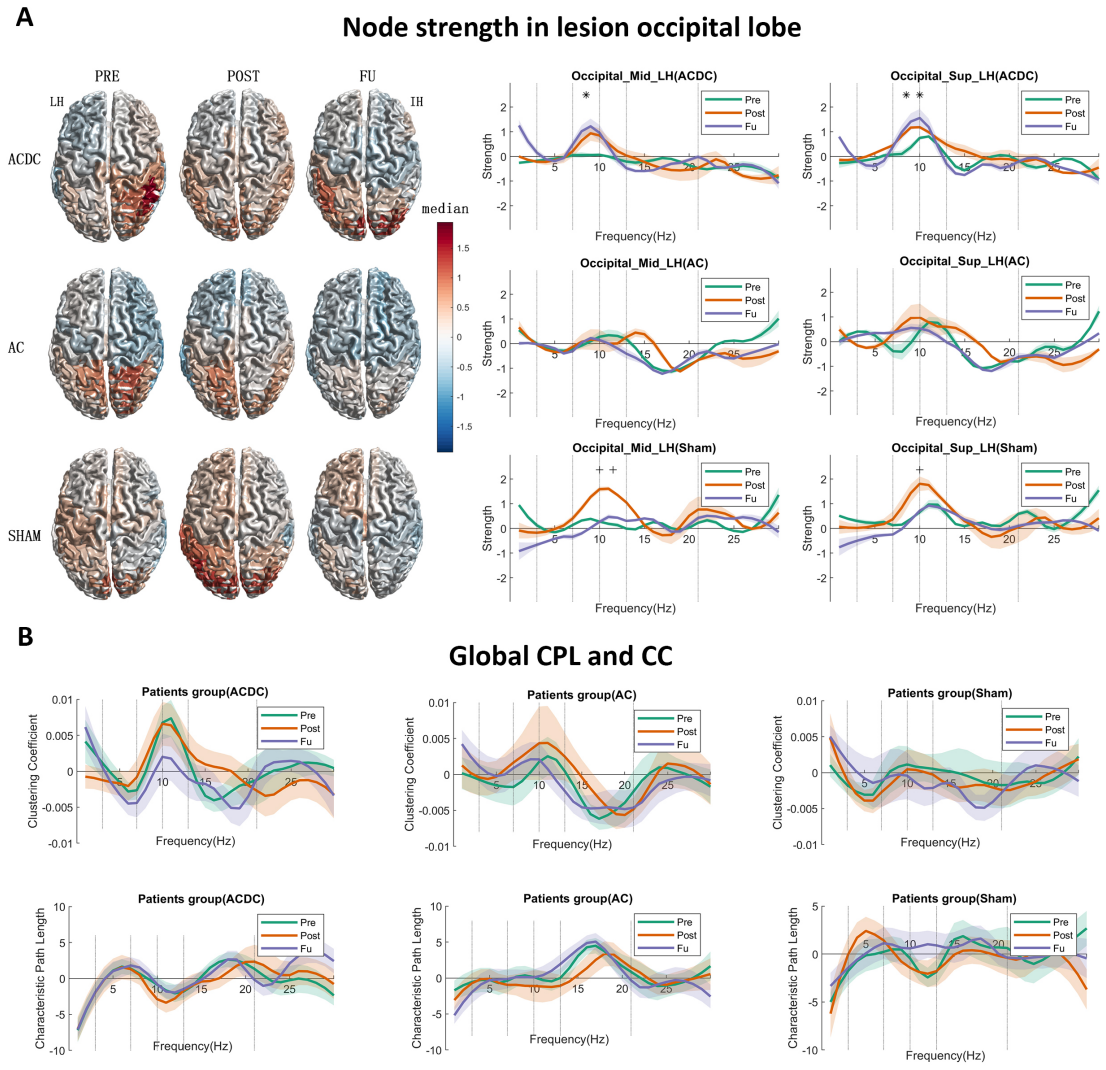

Figure 22: Part A: The left side displays the surface plot of the median node strength per group in the alpha band. Baseline (PRE): ACDC and AC group have stronger connectivity than the SHAM group in the intact hemisphere (Parietal and Occipital). After treatment (POST): ACDC and AC have lower node strength than the SHAM group (Parietal and Occipital). Follow-up (FU): ACDC has stronger connectivity than the AC and SHAM group. Right part: Line plot of the single occipital lobe from 1-30Hz with control baseline corrected. In ACDC, the middle and superior occipital region have greater strength at POST and FU than PRE ($p<0.05$). Meanwhile, the AC group shows a similar pattern for a three-time point ($p>0.05$) in the above two ROIs. The SHAM group's node strength was significantly enhanced after treatment and then dropped to the original level. Part B: this shows the global Clustering Coefficient and Characteristic path length for three groups. The ACDC group had decreased CC at follow-up, indicating that information transfer in the whole brain needed to pass fewer nodes than baseline (i.e., it is more efficient. Here, the connections are more ordered or less diffuse. No significance was observed in the other groups.

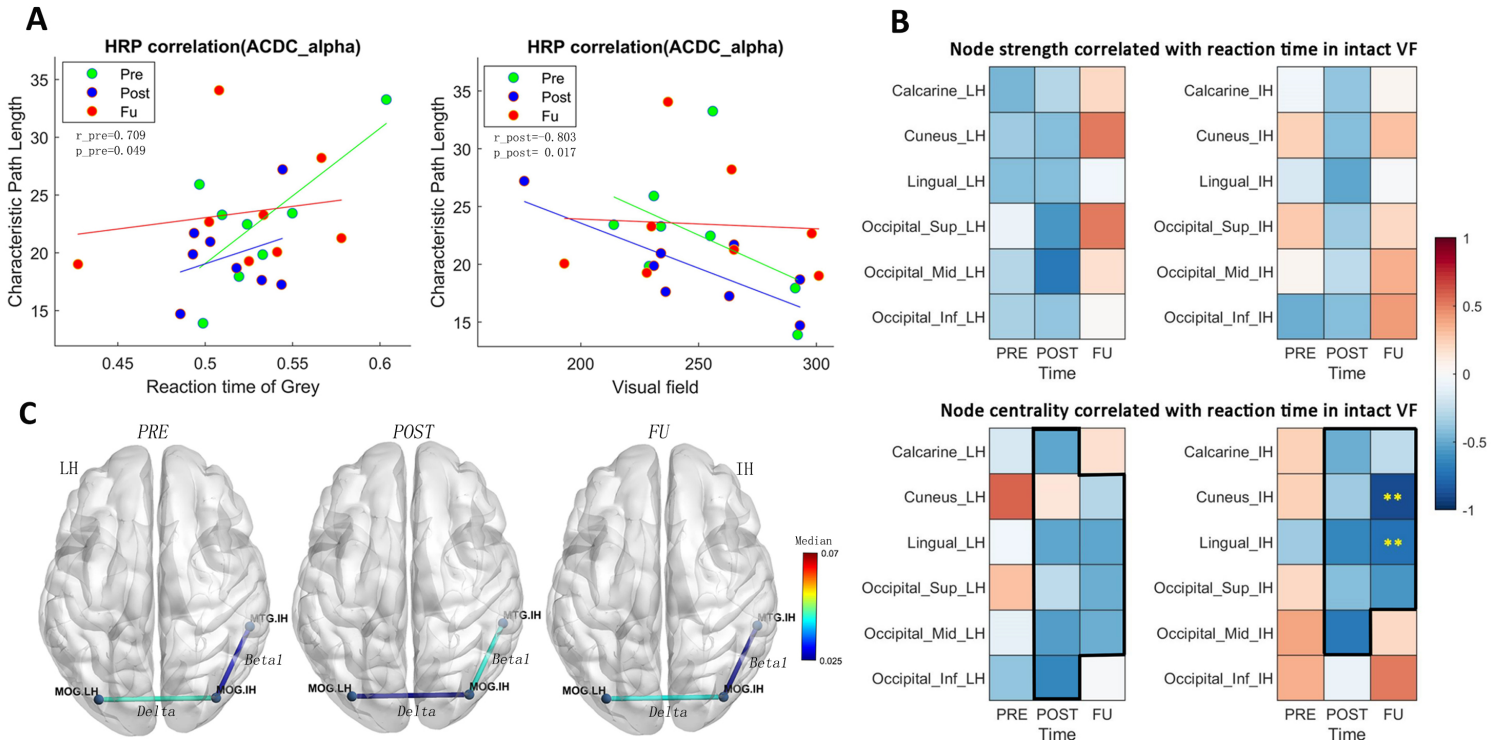

Figure 23: PartA: CPL in the alpha band of ACDC patients correlates positively with RT of residual visual area before treatment and correlates negatively with the intact visual field after treatment. It indicates that the larger the intact visual field in the ACDC group after treatment, the lower is the the CPL in the ACDC group in the alpha band. A lower CPL is a sign of decreased average shortest path length for in the resting-state of brain functionality. When neural processing in the brain has a lower CPL, this can be interpreted as a biomarker that brain process is globally enhanced, more efficient. Part B: Heat map showing correlation coefficients (ranging from -1 to +1) between brain node measures and reaction time in the intact VF of the ACDC group. The upper panel shows a trend of a treatment effect in the intact hemisphere (IH) and the lesioned hemisphere (LH) in both hemispheres; the lower panel shows a clear pattern after treatment: at follow-up, faster reaction time was associated with higher brain node centrality. Significant negative correlation was observed in Cuneus and Lingual in the intact hemisphere. This could indicate that the visual function recovery after brain stimulation could be due to the multi-factor integration of the lesioned and the intact hemisphere. Part C: ACDC significantly reduced the long coherence between the lesion and intact occipital cortex in the delta band after POST ($p<0.05$). Also, low beta was enhanced after POST between the intact occipital and intact temporal ($p<0.05$). Each connectivity was measured between LH and IH Occipital lobe, LH: Lesion Hemisphere, IH: Intact Hemisphere. MTG: Temporal_Mid; MOG: Occipital_Mid. LO: Lesion $\text{Occipital}_{M}idlobe$; $IO : IntactOccipital_{M}idlobe, IT : IntactTemporal\_Midlobe$.

4.3.5 Global small world networks

According to graph theory, a network structure can be characterized by two opposing poles: a high cluster coefficient with a long path length (an "ordered" network) on the one hand and low clustering with a short path length (a "random" network). If the network is between those two poles attributed, it has a proper balance between "stability" and "efficiency." Then it is called a small-world network. Patterns of anatomical connectivity in neuronal networks are sometimes characterized by high clustering and a small path length (Watts and Strogatz, 1998). We calculate the global CPL and CC using the 30% threshold of connectivity matrix as a criterion for three treatment groups to identify the small world network dynamic changes. Using these network parameters, we performed a two-way 3 (Group: ACDC, AC, and Sham) x 3 (Time: Pre, Post, and Fu) mixed-design ANOVA with repeated measurements on the time variable. The compound symmetry assumption was checked before statistics were performed. The regular p-value calculations in the repeated measures were reported if the theoretical distribution of the response variables had the same variance provided the compound symmetry assumption was not violated; p-value calculations were corrected with Greenhouse-Geisser approximation and the posthoc test was estimated with a significant level of $p<0.05$ after a mixed-design ANOVA test. The family-wise error rate was controlled by the Tukey-Kramer test following estimation of the homogeneity of variances. No significance was observed for the global CPL and CC (see Fig. 22B). However, a trend was noted in that the global CC of ACDC was decreased in FU while the global CPL remained at the same level as before, a clear sign of a more efficient small-worldness network after ACDC treatment.

4.3.6 Correlation between brain network measure and reaction time (RT)

The functional meaning of the network dynamics can be explored with correlation analyses. We found a negative correlation between the intact visual field and characteristic path length (global CPL), which was significantly different at POST ($r=-0.80$, $p=0.017$) in the ACDC group (See Fig. 23A), this indicates that a larger visual field is associated with lower characteristic path length after treatment. Furthermore, a positive correlation was observed between reaction time in areas of residual vision and characteristic path length at PRE ($r=0.70$, $p=0.049$), suggesting that slower reaction time of the residual visual field was associated with higher characteristic path length. The correlation between brain network measure at sub-regions of occipital lobe and reaction time in intact VF shows a trend of a treatment effect as well. Node strength correlated negatively with both the intact and the lesioned hemisphere (See Fig. 23B), indicating that better visual function is supported by higher node strength in the brain. As for centrality, which is a measure to quantify how many shortest path length go through one node, the results show that after treatment and follow-up, that better visual function is supported by a state where the brain has a higher capacity to compensate spontaneously.

The centrality of Cuneus ($r=-0.88$, $p\leq0.01$) and Lingual ($r=-0.73$, $p\leq0.01$) in the intact hemisphere were significantly correlated with the reaction time (See Fig. 23B), demonstrating that ACDC may have long-lasting modulation effect than the other two groups (see follow-up). Thus, ACDC enhances both hemisphere's brain connectivity, and we could especially assume that the 'silent' neuron was reactivated. More functional connectivity could be rescheduled and transferred around the lesion part.

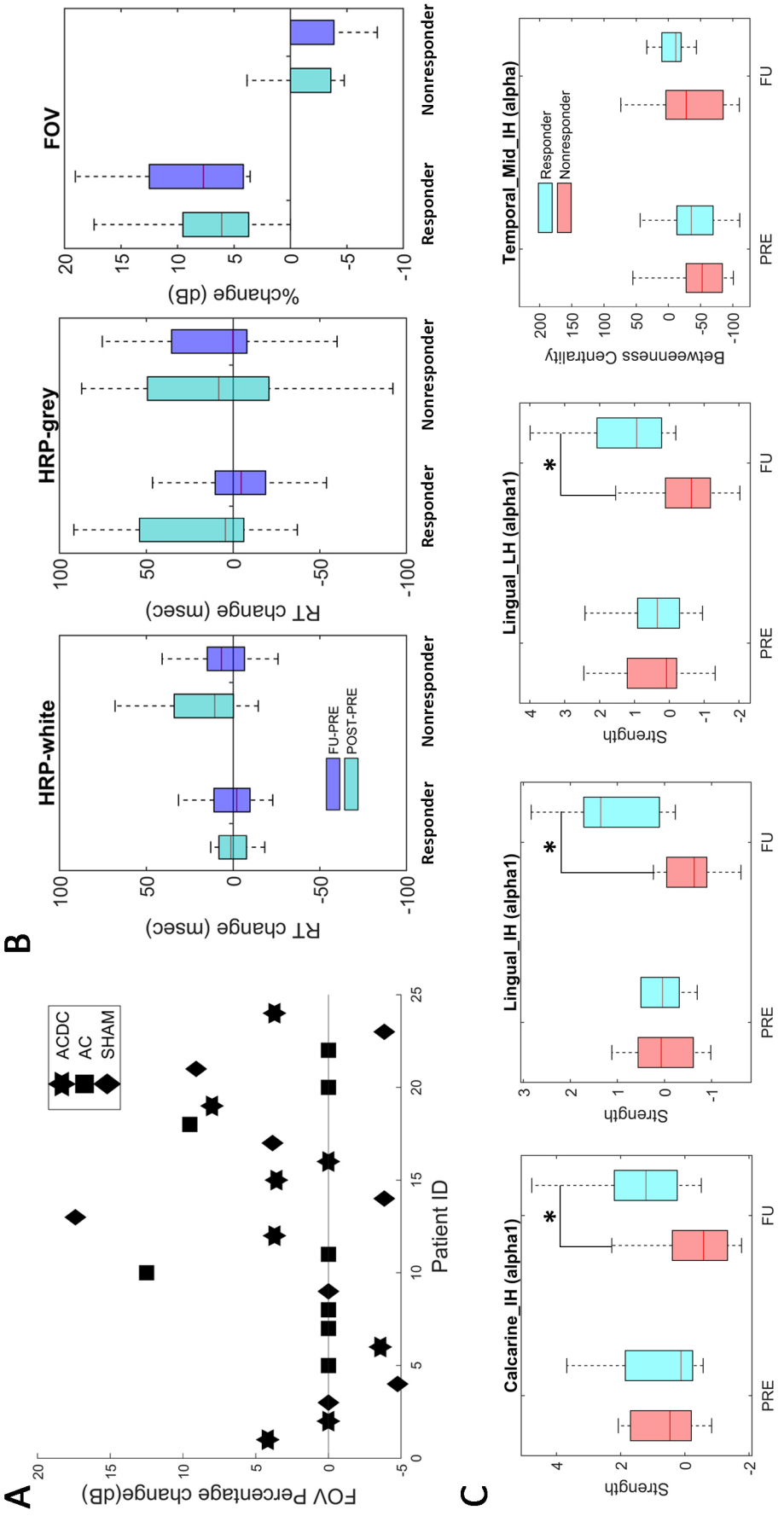

Figure 24: Part A: percentage change of FOV per group for responders with values above zero (n=10) and non-responders (n=14). Part B, boxplot of absolute median change (HRP) and percentage of FOV (Unit: dB) in responder and non-responders. Both groups had comparable reaction times (RT), but (per definition) the percentage change of FOV shows the responders was significantly higher (z=4.17, $p<0.001$). Part C: The local node strength in the low alpha band was significantly enhanced in responders in Calcarine and Lingual areas of both hemispheres (* $p<0.05$). The FU centrality of Temporal_Mid_IH was higher than the PRE ($p>0.05$).

4.3.7 Global brain connectivity

The connections coherence from lesion occipital and intact occipital to other brain regions were calculated, as shown in Fig. 23C. A two-way mixed-designed ANOVA test was conducted on brain network measures between Group (ACDC, AC, Sham) and Time (before treatment: PRE, after treatment: POST, and follow-up: FU). The post-hoc analysis has been performed for the pairwise comparison with a significant sign ($p<0.05$), the family-wise error rate (FWER) was adjusted. A significant coherence was observed between the lesioned occipital (LH) and the intact occipital (IH) region in three measurements ($F(2, 42) = 6.509$, $p = 0.003$), and the neural correlation in the delta band was significantly declined between the lesion occipital and intact occipital lobe after ACDC. Post-hoc analysis indicates that coherence after POST was lower than the PRE (MD $\pm$SEM=-0.014 $\pm$0.005, p=0.036), with a trend at FU (MD =-0.016 $\pm$0.007, p=0.069). A significant coherence was also observed between intact occipital (IO) and intact temporal (IT) in three measurements ($F(2, 42) = 6.16$, $p = 0.004$). The coherence between IO and IT was enhanced after POST and significantly declined at follow-up in the ACDC group in the low beta band. Post-hoc analysis indicates that the coherence of FU was lower than at POST (MD $\pm$SEM=-0.017$\pm$0.006, p=0.018). And there was a trend of coherence enhancement after POST when compared with PRE treatment (MD $\pm$SEM=-0.018 $\pm$0.007, p=0.054).

4.3.8 Responder and non-responder

To further clarify the role of brain FCN reorganization in vision recovery and validate the meaning of our correlation results, we compared responders and non-responders. To this end, we used the contralateral visual field as obtained by standard Oculus perimetry as a criterion to classify each patient as either a responder or non-responder, irrespective of which treatment they received.

As shown in Fig. 24A, patients above the zero-line were considered responders (n=10) and all others non-responders (n=14). We performed a two-way ANOVA test (group: responder and non-responder, time: POST vs. PRE, FU vs. PRE) to investigate HRP changes which were not, but the Mann-Whitney U-test revealed that the FOV was greater in the responders (z=4.17, p<0.001) at Fig. 24B (Right part). Of note: this difference was the result of the definition of responder and confirmed that both groups are, in fact, different. It does not demonstrate treatment efficacy.

4.3.9 Local brain network measure dynamics change

To investigate the local node strength and centrality changes in responder and non-responder groups. We performed a two-way repeated measure ANOVA test (Groups: responder and non-responder, time: baseline and Follow up).

Both the node strength on Calcarine ($F(1, 22) = 6.42$, $p = 0.018$) and lingual lobes ($F(1, 22) = 7.38$, $p = 0.012$) of lesion hemisphere in low alpha band were observed significantly between the responder and non-responder group during Follow up. The post hoc result shows the node strength both in Calcarine (MD $\pm$SEM =-1.56$\pm$0.57, p=0.013) and lingual (MD$\pm$SEM = -1.68 $\pm$0.49, p=0.002) of lesion hemisphere in responder group are higher than the non-responder group, see Fig. 24B.

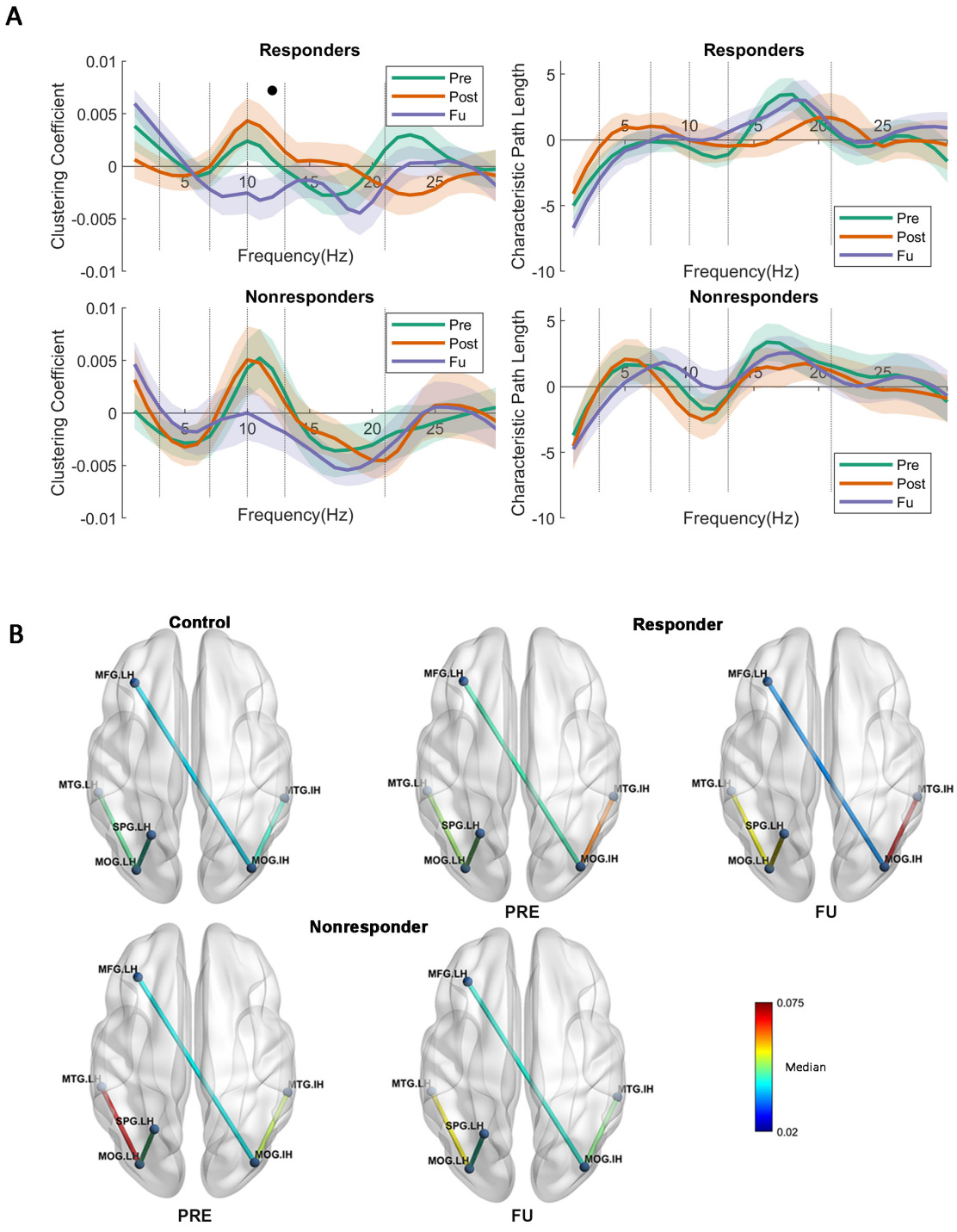

Figure 25: Part A: Global clustering coefficient and characteristic path length show no interaction or main effect for characteristics path length (two groups*three-time points). But a main effect was observed in the responders when comparing FU and POST, namely a lower clustering coefficient. Part B: the global coherence. From B, we could see the strength of the intact middle occipital increased while the centrality decreased, which is very interesting, considering C, we may suggest that intact middle occipital get rid of redundant connections from various regions but enhanced the connection with intact temporal, as the temporal could help the vision loss patient to handle the daily perception or movement identification. The long coherence between lesion frontal and intact occipital was observed significantly reduced at FU, the coherence was lower than the in PRE in the alpha band. The coherence between the lesion temporal and lesion occipital was significantly changed, both the responder and non-responders show higher coherence than the control subject.

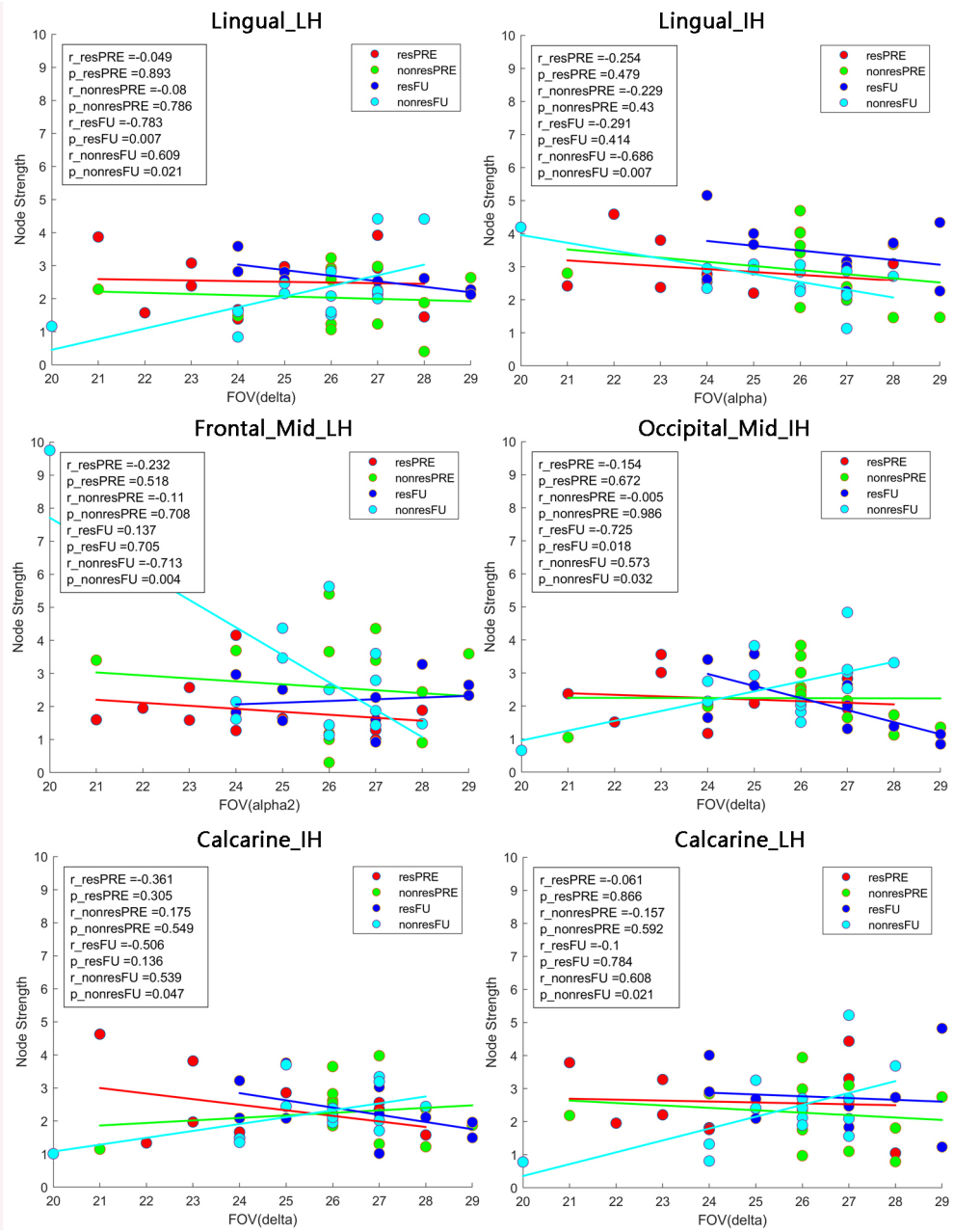

Figure 26: Pearson correlation between the FOV and node strength. In non-responders, we observed a positive correlation between FOV and node strength in the lingual_LH and Calcarine_LH in the Delta band. In the alpha band, node strength of both the lingual_lH and middle frontal_LH was negatively correlated with FOV. resFU: Responders at FU; nonresFU: non-Responders at FU; resPRE: Responders at baseline; nonresPRE: Non-Responders at baseline.

Both the node strength on Calcarine (F (1, 22) = 9.60, p= 0.005) and lingual lobes (F (1, 22) = 5.76, p= 0.025) of intact hemisphere in low alpha band were also observed significantly between the responder and non-responder group during Follow up. The post hoc result shows the node strength both in Calcarine (MD ±SEM = -1.56±0.65, p=0.026) and lingual (MD±SEM = -1.503±0.427, p=0.002) of intact hemisphere in responder group are higher than the non-responder group.

No significant was observed for brain network measure centrality. However, the centrality of intact middle occipital at FU was lower than PRE in the responder group (p=0.32, MD=-44).

4.3.10 Global network measures for responder and non-responder

Global network features are those that describe the state of the whole brain, irrespective of region. We first calculated the global clustering coefficient and global character path length, followed by two-way repeated ANOVA (two groups × three-time points). The p-value was corrected by the Tukey test in post-hoc analysis. The only significant finding was that global CC in FU was significantly lower than the POST (MD ±SEM =-0.0068±0.0027, p=0.05) in the high alpha band (Fig. 25A). This suggests that responders need fewer connections to handle the neuronal synchronization in the resting state.

4.3.11 Global coherence for responder and non-responder

To investigate the long coherence fluctuation irrespective of the stimulation protocols, a two-way repeated measure ANOVA was performed (three groups: control, responder, and non-responder, and two-time points: PRE and FU). The p-value was adjusted for multiple comparisons by the Tukey-Kramer test for post-hoc analysis. A main effect on coherence was observed between intact occipital and lesion frontal in the alpha band (F (1, 45) = 4.032, p=0.05) (Fig. 25B). The FU coherence between the occipital_IH and frontal_LH was significantly lower than baseline in responders (MD± SEM = 0.0069± 0.003, p=0.025). And an interaction effect was observed when investigating the difference between the control and responders during FU (F (2, 45) = 4.04, p=0.024) in the alpha band. Furthermore, at FU, the coherence between the occipital_IH and temporal_IH was significantly higher in non-responders when compared to controls (MD ±SEM = 0.0140±0.0053, p=0.030).

4.3.12 Correlation between FOV and brain network measures

Pearson correlations were calculated to investigate the relationship between visual functionality measurements (FOV: see Fig. 26 and HRP: see Fig. 27) and node strength. We observed significant correlations both in the Lingual_LH (r_resFU=-0.783, p=0.007) and middle occipital_IH (r_resFU=-0.725, p=0.018), where responders with higher FOV showed lower node strength in the delta band, and higher node strength in non-responders in Lingual_LH (r_resFU=0.609, p=0.021) and Middle Occipital_IH (r_resFU=0.573, p=0.032). This suggests that in both hemispheres, responders with higher FOV have lower delta band strength while non-responders have higher delta band strength. The same delta band pattern was also noted in both hemisphere of Calcarine (Lesion hemisphere: r_nonresFU=0.608, p_nonresFU=0.023, Intact hemisphere: r_nonresFU=0.539, p_nonresFU=0.047) in non-

responders. Delta band node strength was positively correlated with FOV in non-responders. This may be one possible reason why non-responders failed to improve their vision because of the delta band oscillation in the visual cortex. High alpha-band node strength correlated significantly with FOV in Lingual_IH (r_nonresFU=-0.686, p=0.004) and middle frontal_LH (r_nonresFU=-0.686, p=0.007) in non-responders. This indicates that alpha-band node strength decreases with higher FOV measures in non-responders.

4.4 Discussion

We used graph theory to analyze the local and global brain network changes after non-invasive brain stimulation for patients with vision loss caused by stroke. The study aimed to find an evidence-based stimulation protocol for clinical use concerning stroke rehabilitation after brain damage. This was the first study to modulate the brain networks with non-invasive brain stimulation for unilateral occipital stroke patients suffering persistent visual field loss.

4.4.1 Behavior performance

Regarding behavior performance, visual field parameters (FOV and HRP) are considered equally important and constitute the primary outcome measures. The ACDC group patients showed a significant percentage improvement over baseline of FOV and faster reaction times, indicating enhanced visual functions. In contrast, AC and SHAM patients at POST and FU showed a slower reaction time and no change over the baseline of the FOV. But the combined tACS and tDCS enhanced visual performance compared to baseline, which was not observed in the other two groups. The output of observable behavior performance enhancement of visual functions was to be ACDC >AC >SHAM. Because only the ACDC had improved visual performance, this raises the question as to possible brain FCN reorganization in this group.

4.4.2 Local and global network alteration after NIBS

Neuroplasticity is a critical factor in many neurological or neuropsychiatric diseases (Lefaucheur et al., 2017) and modifying cortical activities by NIBS might be a promising therapeutic approach for clinical application (Bland and Sale, 2019). For example, tDCS shifts the suprathreshold of the resting state membrane potentials toward depolarization or hyperpolarization (Gorman, 1966). Another approach is tACS, which entrains the neural oscillation in a frequency and phase-specific manner (Ali et al., 2013) and arouses the endogenous network coupling or decoupling in a long-lasting plasticity manner (Polanía et al., 2015; Reinhart and Nguyen, 2019). Vision loss in the blind is induced not only by primary tissue damage but also can be interpreted by a breakdown of synchronization in brain networks (Sabel et al., 2011b). Here, the intact hemisphere hyperactivity may be a possible mechanism of spontaneous compensation (Crofts et al., 2011; Bönstrup et al., 2018) which may – or may not – be beneficial for neuron rehabilitation. In fact, it could be a possible barrier for the recovery of the disturbed balance between both hemispheres. The above-normal hyperactivity of the intact hemisphere has the potential to inhibit the lesioned hemisphere's residual function (Corbetta et al., 2005; Oliveri et al., 1999). Lateralized anode and cathode position tDCS protocols were thought to modulate cortical

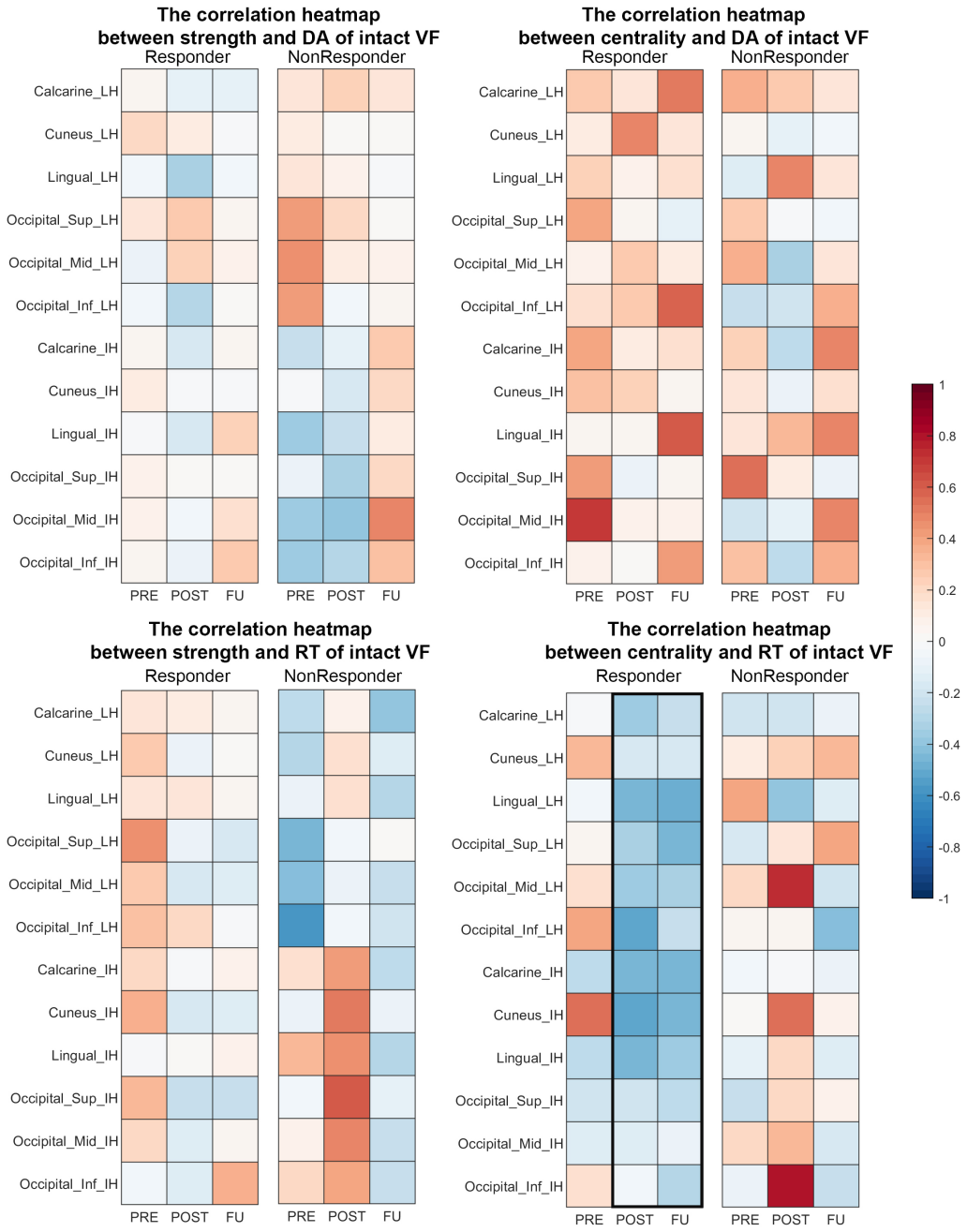

Figure 27: Correlation heat map between brain network measures (strength and centrality) and visual performance (DA: detection accuracy; RT: reaction time) in responders. At POST and FU, there was a trend that faster reaction time was associated with higher centrality in both hemispheres. DA: detection accuracy, VF: visual field, RT: reaction time.

imbalance between excitation and inhibition (Gall et al., 2015). At the same time, tACS is the leading technology that allows manipulation of phase coherence between distant brain regions (Bland and Sale, 2019). The long-lasting effects of tACS were reported in cognitive tasks (Cappelletti et al., 2013; Snowball et al., 2013; Brevet-Aeby et al., 2019; Ciechanski and Kirton, 2017; Fertonani and Miniussi, 2017). Based on the above, the active tACS electrode was positioned at Fpz to entrain intrinsic neuron oscillation with an external matched frequency (5-30Hz). This randomized and sham-controlled clinic trial was finally evaluated for persistent visual field loss recovery with a sequential approach of tDCS followed by tACS.

4.4.3 Inter-hemispheric balance after NIBS

Cortical network reorganization after an injury is a widely recognized phenomenon (Liepert et al., 2006). One study reported HH patients with damage on the left primary visual cortex who showed greater activation on other lobes in the lesion hemisphere and intact hemisphere associated with the visual cortex (Wang et al., 2010). Another study showed that bilateral SMA activation was increased after intensive rehabilitation of postural balance (Fujimoto et al., 2014). Others suggested that plastic reorganization of cognitive resources serve to compensate for impairment in stroke patients during motor rehabilitation tasks (Huo et al., 2019). However, such studies of cortical balance and recovery were not carried out with hemianopic stroke patients. In the present study, we first applied the cathodal tDCS over the intact visual hemisphere with the goal to inhibit the increased excitability caused by brain network reorganization after the stroke, which was then immediately by tACS applied on Fpz to entrain oscillations for both hemispheres. In the ACDC group, the middle and superior occipital lobe of the lesioned hemisphere had significantly higher strength in POST and FU compared to baseline and showed greater network strength in the intact middle occipital lobe. An enhancement of the lesioned hemisphere in the ACDC group was also observed in the superior occipital lobe. The strength of both the AC and sham groups fell back to slightly below the original level during follow-up. Both occipital lobes' enhanced strength could demonstrate that inter-hemispheric connections were more balanced in the ACDC group. Because this correlates with visual performance in the ACDC group. This observation is compatible with the hypothesis that post-lesion FCN plasticity reduces the imbalance between the lesioned and the intact hemisphere. As we showed, the unique protocol design of ACDC is able to modulate brain plasticity between the lesion and intact hemisphere, where the continuous stimulation can produce sustained and long-lasting neuronal modulation of the brain's neural networks. But in stroke patients, ACS alone is apparently ineffective.

The strength of Calcarine_IH increased in the ACDC group while the other two groups did not show similar patterns. The same change was also observed in the responder group. The centrality of both Calcarine_IH and Lingual_IH positively correlated with the reaction time in PRE and correlated negatively with RT both in POST and RT. This shows that the ACDC modulation enhanced the efficiency of information transfer on these two brain regions, which is associated with recovery of visual function (faster reaction time). Regarding the issue of global brain network modulation, a lower CC was only observed in the ACDC group compared to the baseline, which demonstrates that the ACDC reduces alpha-band whole-brain connections. Therefore, our interpretation is that reduced connections are a sign of greater efficiency of visual processing, where less

connectivity (greater processing efficiency) could comprise a possible mechanism of visual recovery.

4.4.4 Correlation of visually guided behavior and global network FCN measures

Characteristic path length (CPL) is the average shortest path length in the network; a lower CPL indicates fewer intermediary nodes are needed to transfer information between two unlinked nodes. In this case, the efficacy within a network is considered to be high. We found a significant positive correlation between the grey dots' reaction time and alpha band CPL in the ACDC group at baseline, which disappeared at follow-up. This suggests that vision processing after ACDC modulation needs fewer nodes, i.e., fewer steps to process neural information. On the other hand, in the ACDC group, a significant negative correlation was observed between the number of white dots in HRP and the CPL after treatment. This also suggests that ACDC decreased in the whole brain alpha band CPL, which was associated with an enlarged visual field. In contrast, CPL shows a very low negative correlation at FU. In summary, we suggest that ACDC can enhance processing efficiency in the alpha-band, a possible mechanism of vision recovery.

4.4.5 Global coherence after brain stimulation

The brain network changes in global coherence at both POST and FU show that NIBS can trigger brain plasticity by altering functional interaction between multiple brain regions. Specifically, ACDC reduced the functional connectivity between the lesion and the intact occipital lobe in the delta band and enhanced the connectivity between the intact occipital and the intact temporal lobe in the low beta band. In contrast, in the sham and ACS groups, no significant network changes were observed. Therefore, the combination of tACS and tDCS is apparently able to modulate neural plasticity by increasing the efficiency of communication between remote regions of the brain, possibly by improving inter-hemispheric balance.

4.4.6 The challenge and efficacy of Sham and AC design

The design of a proper sham condition is one of the biggest challenges in NIBS studies because NIBS can elicit cutaneous sensations that gradually disappear due to habituation, and tACS induces phosphene perception (Schutter and Hortensius, 2010). We used 5 Hz burst/min current bursts rather than "no stimulation" in the Sham tACS group. The current level was ramped up for the 30s, then stopped, and at the end of the session, ramped down for another 30s in the Sham tDCS group (Gall et al., 2015). In this way, we ensured a comparable effect and duration of cutaneous sensations for all the patients during stimulation with this unique design. However, in the sham group, the strength of temporal_mid_IH increased significantly after ten days of stimulation and return to the baseline level at follow-up. This suggests that the sham condition was not neutral but altered the strength, which might mean that the temporal lobe is sensitive to slow burst current in sham tACS, though no long-lasting effect was observed. Yet, node strength in the occipital cortex did not change after ACS.

4.4.7 Comparison of responders and non-responders

Compared to non-responders, responders had fewer grey and more white visual field sectors. This supports the hypothesis that 'areas of residual vision' (grey sectors) can be activated, improve the regions of partial vision (Sabel and Gudlin, 2014). Most patients with residual structures and functions spared by the damage have such "grey" regions where the function is neither completely lost nor normal (Sabel et al., 2018). The faster reaction time of white and grey regions demonstrates that visual processing was enhanced in responders compared to baseline. In addition, the responders had significantly higher FOV than non-responders, both after treatment and at FU. This raises how the local and global brain network compares between responders and non-responders, irrespective of their NIBS treatment.

4.4.8 Local and global network in responders

The group of responders (irrespective to which group each patient belonged) showed significantly enhanced strength in the low alpha band in the lingual and calcarine lobe of both hemispheres which non-responders did not. The lingual gyrus located between the middle of the temporal lobe and occipital lobe is relevant for complex visual processing such as object shape and contour information (Karnath et al., 2009; Schankin et al., 2020). The calcarine sulcus is mainly involved in the primary visual cortex (V1) with a role in early-stage visual processing, creating a bottom-up saliency map from visual inputs to guide the shifts of attention (Yan et al., 2018; Zhaoping and Ackermann, 2018). The strength enhancement in both hemispheres could be a sign of compensation following the occipital damage. Similarly, the strength of the middle occipital region of the intact hemisphere was enhanced. We conclude that the reorganization occurs in two hemispheres symmetrically as a consequence of the occipital lobe. The correlation between network strength and behavior performance indicates that the delta band and alpha band play a vital role in vision recovery. Possibly regions with less alpha and higher delta are less responsive to the NIBS-induced oscillations, at least with regard to behavior output.

While in the delta band of the lingual and calcarine node, non-responders had higher connection weights with higher FOV values; responders had fewer connection weights with higher FOV. Thus, delta band connectivity might play a critical role in enhancing visual functions and be a possible recovery biomarker of brain network reorganization. The same was noted in the intact middle occipital lobe, wherein responders better vision was associated with lower delta band connectivity strength of the intact middle occipital, while the non-responders had higher node strength. The pattern is consistent with the neural correlation between the intact and lesion occipital lobe in the ACDC group. Here, a lower coherence in the delta band between two occipital lobes was associated with visual field parameter improvement. Similarly, the global CC of the responder group in FU was significantly decreased in the high alpha band compared to baseline. Thus, this finding also suggests could responders (with better vision recovery) needed fewer whole-brain connections in the high alpha band.

4.4.9 The correlation between the FOV and network measures

In non-responders, greater visual acuity correlated with lower strength and FOV in the alpha band, especially at the frontal and lingual region. We also observed the neuron correlation between intact occipital and lesion frontal was deceased during in the responders. This observation is consistent with our prior studies (Bola et al., 2014) that the connection between the frontal and occipital cortex was enhanced after optic nerve damages. Thus, local and global patterns of decreased connections between the intact occipital cortex and the lesioned frontal cortex signal this a physiological correlate of vision recovery. The middle frontal lobe plays an essential role as a visual information-processing bridge that was weakened after ACDC treatment.

4.4.10 The coherence between the intact occipital and intact temporal lobe

In responders, the FU coherence between intact occipital and intact temporal was significantly higher than at baseline. It is known that the temporal lobe is responsible for handling perception and movement identification. Therefore, an enhanced connection between two lobes following NIBS suggests that the intact temporal lobe adjusts the internal information transmission state more rapidly. It may temporarily disengage connections with other less important regions, providing more support for the visual cortex to process visual motion information. The centrality of the intact temporal lobe demonstrates how much information is transferred through this area. In responders, we noticed a trend of local node enhancement in centrality and strength during FU compared with baseline and control. In responders, the centrality of Occipital_mid_IH remained unchanged compared to baseline, whereas the centrality of Temporal_mid_IH increased. Considering the global coherence enhancement between the intact occipital and intact temporal regions, we conclude that the communication between the intact occipital and temporal lobe plays a critical role in visual function enhancement. We are cautious to considering it to be due to brain stimulation. However, we assume that this kind of enhancement between intact occipital and intact temporal is adaptive for brain network reorganization after brain damage.

In summary, occipital damage, following stroke creates partial vision loss with brain network alteration in the delta and alpha band, and ACDC, but not AC alone, improves visual functions. As we showed now, brain network plasticity patterns such as interhemispheric (im) balance and the long-lasting plasticity were consistent with behavior performance in the ACDC group. This suggests that modulating brain network plasticity is a promising tool to induce recovery of vision recovery. An analysis of responders vs. non-responders (irrespective of the treatment they received) also helped us understand NIBS effects, highlighting the role of a reduction of the coherence between the LH and IH occipital lobes in the delta band and a reduced high alpha-band coherence between the frontal and occipital; these two FCN patterns might comprise biomarkers of vision recovery and shed light on the role of coherence between intact occipital and intact temporal regions. Future experiments are needed to confirm this proposal.

4.5 Conclusion

Our exploratory clinical trial of hemianopic stroke patients showed that ACDC, but not ACS treatment, is able to induce greater hemispheric balance of brain functional connectivity networks in the alpha band, which correlates with vision recovery. In addition, ACDC decreases delta band coherence between the lesioned and intact occipital cortex and modifies the connections with other regions. A lowered global clustering coefficient observed in responders may be the physiological mechanism of vision recovery. The brain´s FCN can process visual information with fewer functional connectivities in the alpha band. Thus, brain FCN reorganization is relevant for the post-lesion response and plasticity of the damaged visual system. The results can help guide us in the development of more effective stimulation protocols for vision restoration.

5 Study 3: Interhemispheric Cortical Network Connectivity Reorganization Predicts Vision Impairment in Stroke

(This work has been published by 43rd Annual International Conference of the IEEE Engineering in Medicine and Biology Society)

5.1 Background

Stroke of the brain is a common cause of death and disability in the elderly, which is steadily increasing. Until 2013, there were almost 25.7 million stroke survivors, 6.5 million deaths from stroke worldwide (Feigin et al., 2017). About 30-50% of the stroke cases have damage to the visual pathway, leading to homonymous hemianopia (HH), in which the same half of the visual field in both eyes is lost. This visual field defect significantly decreases daily functional abilities and quality of life (Gall et al., 2010a). With secondary risks of falling, loss of the ability to read, and anxiety and depression (Ribeiro et al., 2015b).

Graph theory-based network analysis is essential in neuro-science to explore brain functional connectivity (FCN) network synchronization and reorganization after a stroke. It is typically characterized by graph parameters such as strength, which is the sum of weights of links connected to one node (Newman, 2004).

Vision loss in the blind is a result of both primary losses of neurons through tissue damage and a breakdown of synchronization in brain networks (Sabel et al., 2011a). Disturbed synchronization in patients with vision loss might aggravate the functional consequences of reduced visual input (Bola et al., 2014). Wang et al. (Wang et al., 2012) reported HH patients with left primary visual cortex damage to have less brain functional activity than healthy subjects. Another study (Guo et al., 2014) showed that the newly forming FCN connections and compensatory connections mainly originated from the infarction area and influences contralesional cortices.

Weighted graphs with thresholds are able to reveal the level of efficiency in large-scale networks analysis (Telesford et al., 2011), allows easy extraction of meaningful information (Serrano et al., 2009) compared to binary graphs. Fornito et al. (Fornito et al., 2010) reported network scaling effects in human resting-state fMRI under the proportional thresholds from 5% to 40%. Buckner et al. (Buckner et al., 2009) reported the hubs for adaptive task control at the proportional thresholds from 2% to 10%. Heuvel et al. (van den Heuvel et al., 2009) reported the efficiency of functional brain networks and intellectual performance from a correlation coefficient of r=0.3 to 0.5. In all these studies, the authors used a relatively narrow range of network density, and this could be a limitation with risks of inadequate or faulty interpretations. Previous graph theory studies on HH (Wang et al., 2012; Guo et al., 2014) used scalp electrode connections without considering the network density; the stability of such patterns is still unknown. Therefore, in the present study, we characterized the cortex level's brain functional network dynamics in HH patients after a stroke, using multiscale proportional threshold-based densities for brain connectivity matrix.

Stroke biomarkers could provide a diagnostic inference for effective personalized therapy in stroke patients. Several researchers have proposed various prediction biomarkers such as fluid and tissue analysis for stroke prevention (Kim et al., 2013; Jickling and Sharp, 2015). Others utilized the brain functional network to predict the impairments in stroke with deep learning technology (Lindow et al., 2016; Jiang et al., 2013; Siegel et al., 2016). Therefore, we evaluated the potential for predicting functional loss in patients with stroke using deep learning technology through the brain network. There are many and highly sophisticated deep learning methods in the market; however, deep learning requires

high computation power and colossal data size, limiting its application in brain science. Especially the use of small amounts of high-dimensional data is still facing significant challenges.

LSTM (Long Short-Term Memory) (Huang et al., 2015) was a particular type of recurrent neural network (RNN) (Hochreiter and Schmidhuber, 1997) that is often used to model contextual information in natural language processing tasks. However, RNN models feed the data into the network only in a one-directional manner. In the present study of stroke patients, we consider both internal connections and external isolation between the lesion and intact hemisphere of the brain to evaluate if the Bi- LSTM can capture a better network feature presentation in bi-directional learning from both hemispheres.

We hypothesize that the Bi-LSTM can learn brain network patterns by paying specified attention to the FCN state of the lesioned and the intact hemisphere. We, therefore, implemented the Bi-LSTM model along with other traditional algorithms on the multiscale brain functional connectivity matrix to reveal brain network alteration patterns in occipital stroke patients.

Specifically, we addressed the following two questions: (i) how does the frequency band and the density of the brain connectivity matrix influence the performance of the deep neural network for predicting stroke patients; and (ii) how does the predictive performance of the model fit the characteristics of electrophysiological data using the statistics and visualization of the FCN-"strength" changes in the middle occipital node.

5.2 Method

5.2.1 Subject

We recruited 24 Patients with partial vision loss as a result of occipital stroke (see more detail (Gall et al., 2015)) and 24 age-matched healthy subjects with normal vision or corrected to normal vision. All subjects were instructed to keep their eyes closed while resting-state EEG was recorded for the duration of five minutes (Table 4). Patient and control subjects were statistically comparable in age ($p>0.05$). High dense array EEG was recorded using a HydroCell GSN 128 channel net (EGI Inc.). The ethics committee of the University of Magdeburg approved the study in compliance with the declaration of Helsinki. All subjects were asked to sign a consent form. See Chapter 3 for more detail.

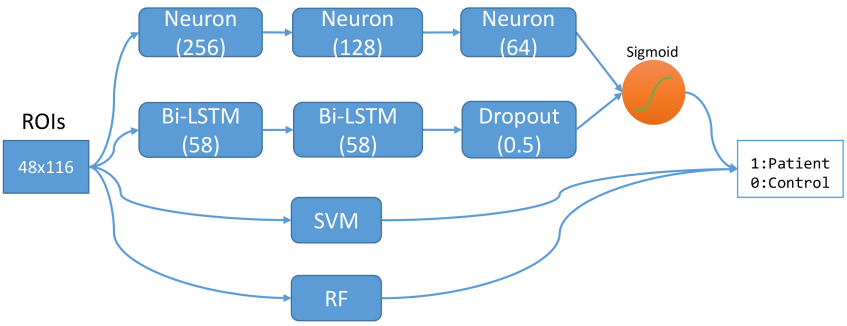

Figure 28: We evaluated a two-layer Bidirectional LSTM (neurons: 58, 58) algorithm and compared it with other traditional algorithms such as deep forward neural network architecture with three hidden layers (neurons: 256, 128, 32), support vector machine (SVM), and random forest (RF). Data input shape (1×116) from AAL atlas. Output label was 1: patient and 0: control subject.

Table 4: Patient information summary

	Total	Lesion side	Age	Lesion Months
Patient	24	10 left, 14 right	58.375±10.87	40.95±39.21
Control	24	NA	57.375±10.56	NA

5.2.2 Data prepossessing

A digital 1-145 Hz bandpass filter was applied as well as a 50 Hz notch filter. The data was down-sampled to 250 Hz and then referenced by the common average reference method. EEG recordings were segmented into 2 seconds long per epoch. Components of eye-blinks and cardiac activity were removed by independent component analysis (ICA). The signal was decomposed as six frequency bands: Delta (1-3Hz), Theta (4-7Hz), Alpha1 (8-10Hz), Alpha2 (11-13Hz), Beta1 (14-21Hz), Beta2 (22-30Hz). see Chapter.3 for more detail

5.2.3 Source reconstruction

The forward model was calculated using the symmetric boundary element method (BEM) (Fuchs et al., 2001). The inverse model was calculated with a beamforming method using the partial canonical correlation method (Rao, 1969), which implements Dynamical Imaging of Coherent Sources (DICS) (Gross et al., 2001). The default template for MRI was from MNI (Colin 27) at 8mm resolution (Holmes and Hoge.etc, 1998). The AAL-VOIs atlas (AAL) is an automatic anatomical labeling result (Tzourio-Mazoyer and Landeau, 2002), which includes 120 structure definitions, and 116 were used in this study. See Chapter 3 for more detail.

5.2.4 Brain connectivity and threshold

Functional connectivity was based on the statistical synchronization to quantify the interaction between different brain region pairs (Pereda et al., 2005). Here we used the imagery part of coherence (Nolte et al., 2004a),

Finally, the connectivity matrix (116×116) was sparsed from density 0.1 to 1 per frequency band for patients and controls. All self-connections were removed before analysis, which means only$[0.1 \sim 1]$ strongest weight edges were kept for each subject in both groups consistently. In this case, the density defined as the proportion of existing edges out of all possible edges was equal for each graph per subject (Bola and Sabel, 2015). Fixing the probability for an edge also excludes the criteria of Erdo¨s-R´enyi random networks for group analysis (Van Wijk et al., 2010).

5.2.5 Evaluation method

A deep neural network (DNN) is an artificial neural network (ANN) with multiple layers between the input and output layers (Bengio, 2009). The hidden layer and activation functions can improve expressive ability. In this paper, we implemented a two hidden layer (58, 58) Bi-LSTM model and three hidden layers (256, 128, 32) deep forward network to predict the vision impairment stroke patients with a support vector machine(SVM) and Random forest(RF) as the baseline shown in Fig. 28, Brain node strength was calculated per frequency and density. We proposed three feature extraction methods: Model I): The

Table 5: Final peak performance of the evaluated models

	Model	Pooled Control	Flipped Patient	Accuracy	Sensitivity	Specificity
SVM	I	Yes	Yes	67%	58%	75%
	II	No	Yes	**73%**	63%	**83%**
	III	No	No	67%	54%	70%
RF	I	Yes	Yes	63%	54%	70%
	II	No	Yes	63%	58%	63%
	III	No	No	60%	63%	41%
DNN	I	Yes	Yes	**81%**	67%	**96%**
	II	No	Yes	70%	75%	67%
	III	No	No	67%	75%	58%
Bi-LSTM	I	Yes	Yes	63%	58%	67%
	II	No	Yes	**73%**	**70%**	**75%**
	III	No	No	63%	63%	63%

node strength of control subjects between the left and right hemispheres was pooled. The brain of the right stroke patient was flipped so that only the lesion hemisphere and intact hemisphere were showed. Model II): The controls were not pooled, and the patient data was flipped. Model III): The controls were not pooled, and the patient data was not flipped (see Tab 5).

5.2.6 Training the model

All training sessions were implemented in Google Colab, Sklearn, and Keras. Forty-eight subject data was shuffled before a three-folder cross-validation in the training session. For both Bi-LSTM and DNN, we took Adam as the optimizer and binary-cross entropy as the cost function. The performance was evaluated with three metrics: overall accuracy, sensitivity, and specificity. A non-parametric Mann- Whitney U-test was performed between the lesioned hemisphere and the control hemisphere and between the intact and control hemispheres. Data prepossessing, source reconstruction, and brain connectivity were conducted with the Fieldtrip toolbox (Oostenveld et al., 2011).

5.3 Result

5.3.1 Model performance

We evaluated Bi-LSTM, DNN, SVM, and RF to scout for appropriate prediction biomarkers (Frequency bands or network density), which can identify the presence of vision impairment in patients with occipital stroke. As shown in Tab 5, the DNN yielded the highest accuracy (81%) in model I; however, the sensitivity (67%) was relatively low, and the specificity was significantly higher (96%). This demonstrates that pooling the left and right hemispheres for the controls may lead to an over-fitting in testing data. The same phenomenon appeared in SVM performance. The Bi-LSTM shows a balanced performance between sensitivity (70%) and specificity (75%) with an overall accuracy of 73% in model II, suggesting that flipping the hemisphere could enhance the feature patterns learning during training. As shown in Fig. 30, the log loss of model II shows the Bi-LSTM demonstrated the ability to learn the feature patterns and continuously reduce losses. For RF, the result is not satisfied as expected.

Figure 29: The plot shows the low and high alpha band strength distribution from density. 0.1 to 1 in the middle occipital lobe. This dynamic change of network properties shows that the reorganization of the brain after the damage is mainly based on the formation of massive weak connections in the high alpha band. In contrast, the low alpha band did not show huge links. SVM learned feature patterns in the high alpha band from the evaluation models. Bi-LSTM learned the low alpha feature patterns and achieved a balanced performance between sensitivity and specificity.

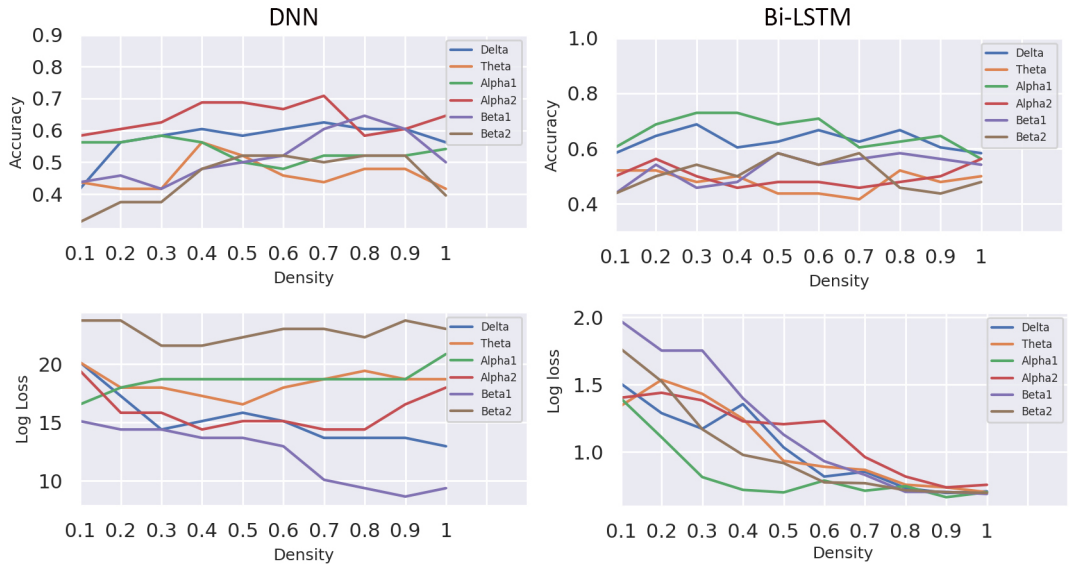

Figure 30: Compared to the Bi-LSTM, the DNN shows a slice better performance in model I in the high alpha band. However, here the log loss is relatively stable and higher than the Bi-LSTM. Bi-LSTM shows a balanced performance between sensitivity (70%) and specificity (75%), with an overall accuracy of 73% in model II in the low alpha band. Eliminating the structure influence of individual algorithms, the result suggests that flipping the patient's hemisphere could enhance the feature pattern learning, while the controls should not be pooled.

5.3.2 Biomarker in Brain network

Stroke biomarkers can be used as a guiding tool for more effective personalized therapy (Kim et al., 2013), and help improve the diagnosis of stroke and determine the cause of stroke (Jickling and Sharp, 2015). Unlike the traditional approach, we aimed to find the characteristics representing the network reorganization after a stroke with a bi-directional LSTM algorithm. This algorithm has been used for natural language processing for a long time. Here, we explored the two-directional feature learning efficiency from intact and lesion hemispheres. As shown in Fig. 30, the peak accuracy was achieved in the low alpha band from density 0.3 to 0.5 with Bi-LSTM. The result is compatible with the hypothesis that brain network reorganization in the low alpha band after a stroke can help to identify occipital stroke patients. Therefore, the network threshold should be taken into account for brain network analysis or biomarkers prediction in neurological disease.

In our patients, the middle occipital lobe area is most affected by ischemic stroke (Posterior cerebral artery infarcts). To further confirm the patterns from the network characteristics, we specifically selected the middle occipital lobe for further statistical analysis. As shown in Fig. 31, the strength of the alpha band in both lesion and intact hemisphere was found significantly lower than in controls for a density >0.3, which is consistent with our prediction result.

5.4 Discussion

A correct diagnosis of ischemic stroke and its causes are essential to treat and prevent stroke (Jickling and Sharp, 2015). While MRI images used in the clinic to identify the lesion location are structurally meaningful, they provide no information about the functional state of the tissue at or around the lesion site (locally) or in other brain regions

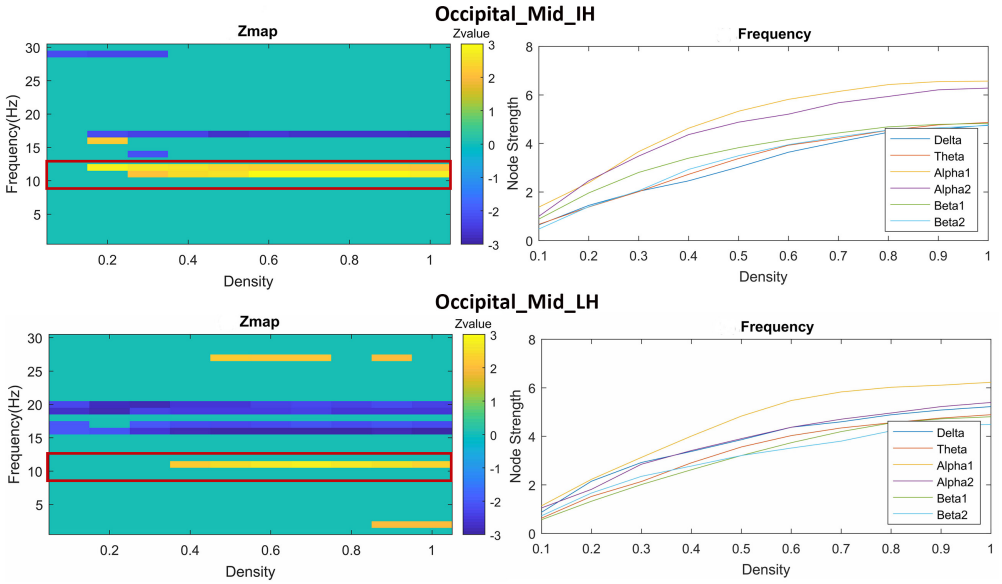

Figure 31: Left part: Z-value distribution between the lesion /intact hemisphere and the control hemisphere at the middle occipital lobe. Significant patterns show that both intact hemispheres have higher strength in the alpha band (8-12 Hz) than controls when selecting a density>0.3 (red-box). The strength in the low beta band (13-21) of both lesion and intact hemisphere was lower than the controls. Right part: the high alpha band strength of intact hemisphere was higher than the lesion hemisphere.

(globally). This can only be achieved with EEG recordings that provide electrophysiological information about the activity of neurons and their interactions. Therefore, assessing brain network reorganization in a quantitative manner offers a new "functional" dimension to characterize brain damage and recovery. Traditional biomarkers such as blood, other body fluids, or tissues have been proposed to predict neurological disease states physiologically (Kim et al., 2013). In contrast, the present study aimed to find a 'biomarker' based on a multiscale brain network and deep neural network. We evaluated the pattern learning efficiency of Bi-LSTM with a bidirectional vector from two hemispheres. The result demonstrates that the brain node strength in the low and high alpha band could be utilized to predict functional (vision) loss in occipital stroke patients. The Bi-LSTM achieved an excellent performance that was more specific and effective than other traditional algorithms of hemisphere pattern learning. Furthermore, the result from Model II illustrates that hemisphere flattening in unilateral stroke patients and no-pooling in controls has a palpable classification performance to discriminate between visually impaired stroke patients and normal subjects.

Alpha phase synchronization is known to relate to different behavioral states and neuronal effects of visual-spatial attention (Lobier et al., 2018). With the present study, we confirmed the role of the high alpha band in visual processing because, in this frequency band, brain damage leads to reorganized FCN patterns with a more significant number of functional connections of intermediate density. Future studies should explore how this understanding of brain FCN can be used for clinical diagnostics and rehabilitation. This new perspective is consistent with our earlier findings that both low and high-alpha brain network alternation is critical in the brain network reorganization of stroke patients. Our future studies will evaluate if and how the strong connections from the lesion side can handle information processing after a stroke; and how the contralateral, "intact" functional regions might help compensate for the loss of vision.

More generally speaking, deep learning technology with optimized structures can help extract functionally relevant parameters by using FCN pattern characterization without predefined features. Bi-LSTM achieved a more balanced performance (in both accuracy and log loss) than other methods. Considering the mechanism of Bi-LSTM in natural language processing, we propose that the Bi-LSTM method is a valuable procedure for capturing brain network states of the lesion and intact hemisphere. Integration of bidirectional data input (intact vs. lesioned hemisphere) through LSTM cell can enhance the performance and stability of the model. Although the model's final performance did not reach a high accuracy rate for all models in this study, we believe that the expected results can be obtained using a more extensive data sample with Bi-LSTM. Moreover, the performance can inspire us to understand brain network reorganization after an occipital stroke in the clinical context of diagnosing vision loss and predicting its recovery potential.

5.5 Conclusion

This study evaluated the potential of predicting vision impairment in stroke patients with deep neural networks and multiscale brain networks. The prediction model and statistical analysis results show that brain node strength in the low and high alpha band under specific density could be a predictor to characterize brain network reorganization in stroke patients. Furthermore, the Bi-LSTM gained a balanced performance between sensitivity and specificity, proving its feature learning capacity for hemisphere feature extraction. Further investigation is needed to extend this algorithm with more data samples and an optimized network structure. In the future, these results may inspire others to gain more insight into stroke clinical diagnostics and interventions, and it highlights the value of Bi-LSTM in functional predictions of brain diseases.

6 Study 4: Decoding Resting-state EEG to Predict Visual Field Defect in Stroke

(This work has been published in 10th International IEEE EMBS Conference on Neural Engineering (Xu et al., 2021))

6.1 Background

Stroke is one of the leading causes of death and disability globally (Campbell, 2019). One-third of stroke patients may lose part of the visual field in both eyes called homonymous hemianopia (HH). HH is the main consequence of an occipital lobe damage (Goodwin, 2014), which can significantly negatively affect the quality of life such as walking and reading. Occipital damage will cause the vision loss or inhibition of lesion visual cortex activity, which will further affect the neural synchronization that physiologically manifests as a dynamic change in the brain network's plasticity. The relationship between neural oscillation or synchronization and visual field loss is quite promising and worth investigating. Decoding resting-state Electroencephalography (rsEEG) to predict the visual field distribution could be an essential reference for a better understanding of the compensation of visual functions after a stroke. The result could be beneficial for clinical diagnostics and treatment.

Deep learning technology has attracted lots of attention in visual field prediction based on different types of patterns of clinical data. Choi et al. (Choi and Kwon, 2016) proposed an assembled deep neural networks to enhance post-treatment ischemic stroke prognosis. Christopher et al. (Christopher et al., 2020), and Hashimoto et al. (Hashimoto et al., 2020) utilized the deep learning technology to predict the visual field damage from spectral-domain Optical Coherence Tomography in glaucoma. Park et al. (Park et al., 2019) built a visual field prediction algorithm using a recurrent neural network(RNN). Wen et al. (Wen et al., 2019) demonstrated that deep learning networks could be trained to forecast future 24-2 Humphrey Visual Fields. As mentioned above, these researchers rely on the visual field chart or Optical Coherence Tomography (OCT), not the electrophysiological data. Little is reported and known if there is a possibility of decoding the neural oscillation or synchronization to predict the status of visual field loss in HH patients after a stroke.

We propose a frequency spectrum based on 2DCNN and brain connectivity-based 3DCNN to predict the visual field defect after a unilateral occipital stroke. The visual field defect location and percentage (Black, Grey, and White area) were decoded with deep learning technology. We also explored and visualized the pattern of brain oscillation and neural synchronization in these patients.

6.2 Method

6.2.1 Subject information

Twenty-four occipital stroke patients and 24 controls were recruited; more information of the patients, such as the lesion pathology and the inclusion criteria, were previously described here (Li, 2016). High density array EEG was recorded using a HydroCell GSN 128 channel net (EGI Inc.). The ethics community of Otto-von-Guericke-University approved this study in agreement with Helsinki's declaration, and all the subjects signed their consent.

6.2.2 Data collection

Patients were randomly divided into three groups and received non-invasive brain stimulation to recover visual performance. Five minutes of resting-state EEG with eyes

closed per subject were recorded three times: before treatment, post-treatment, and follow-up. both the EEG data and high-resolution perimetry (HRP) (Kaiser et al., 1994) data were recorded for patients. The EEG data of control was collected only once, and HRP was not tested (all white) for control since HRP was binocular visual test.

6.2.3 Data preprocessing

A digital 1-145 Hz bandpass filter with a 50 Hz notch filter was used to remove the current interference. The data were down-sampled to 250 Hz. EEG recordings were segmented into 2 second-long epochs after common average reference. Eye-blinks and cardiac activity were rejected by independent component analysis (ICA) and visual checking. A 1-30Hz bandpass filter was applied. Finally, 100 clean trials for each subject per recording were kept. Finally, total trials were 9600, including the 24*3*100(patient*times*trials) and 24*1*100(controls*times*trials).

6.2.4 Feature extraction

Frequency decomposition with Fourier analysis was performed, the multitapers method was included in Fourier analysis, which allows better control of time and frequency smoothing. The frequency spectrum was averaged in the time unit since there was no task during the recording. Finally, a 128*30 spectrum matrix was generated per trial, where 128 represents the number of channels, and the 30 represents the frequency bin from 1 to 30 Hz. Here instead of the frequency band (128*4, here Delta, theta, alpha, beta band), we believe that frequency bins (128*30) could enrich the spectrum's context information.

The cross-spectral density was computed from the Fourier coefficients during the frequency decomposition to calculate the sensor level functional brain connectivity for each subject. We used the imagery part of the coherence to estimate the phase synchronization between pair channels (Nolte et al., 2004b). Finally, a 128*128*30 sensor level-based brain connectivity matrix was generated per trial. Meanwhile, the group of electrodes was selected in the location of the left occipital Lobe (LO) [E65, E66, E67, E70, E71] and right occipital lobe (RO) [E76, E77, E83, E84, E90] for feature visualization as shown in Fig. 36.

6.2.5 Label generation

To quantify the visual impairment, the visual field was evaluated in patients by HRP. In this Perimetry test, white regions show the intact visual field, and grey regions represent areas of residual vision, and black regions are considered fully blind areas. The raw HRP data was recorded as a 21*21 matrix which is too large for it may lead to poor performance and make no sense for our hypothesis; hence we reduce the size and complexity of labels with two methods: The percentage of each category per subject were regarded as the label1, which was indirect information presentation of the visual field; the label2 represented the location of the visual field in a reduced dimension HRP from 21*21 to 2*2, max-pooling was applied when decreasing the matrix dimension, only the black and white area was considered, see Fig. 33.

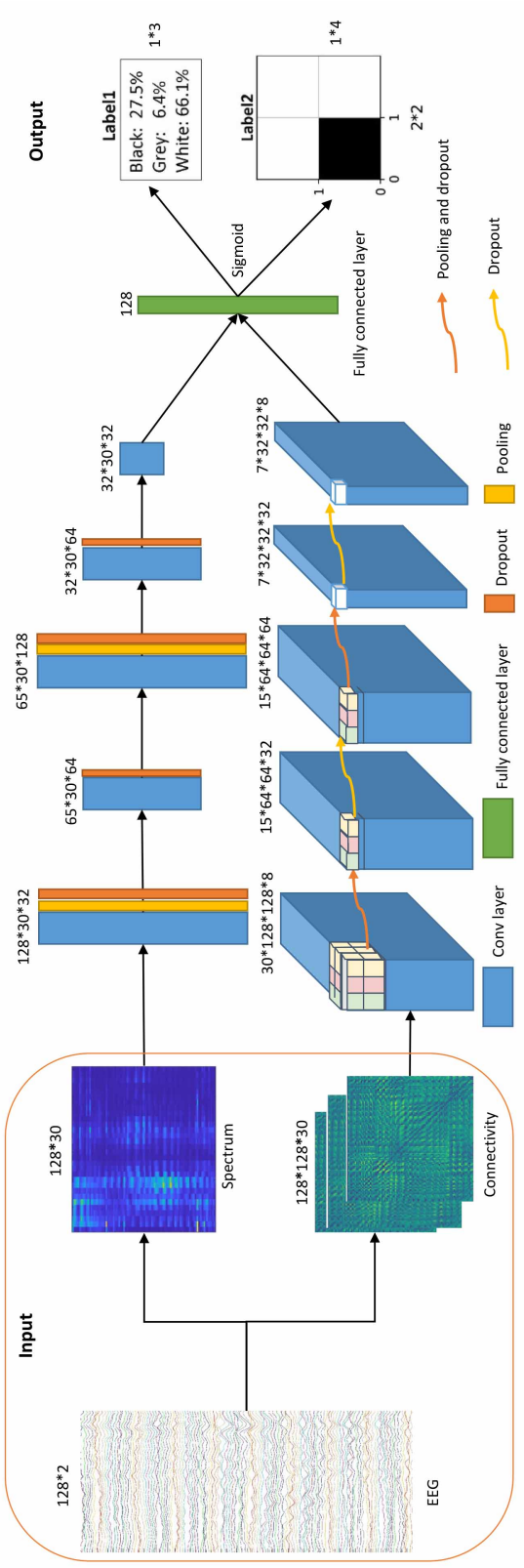

Figure 32: Proposed CNN architecture for visual field decoding. The upper one's input feature is the frequency spectrum (Channel*Frequency:128*30), The input feature of the lower one is the sensor-based brain connectivity matrix (Channel*Channel*Frequency:128*128*30). Both structures follow a five convolutional network layer with a fully connected network layer of 128 neurons, the final output with sigmoid activation function was label1 (1*3) and Label2 (1*4, binary).

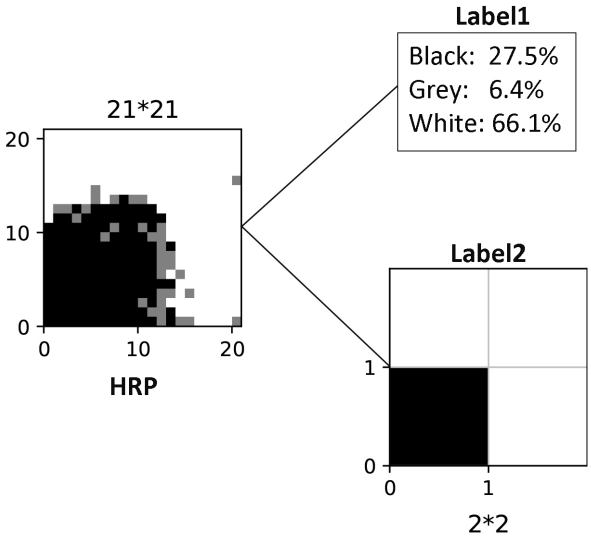

Figure 33: The original HRP was converted into two categories: percentage and location. The percentage presents the indirect information of visual field: Black, Grey, and White (1*3 vector, for example: [75%, 10%, 15%]). The location distribution presents the visual field defect location considering the mostly hemianopia patient lost their vision by the quarter as a unit (1*4 binary vector, for example: [1, 0, 0, 1], 1: black, 0:white).

6.2.6 Metrics

The percentage prediction of the visual field distribution is based on a nonlinear regression model. For this, we use MSE (Mean square error) to calculate the loss for training. R2 score is promoted to evaluate the model performance, the high peak score is 1.0, and it could be harmful if the model is unexpectedly worse. The visual field location has a binary output (in a 1*4 matrix: 1: black and 0: white), the accuracy metric was applied to evaluate the performance.

6.2.7 Proposed networks

We proposed a 5-layers CNN architecture as the network's backbone for the spectrum-based 2DCNN and connectivity-based 3DCNN model. This concave network architecture design is mainly to learn local features by reducing dimension and input this feature into the fully connected network after upsampling. The 2DCNN model for frequency domain is shown in the upper part of Fig. 32. For the connectivity domain, we use a similar model as 2DCNN but revised some details, shown in the lower part of Fig. 32, the input was marked 3D data. The size of the output layer following the fully connected network is adjusted for different labels. For example, the size is set as 3 for the percentage label and 4 for the location distribution label. Thus, each grid has a binary output(0/1).

6.2.8 Training process

We fit the model using the Adam optimizer, using default parameters described in (Kingma and Ba, 2014), minimizing the binary cross-entropy loss function in the brain connectivity domain and MSE (Mean square error) in the frequency spectrum domain. The reactivation function is the exponential linear unit (ELU). The dropout probability was set to 0.5 to prevent over-fitting when training on limited sample sizes. 5 fold cross-validation

Table 6: The performance of visual field percentage

Model	Feature	Control	Data split	Label	R2
2DCNN	Spectrum	No	Cross subjects	Percentage	<0
	Spectrum	Yes	Cross subjects	Percentage	<0
3DCNN	Connectivity	No	Cross subjects	Percentage	<0
	Connectivity	Yes	Cross subjects	Percentage	<0

(train-test spilt rate: 0.8 for training and 0.2 for test) was applied. We ran 50 training iterations (epochs) and saved the model weights, producing the lowest validation set loss. Within-subject evaluation generally uses single-person data, so it is prone to overfitting and low generalization ability. Cross-subject evaluation could help improve the trained models' generalization ability and prevent overfitting. Therefore, this study mainly reports cross-subject training performance. When performing data split, we randomly split into training and test groups based on samples instead of a single trial to ensure no training data would appear in the test part.

All models were trained on Google Colab Pro using Tensorflow and Keras. Data preprocessing and feature extraction were performed with the Fieldtrip toolbox in Matlab (Oostenveld et al.).

6.3 Results

As shown in Tab 6, the R2 score shows the model output a worse prediction performance about the percentage of the visual field. Furthermore, both frequency spectrum and brain connectivity-based R2-score are less than zero, indicating that the brain oscillation feature could not correspond with the percentage of the visual field.

From Tab 7, the frequency spectrum-based 2DCNN model achieved the best performance 67.5% with the control dataset where the brain connectivity-based 3DCNN only achieved the 60.7%. The possible explanation is that the frequency spectrum was more direct information than the brain connectivity. The form of spectrum data is suitable for feature learning in convolutional neural networks. For the spectrum model, the precision of each sub-region was [0.595 0.748 0.667 0.638]. We also evaluated the model based on the frequency band; however, they did not exceed the result as in Tab 7.

The feature map was visualized from frequency spectrum 2DCNN as in Fig. 34A, a clear pattern was observed with light color around 10 Hz; the electrode was located in the occipital and temporal lobe. The feature map from brain connectivity was visualized as shown in Fig. 34B. no clear pattern was observed in this 3DCNN model, which could be why the 3DCNN model shows worse performance than the 2DCNN model.

The topology plot of the frequency spectrum and local node weight were visualized to further investigate the patterns from frequency spectrum and brain connectivity. As shown in Fig. 35, both in the low and high alpha bands, the alpha band spectrum power of the control subject is relatively similar in both hemispheres. While, stroke patients show more activities in the contralateral visual cortex. In Fig. 36, the zero-means of LO or RO is used as a reference to show the distribution of brain node strength. However, no obvious characteristic pattern could be extracted.

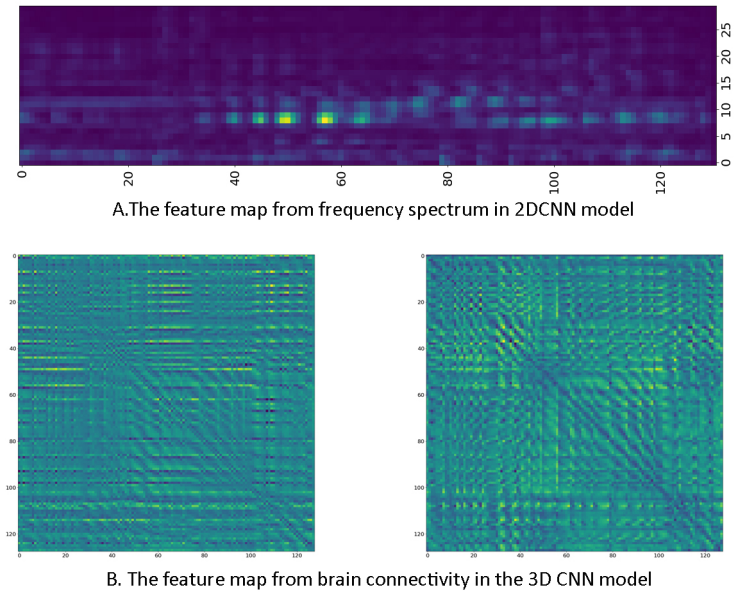

Figure 34: The feature map visualization for frequency spectrum-based model and sensor-based brain connectivity. In A, the region of interest was learned and highlighted (Occipital and temporal electrodes). In B, no clear patterns were learned from the 3DCNN model

Table 7: The performance of visual field Location

Model	Feature	Control	Data split	Label	Acc
2DCNN	Spectrum	No	Cross subjects	Location	0.639
	Spectrum	Yes	Cross subjects	Location	0.675
3DCNN	Connectivity	No	Cross subjects	Location	0.578
	Connectivity	Yes	Cross subjects	Location	0.607

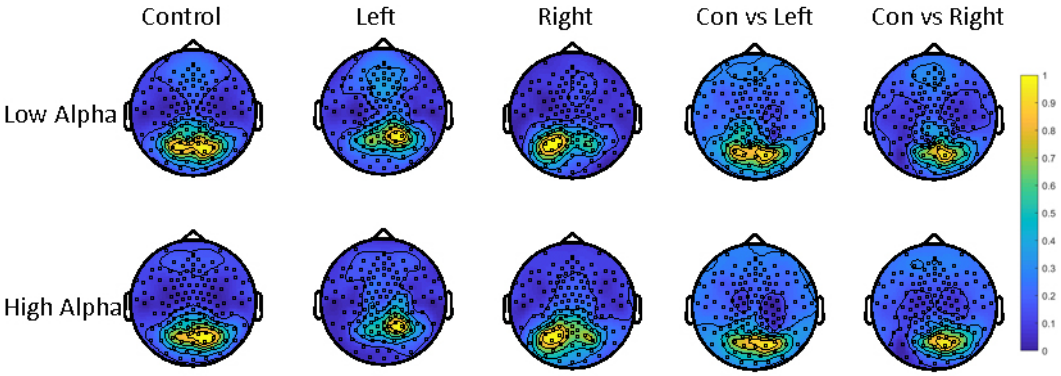

Figure 35: The topology plot of the frequency spectrum over the scalp for control and patient (left and right stroke patients). Higher activity in the contralateral visual cortex was observed both in the low and high alpha band.

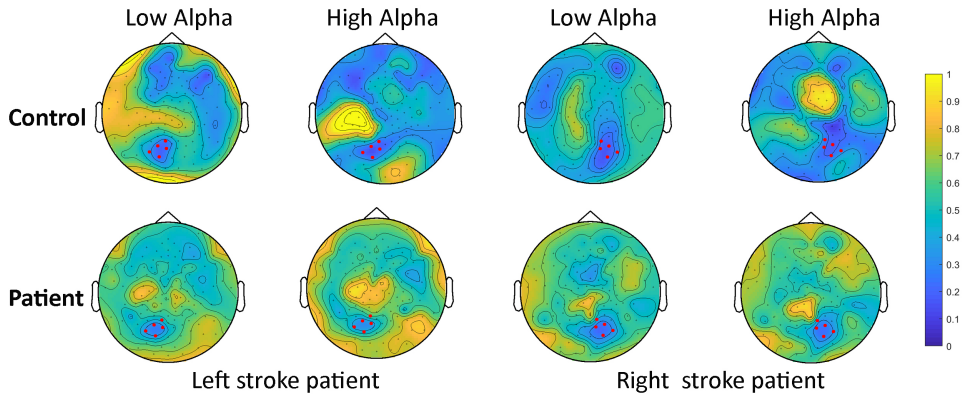

Figure 36: The topology plot of the node strength for control and patient(left and right stroke patients) in the low and high alpha band. The LO or RO was zero-averaged as the reference for other regions. There was no obvious pattern observed for local node weight.

6.4 Discussion

The loss of the visual field in stroke patients causes many inconveniences in life. Clinical diagnosis and treatment can help patients manage the visual field's loss and improve their quality of life. However, there are few studies on the decoding changes in brain state to predict visual field defects. Therefore, based on features extracted from the resting state EEG, we utilized deep learning methods to evaluate the possibility of visual field defect prediction in stroke patients.

The results from the above experiments may present that it is barely possible to predict a patient's percentages of vision field given their electrode-based frequency spectrum and brain connectivity. In contrast, the visual field location was possibly predicted with a large sample and optimized algorithms.

In the case of large samples, it may provide a more appealing prediction performance. On the contrary, patient recruitment and data collection are challenging, so increasing the data sample is feasible but not economical.

Although the 2DCNN model learns some helpful information, the cross-subjects performance is not as satisfactory. In both domains, the score never reaches 70%. One possible reason could be that the 2DCNN and the 3DCNN model cannot thoroughly learn EEG signals' typical pattern, and the variability of lesion location may cause inconsistent brain network patterns.

We consider that the vision field's percentages are not a direct representation of visual functional ability. The percentages of the vision field only reflect the numeric values. For a single value, it could have infinite combinations. For example, the intact vision percentage is 54.4% (240 out of 441 areas are white). In this case, the white areas' locations could be distributed anywhere within the 21 * 21 matrix.

In conclusion, the visual field defect location could be predictable through the frequency spectrum, and the performance could possibly be improved with a large sample. However, predicting vision percentage remains a formidable challenge.

6.5 Conclusion

This study proposed a frequency spectrum-based 2D convolutional neural network and a connectivity-based 3D convolutional neural network to decode the relationship between the brain oscillation and the visual field defect caused by a unilateral occipital stroke. The spectrum-based 2DCNN demonstrated better visual field location prediction than the connectivity-based 3DCNN model, while the visual field percentage was not predictable in our evaluation. The visualization of EEG characteristics and feature maps help make results more explainable. More samples and optimized network structure may yield an improvement in the future.

7 Study 5: Predicting Brain Electrical Stimulation Outcome in Stroke by Clinical-inspired Hybrid Graph Convolutional Autoencoder

(Part of this work has been published to 2nd IEEE International Conference on Human-Machine Systems 2021)

7.1 Background

Noninvasive brain stimulation (NIBS) techniques have been widely used in clinical application and they were found to be effective and safe (Dayan et al., 2013). Two of the most common neural modulation technologies are tDCS and tACS. tDCS can modify excitability of neuronal tissue with direct current. tACS, on the other hand, can entrain the neurons to oscillate at an externally driven frequency. The effect of neuromodulation technology has been clinically confirmed in stroke (Lindenberg et al., 2010), pain (O'Connell et al., 2018), Parkinson's (Tinkhauser et al., 2017), depression (Holtzheimer et al., 2017), and other brain diseases. Regarding stroke, NIBS techniques were used to enhance different functional domains, including vision loss after a unilateral occipital stroke, which could possibly be benefited from NIBS (Gall et al., 2015; Sabel et al., 2020b).

There has been little study of brain network-based clinical outcome prediction after brain electrical stimulation with machine learning (Butson et al., 2006; Chaturvedi et al., 2006; Mohammed et al., 2017). Kyriaki et al. (Park et al., 2021) presented a random forest technique to predict the unified Parkinson's disease rating scale improvement after deep brain stimulation. Another similar work is that of Kwang et al. (Kostoglou et al., 2017) who applied deep learning techniques to microelectrode recording signals to predict motor function improvement in Parkinson's disease. However, these invasive brain stimulation studies are not based on physiological signal phase coupling and did not consider the behavior data. Indeed, considering the unknown underlying mechanism for NIBS and personalized variance, the prediction of the clinical outcome after noninvasive brain stimulation therapy is very challenging and rarely investigated.

Deep learning has achieved great success in computer vision, audio recognition, and natural language processing (LeCun et al., 2015). Current deep learning technology is mainly based on Euclidean geometric distance, such as the convolutional neural network (CNN). However, the non-Euclidean geometric distance data emerged increasingly, such as social networks and brain networks in graphs with complex relationships presented by node and edges. Graph neural network aimed handling non-Euclidean geometric distance in many applications. One of the most highlighted networks is the spatial-based graph convolutional network (GCN). The spatial GCN could derive the updated presentation of the central node with its connected neighbors in a weighted network, which is equivalent to the node strength in graph theory analysis.

The spatial-based graph convolutional network can obtain the characteristics of the central node from its connected neighbor nodes, which matches the strength (information propagation) and centrality (message passing) in graph theory analysis. The strength is the local feature presentation of pre-defined nodes with its neighbors. Centrality is the global feature presentation of pre-defined nodes with all the nodes in the graph. The readout layer mainly aimed to generate the whole level presentation based on nodes and then feed the node features into a fully connected layer for training.

GCN pooling is a down-sampling strategy to reduce the size of parameters for a smaller presentation in a graph. The pooling operation could relieve the over-fitting, permutation invariance, and computation issues (Zhou et al., 2020). Mean pooling was one of the most effective methods to implement the pooling operation. The DiffPool was proposed to generate a hierarchical presentation of graphs (Ying et al., 2019). The critical point in

this method is to compress the nodes into a lower number while keeping topological and feature information. For example, a mean pooling strategy could help generate lower-size and higher-level presentations between two brain nodes from a sub-nodes connectivity matrix in neuroscience.

This study evaluated a proposed hybrid convolutional autoencoder (HGCAE) to predict the clinical outcome based on brain network measures and behavioral data obtained from patients with unilateral stroke. Brain node strength and centrality are generated by an equivalent filter of graph convolutional network. Pairwise coherence between high-level nodes was derived by the mean pooling layer on sub-nodes. The visual performance was also considered during the training session. The overall goal of our research was to promote the development of novel approaches of predicting outcome in clinical neurology.

7.2 Method

7.2.1 Subjects information

24 patients ($Age, n = 24, Mean \pm Sd, 58.375 \pm 10.87$) with partial vision loss led by a unilateral occipital stroke were recruited (see more detail for clinical trial (Sabel, 2019) and treatment (Gall et al., 2015)). High dense resting-state EEG was recorded before brain stimulation therapy using a HydroCell GSN 128channel net (EGI Inc.). The ethics committee of University Magdeburg approved this study and all the subjects have signed the consent. For more details, see Chapter 3.

7.2.2 Data preprocessing

A digital 1-145 Hz bandpass filter was applied on data as well as a 50 Hz notch filter. The data was downsampled to 250 Hz and then referenced by the common average reference method. EEG recordings were segmented into 2 seconds long each epoch, 100 trails were picked out per subject. Independent component analysis (ICA) removed the eye-blinks and cardiac activity.

7.2.3 Source reconstruction

Only the Alpha band frequency ($8 \sim 12Hz$) was decomposed for brain source reconstruction. The forward model was calculated using the symmetric boundary element method (BEM) (Fuchs et al., 2001). The inverse model was calculated with a beamforming method using the partial canonical correlation method (Rao, 1969), which implements Dynamical Imaging of Coherent Sources (DICS) (Gross et al., 2001). The default template for MRI was from MNI (Colin 27) at 8mm resolution (Holmes and Hoge.etc, 1998). The AAL-VOIs atlas (AAL) is an automatic anatomical labeling result (Tzourio-Mazoyer and Landeau, 2002), which includes 120 structure definitions, and 90 were used in this study.

7.2.4 Functional connectivity and brain network

Using the source reconstruction, we re-sampled the trials with bootstrap method which generated 50 connectivity matrices per subject as output. Then we used the imagery part of coherence (Nolte et al., 2004a) to calculate the brain connectivity, which is insensitive to false connectivity arising from volume conduction to measure the functional connectivity

with resting-state EEG data. The connectivity matrix of each subject was thresholded with a network density of 0.3, which means only 0.3 strongest weight edges were kept for each subject. In this manner, the density defined as the proportion of existing edges out of all possible edges was equal for each graph per subject (Bola and Sabel, 2015). Fixing the probability for an edge also excludes the criteria of Erdos-R´enyi random networks for group analysis (Van Wijk et al., 2010). The connectivity matrix (90×90) was generated for graph network analysis.

Weighted graph analysis attracted lots of attentions from the neuronscience area, Which can keep the information and avoid all issues related to selecting an appropriate threshold comparison with the binary network (Hagmann et al., 2008; Stam et al., 2008). In this study, we applied the graph theory analysis with the brain connectivity matrix for feature engineering in predicting the noninvasive brain stimulation output performance.

7.2.5 Node local aggregation

In graph theory, node strength is the sum of weights of links from its neighbors connected to the node, demonstrating the importance of information exchange with neighborhood nodes, consistent with the information propagation in GCN (Monti et al., 2017). Here, the brain was parcellated with an AAL mask. The node strength (1×90) was calculated with a weighted connectivity matrix (90×90). The whole-brain node strength was averaged as the global strength.

7.2.6 Node global aggregation

Node betweenness centrality is the fraction of all shortest paths in the network that contain a given node, which match the messaging pass in GCN (Yadati et al., 2018). A higher value of betweenness centrality in node indicates that it participates in a more significant number of shortest paths, where the node will be considered to play an essential role in the whole brain network information transfer. Node betweenness centrality (1×90) was calculated by Brandes algorithm with a weight connectivity matrix (90×90) (Brandes, 2001). The entire brain node's centrality was averaged as the global centrality.

7.2.7 Edges with GCN pooling

Inspired by the pooling modules in GCN (Ying et al., 2018), the coherence between pairwise nodes were segmented from left or right Occipital (LO or RO) linked to the rest of the brain regions [RO] to [RT,RF,RP,LT,LF,LP,LO] or [LO] to [RT,RF,RP,RO,LT,LF,LP](T: Temporal, F: Frontal, P: Parietal) as shown in Fig. 37. The pooling layer averaged the sub-nodes in these regions for a higher-level node presentation. The coherence matrix (1×7) from each hemisphere was contacted during the training session.

7.2.8 Visual field

Binocular visual fields were tested using a particular high-resolution computer-based campimetric test battery as previously described (Kasten et al., 1997). For each patient, three measurements were performed. The visual field areas were categorized as intact shown in white (three correctly detected stimuli per location), partially damaged regions shown in grey (one or two stimuli seen), and impaired, blind areas shown in black (no

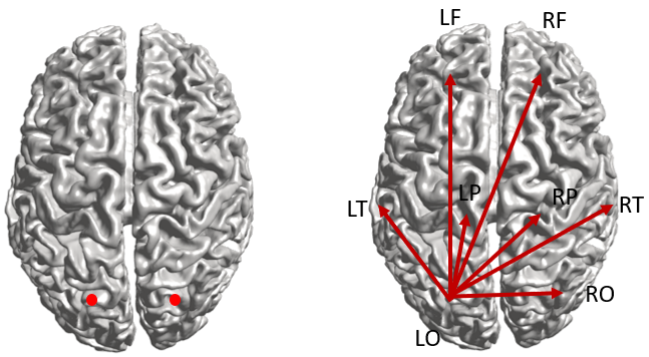

Figure 37: Local node strength (left) and global pairwise coherence (right)

stimulus detected). The reaction time $(0 - 1s)$ of the intact visual field(white and grey grids) was recorded simultaneously. The HRP parameters include a 1×5 vector.

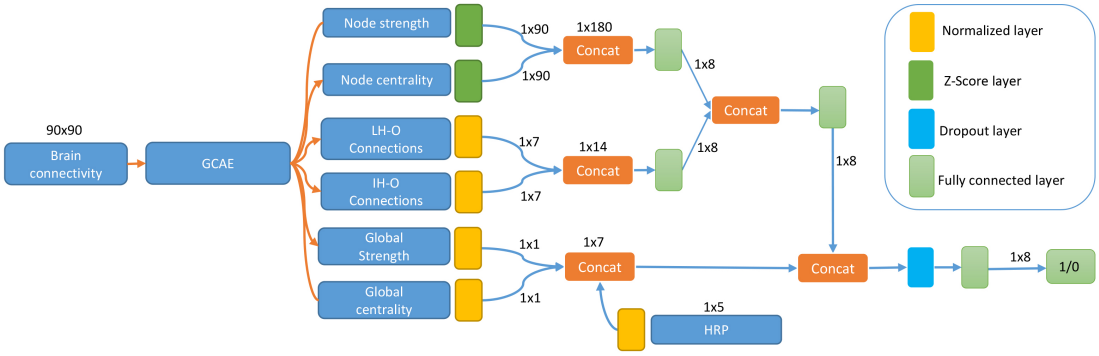

Figure 38: Proposed HGCAE structure for brain stimulation therapy output prediction in stroke

7.3 Frame structure

The proposed network structure includes: graph convolutional autoencoder, readout layer, pooling layer, and multiple layer perception (MLP). GCN autoencoder (including the readout and pooling layer) can generate the network embedding of clinical inspired feature and train the MLP involved in the parameter optimization. The brain connectivity matrix was fed into the GCN autoencoder to derive the feature matrix, such as local node and global pairwise coherence. Local node strength and centrality were z-scored before concatenation, followed by a fully connected layer (8 neurons). The coherence between higher-level nodes were normalized before concatenation. Both outputs were concatenated into another fully connected layer (8 neurons). Meanwhile, the global strength and centrality were concatenated with HRP parameters and then contacted with the output from local node strength and centrality with a dropout of 0.75 as well as the sigmoid activation function, see Fig. 38.

7.4 Label generation

All the patients have been given noninvasive brain stimulation after this study. The visual field was tested by HRP, and displayed as visual field charts. The contralateral

Table 8: The classification report with HGCAE

class	Precision	Recall	F1-score	Support
Non-responder	0,86	0,56	0,68	200
Responder	0,68	0,91	0,78	200

eye's FOV was measured by OCULUS Twinfield®[2]. For the details of NIBS protocols, see (Gall et al., 2015). The visual field parameters were measured before treatment and two months later after treatment. Compared with before treatment, the patients with enhanced visual performance (Positive percentage change of FOV) were categorized as responders (Label: 1), or, non-responders (Label: 0).

7.5 Training detail

The model was trained on Google Colab by using the Adam optimizer with the default parameters described in (Kingma and Ba, 2014), minimizing the binary cross-entropy log loss function. The reactivation function is the Rectified Linear Unit (RELU). The dropout probability was set to 0.75 to prevent over-fitting when training on limited sample sizes. Data was split with 800 trials from 16 subjects for training and 400 trials from 8 subjects for the validation. We ran 30 training iterations (epochs). Loss_weights were settled as [0.2, 0.2, 0.1, 0.2, 0.2] for [local node, local centrality, HRP, LO-coherence, RO-coherence]. Data preprocessing and feature extraction were performed with the Fieldtrip toolbox (Oostenveld et al., 2011) on Matlab.

7.6 Result

The final performance of HGCAE shows the proposed model gains at a higher sensitivity of 91% and lower specificity of 56% as well as the global mean accuracy of 74% on the validation dataset, see Tab 8 and Fig. 39, The model's performance is in line with clinical expectations because higher sensitivity is expected to help the clinician decide if further treatment is and which treatment conditions are more preferred. Those patients who can get the most extraordinary potential recovery possibilities from non-invasive electrical stimulation therapy can receive treatments, which effectively saves medical resources and achieve precision medicine.

Specifically, the precision of the non-responder prediction accuracy was 86% and the responder prediction was 68%. This indicates that more negative samples are predicted to be positive and fewer positive numbers of examples are predicted to be negative. This phenomenon could be considered over-fitting because our model is more sensitive to positive samples. As can be seen in Fig. 41 and Fig. 42, the visualization of brain node strength and centrality showed that the features of positive subjects are more pronounced. The responder's pairwise coherence between temporal and occipital in the intact hemisphere is higher than the non-responder while in the lesioned hemisphere of the non-responder, it is reverse. In the future, it might be possible to optimize the performance through early-stop (see Fig. 40), learning-rate and dropouts.

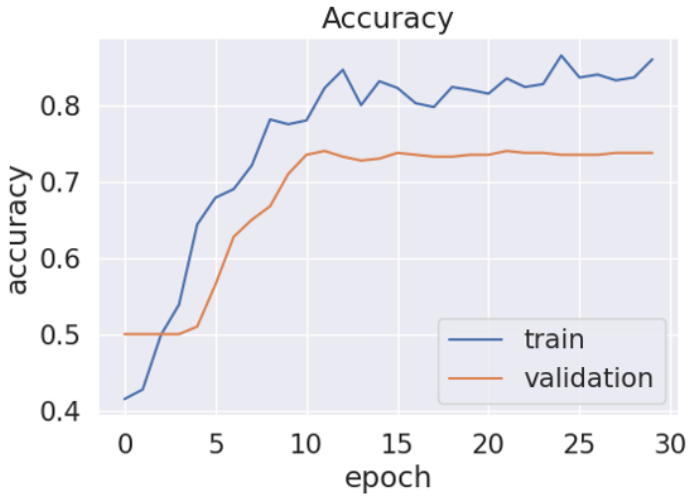

Figure 39: The accuracy of the train and validation dataset

Figure 40: The loss curve of the train and validation dataset

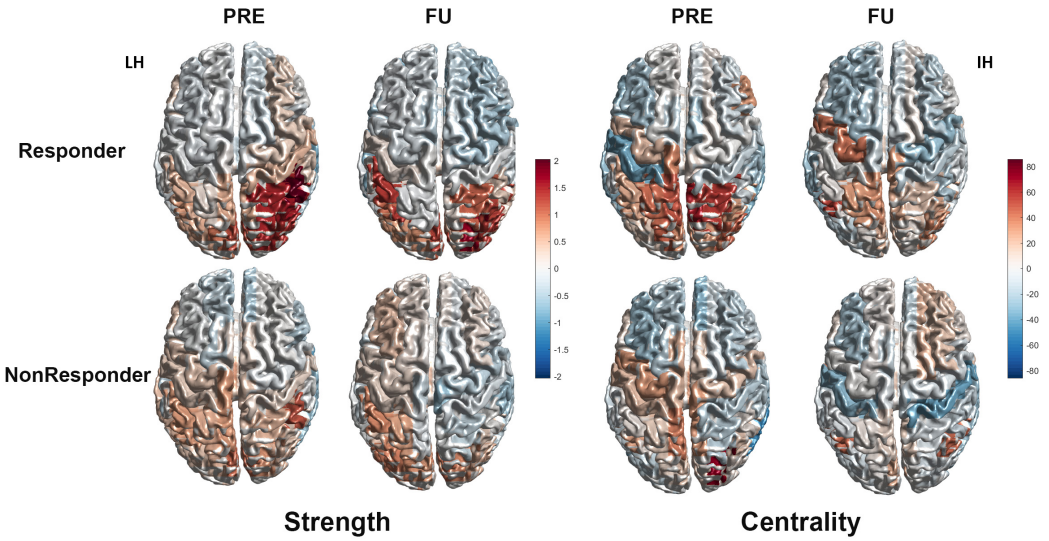

Figure 41: The topology plot of the strength and centrality in patient brain network reorganization after noninvasive brain stimulation before treatment (PRE) and two months after treatment (FU)

7.7 Discussion

Noninvasive brain stimulation (NIBS) has shown its promising potential to improved lost functions in neurological disorders (Woods et al., 2016; Antal et al., 2017). Vision loss after stroke is one example how this new technology can help patients (Sabel, 2019). However, the mechanisms of recovery following brain stimulation are only poorly understood, hindering our progress to better define a more effective usage of this technology. Research regarding the possibility of predicting this therapy efficacy using brain network features are quite rare and worth to be investigated further (Kostoglou et al., 2017; Park et al., 2021). And there is currently still no consensus on mechanisms of action of how NIBS achieves neuromodulation and recovery. We therefore explored the possibility of recovery prediction after receiving non-invasive neuromodulation based on the brain network measures and using behavior data.

The proposed model has achieved relatively high sensitivity in predicting responders. By visualizing the brain network parameters, we found that patients with a stronger capacity for brain network reorganization are more likely to benefit from neuromodulation after a stroke. However, it is probably not be the only factor that influences outcome. One possibility is that electrical stimulation enhances the excitability of the neurons in patients and this might induce adaptive brain network reorganization. Yet, more experiments are needed to study this proposal.

Future studies should also consider other machine learning models and to test more algorithms to evaluated the value of our proposed model's performance. Preferably, such studies should include larger sample sizes of patients. It is worth pointing out that this study did not consider the personalized variability caused by different electrical stimulation parameters during the treatment. Rather, we predicted the possibility of recovery by observing the reorganization of the brain network before treatment and the changes in visual function after treatment. As for the relationship between the possibility of recovery

and different NIBS protocols, further investigation are needed.

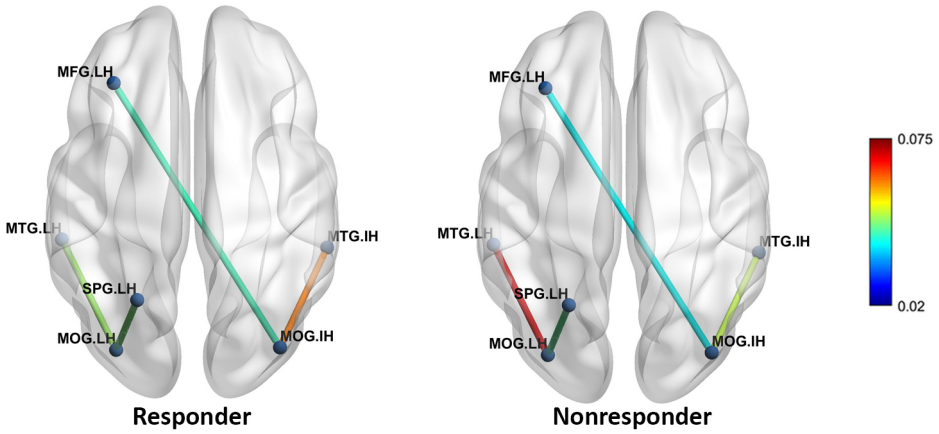

Figure 42: Pairwise coherence between higher level brain nodes, no significant was observed

7.8 Conclusion

This study evaluated the possibility of predicting the effect of noninvasive brain electrical stimulation of the alpha band brain functional network on recovery of vision in patients after occipital stroke. As we showed, brain network dynamic changes can be uncovered with graph theory in combination with a hybrid graph convolutional network autoencoder for NIBS outcome prediction. Our results show that with the HGCAE we can achieved an overall accuracy of 74% as well as 91% sensitivity of predicting recovery of vision after NIBS intervention. Although this is still far away from the valid clinical usage, this outcome prediction approach showed that progress can be made with machine learning, and the results are an incentive to further explore prediction models for the clinical application of non-invasive brain stimulation.

8 General discussion and Future work

8.1 General discussion and conclusion

This chapter first summarizes this thesis's main contributions (neuromodulation with noninvasive brain stimulation and prediction with deep learning) corresponding to the raised questions in the motivation part. The second part of this chapter discusses potential directions for future work inspired by our current work.

8.1.1 Clinical findings from brain damage, reorganization and recovery

The role of brain network reorganization: Graph measures of FCN based on EEG-tracking are a valuable tool to unravel the role of electrophysiological oscillations in brain network reorganization. As shown in Chapter 3, the stroke brain shows both local and global FCN reorganization in the high alpha and low beta band, and this can be both "maladaptive" or "adaptive" in different brain regions. Specifically, the stroke FCN changes towards a more "regular" pattern that is maladaptive in the intact occipital region, possibly creating perceptual deficits causing temporal and spatial visual impairments in the "intact" but crowded visual field. However, FCN can also be "adaptive", enabling temporal gyrus structures to compensate for the loss of vision in the scotoma. Thus, exploring the complex architecture of the brain's FCN using EEG-tracking adds critical temporal dimensions to our understanding of brain reorganization to better explain the normal and abnormal (low) vision. In addition, brain FCN graph analysis might inspire new approaches for the diagnosis and rehabilitation of low vision loss and other neurodegenerative disorders, such as noninvasive brain stimulation.

The brain network dynamic change after NIBS : Noninvasive brain stimulation (NIBS) is already known to improve visual field functions in patients with optic nerve damage as it partially restores the organization of brain functional connectivity networks (FCN). However, because little is known if NIBS is effective also following brain damage, we studied the correlation between visual field recovery and FCN reorganization in stroke patients with central visual pathway damage. Then we analyzed data from a randomized, and sham controlled noninvasive brain electric stimulation clinical trials to modulate the brain plasticity for vision loss patients to validate its vision recovery potential (Chapter 4). ACDC patients obtain improved visual functionality and hemispheric balance while AC and SHAM groups remain at the previous level. The decreased long connectivity changes in the ACDC group in the delta band suggests that the combination of tACS and tDCS could inhibit the low-frequency neural oscillation between the lesion occipital and intact occipital. This raises the question, if FCN parameters can serve as a biomarker to predict vision recovery.

The possible mechanism of vision recovery after NIBS: The less global clustering coefficient in the responder group than the non-responder group suggets that the resting brain state needs fewer connections at paired regions to transfer the information; possibility ACDC could elicit some 'silent neurons' in the lesion location. These fewer connections in the alpha band between lesion frontal and intact occipital represented the plasticity alterations toward improving visual functionality. The connections between intact temporal and intact occipital lobe shows that the intact temporal plays an essential

role in adaptive visual function after stroke. Brain FCN reorganization is therefore relevant for the post-lesion response and plasticity of the damaged visual system. This finding could help guide us in searching for more effective stimulation protocols to induce vision restoration in ways that are more effective and long-lasting than the existing technique of visual rehabilitation in stroke and brain injury.

8.1.2 Visual field decoding with deep learning

Deep learning and graph neural networks attracted lots of attention from the neuroscience community. This thesis proposes a frequency spectrum based 2DCNN and brain connectivity- based 3DCNN for predicting the visual field defect after a unilateral occipital stroke. Next, we evaluated if it is possible to identify patients and controls using brain network biomarkers. Bi-LSTM demonstrated the overall balanced performance. Lastly, inspired by the clinical features, a GCN autoencoder was implemented to predict the responder or non-responders from the brain connectivity matrix. Work described in Chapters 5-7 is now discussed.

Brain network connectivity predicts vision impairment:Chapter 5 explored a multiscale brain network and deep neural network to evaluate brain network patterns for identifying vision impairment patients after occipital stroke. The prediction model and statistical analysis indicate that the low and high alpha band under specific density can serve as a predictor to characterize brain network reorganization. The Bi-LSTM gained a balanced performance between sensitivity and specificity, which could prove useful for the development and application of brain feature extractions. Further investigation should extend this algorithm with more data samples and an optimized network structure. These results may provide insight for clinical diagnostics and interventions in the future.

Decoding resting-state EEG to predict visual field defect: To investigate the relationship between EEG and visual field, Chapter 6 proposed a frequency spectrum-based 2D convolutional neural network and a connectivity-based 3D convolutional neural network to decode the relationship between the brain oscillation and the visual field defect caused by a unilateral occipital stroke. The spectrum-based 2DCNN demonstrated better visual field location prediction than the connectivity-based 3DCNN model, while the visual field percentage was not predictable in our evaluation. The visualization of EEG characteristics and feature maps help make results more explainable. More samples and optimized network structure may yield an improvement in the future.

Predicting brain electrical stimulation outcome in stroke: To investigate the relationship between EEG and visual field parameters, Chapter 7 proposed a frequency spectrum-based 2D convolutional neural network and a connectivity-based 3D convolutional neural network to decode the relationship between the brain oscillation and the visual field defect caused by a unilateral occipital stroke. The spectrum-based 2DCNN demonstrated better visual field location prediction than the connectivity-based 3DCNN model, while the visual field percentage was not predictable in our evaluation. The visualization of EEG characteristics and feature maps help make results more explainable. More samples and optimized network structure may yield an improvement in the future.

8.2 Future work

The studies discussed in this thesis have some limitations:

- Sample size: in this study, twenty-four unilateral occipital stroke patients were recruited for the brain stimulation intervention, to test three stimulation protocols (ACDC, AC, SHAM) with eight patients per group. This small sample size per group may play a critical role in limiting our ability to interpret data. In future studies a larger sample would be preferred to obtain more robust data analysis and result interpretation. Meanwhile, for the prediction part of the brain network, visual field, and brain stimulation responder, the small number of subjects limits the accuracy. A larger sample is expected to improve the final performance in future studies.

- Source reconstruction and data variability: we applied a common fMRI template from MNI when resourcing with a low spatial resolution of the EEG signals. For a better resolution the individual head model for both patients and controls would be preferable. Some researchers reported that intra-individual variability in response to tDCS and tACS was found (Im et al., 2018; Kasten et al., 2019; Laakso et al., 2015; Wiethoff et al., 2014). There are different possible sources of outcome variability. Firstly, the individual anatomy varies between patients, which generates differences in electric fields inside the brain (Laakso et al., 2015). Even in a fixed stimulation montage and intensity, there is substantial variability of spatial distribution and strength were observed with individual anatomical differences (Laakso et al., 2015). In our study, the data was warped into MNI (Montreal Neurologic Institute) space during source reconstruction. Some researchers argue that the standard template would make the anatomy less precise, especially in the lesion area; however, we used the same pipeline and could still demonstrate the brain network consistently with the behavior output. Secondly, there may be other systemic factors (such as blood flow differences, hormonal or nutritional influences) which may influence neurophysiological activity during FU; and thirdly, we recently observed that vision recovery following ACS treatment in patients with optic nerve damage depend on the patients' personality trait (Sabel et al., 2020b). In view of these other intervening variables, it is questionable if an individual brain scan template really enhances the power of prediction.

- Resting-state connectivity vs. Task-based connectivity: brain connectivity could be calculated at rest (with eyes closed) or during a task-specific activity. The FCN in resting-state EEG was our first step to investigate the role of the brain's FCN after damage to characterize its fundamental network structure. The visual task-induced reorganization would be another fascinating perspective for future studies. Of note, MRI studies of neurological functions are also often carried out during the resting state. Future work could be a multi-model data study that combines the rFMRI and visual task-based EEG data. In this way, not only the brain network in resting EEG but also the dynamic brain network in time scale would tell us more details about brain network reorganization.

- Optimized algorithms: in this study, we had implemented several algorithms such as SVM, MLP,2DCNN,3DCNN, Bi-LSTM, and GCN autoencoder. The results are

meaningful in clinical terms and could possibly serve as a biomarker for the visual vision diagnostics. However, the output performance is not state of the art or in the scope of our expectations. The possible reason could be the structure of the proposed algorithms and the fine-tune tracks that could not converge the final loss. Regarding brain connectivity, we would like to explore a more novel structure of the graph neural network for higher performance. The attention mechanism also attracts lots of attention from researchers. The possible way in the future could be the GCN transformer that takes advantage of both the graph data and the global attention features.

In sum, despite these limitations, this thesis demonstrates the value of brain functional connectivity reorganization as a physiological biomarker for normal, abnormal, and recovered vision. The hope is that this new understanding will inspire novel methods for vision diagnostics, recovery and rehabilitation.

References

M. M. Ali, K. K. Sellers, and F. Fröhlich. Transcranial alternating current stimulation modulates large-scale cortical network activity by network resonance. *Journal of Neuroscience*, 33(27):11262–11275, 2013.

C. Allman, U. Amadi, A. M. Winkler, L. Wilkins, N. Filippini, U. Kischka, C. J. Stagg, and H. Johansen-Berg. Ipsilesional anodal tdcs enhances the functional benefits of rehabilitation in patients after stroke. *Science translational medicine*, 8(330):330re1, 2016. doi: 10.1126/scitranslmed.aad5651.

K. Altman, E. Shavit-Stein, and N. Maggio. Post stroke seizures and epilepsy: From proteases to maladaptive plasticity. *Frontiers in cellular Neuroscience*, 13:397, 2019. ISSN 1662-5102. doi: 10.3389/fncel.2019.00397.

C. A. Anastassiou, S. M. Montgomery, M. Barahona, G. Buzsáki, and C. Koch. The effect of spatially inhomogeneous extracellular electric fields on neurons. *Journal of Neuroscience*, 30(5):1925–1936, 2010.

A. Antal and C. S. Herrmann. Transcranial alternating current and random noise stimulation: Possible mechanisms. *Neural Plasticity*, 2016:3616807, 2016. doi: 10.1155/2016/3616807.

A. Antal and W. Paulus. Transcranial alternating current stimulation (tacs). *Frontiers in Human Neuroscience*, 7:317, 2013.

A. Antal, I. Alekseichuk, M. Bikson, J. Brockmöller, A. R. Brunoni, R. Chen, L. G. Cohen, G. Dowthwaite, J. Ellrich, A. Flöel, F. Fregni, M. S. George, R. Hamilton, J. Haueisen, C. S. Herrmann, F. C. Hummel, J. P. Lefaucheur, D. Liebetanz, C. K. Loo, C. D. McCaig, C. Miniussi, P. C. Miranda, V. Moliadze, M. A. Nitsche, R. Nowak, F. Padberg, A. Pascual-Leone, W. Poppendieck, A. Priori, S. Rossi, P. M. Rossini, J. Rothwell, M. A. Rueger, G. Ruffini, K. Schellhorn, H. R. Siebner, Y. Ugawa, A. Wexler, U. Ziemann, M. Hallett, and W. Paulus. Low intensity transcranial electric stimulation: Safety, ethical, legal regulatory and application guidelines. *Clinical Neurophysiology*, 128(9): 1774–1809, 2017. ISSN 1388-2457. doi: 10.1016/j.clinph.2017.06.001.

N. Attal, S. S. Ayache, D. C. De Andrade, A. Mhalla, S. Baudic, F. Jazat, R. Ahdab, D. O. Neves, M. Sorel, J.-P. Lefaucheur, et al. Repetitive transcranial magnetic stimulation and transcranial direct-current stimulation in neuropathic pain due to radiculopathy: a randomized sham-controlled comparative study. *Pain*, 157(6):1224–1231, 2016.

S. S. Ayache, U. Palm, M. A. Chalah, T. Al-Ani, A. Brignol, M. Abdellaoui, D. Dimitri, M. Sorel, A. Créange, and J.-P. Lefaucheur. Prefrontal tdcs decreases pain in patients with multiple sclerosis. *Frontiers in Neuroscience*, 10:147, 2016.

S.-c. Bao, A. Khan, R. Song, and R. K.-y. Tong. Rewiring the lesioned brain: electrical stimulation for post-stroke motor restoration. *Journal of Stroke*, 22(1):47, 2020.

A. T. Barker, R. Jalinous, and I. L. Freeston. Non-invasive magnetic stimulation of human motor cortex. *The Lancet*, 325(8437):1106–1107, 1985.

D. S. Bassett and E. T. Bullmore. Small-world brain networks revisited. *The Neuroscientist*, 23(5):499–516, 2017.

C. Beard, A. J. Millner, M. J. C. Forgeard, E. I. Fried, K. J. Hsu, M. T. Treadway, C. V. Leonard, S. J. Kertz, and T. Björgvinsson. Network analysis of depression and anxiety symptom relationships in a psychiatric sample. *Psychological Medicine*, 46(16): 3359–3369, 2016. doi: 10.1017/S0033291716002300.

Y. Bengio. *Learning deep architectures for AI.* Now Publishers Inc, 2009.

E. J. Benjamin, M. J. Blaha, S. E. Chiuve, M. Cushman, S. R. Das, R. Deo, S. D. de Ferranti, J. Floyd, M. Fornage, C. Gillespie, C. R. Isasi, M. C. Jiménez, L. C. Jordan, S. E. Judd, D. Lackland, J. H. Lichtman, L. Lisabeth, S. Liu, C. T. Longenecker, R. H. Mackey, K. Matsushita, D. Mozaffarian, M. E. Mussolino, K. Nasir, R. W. Neumar, L. Palaniappan, D. K. Pandey, R. R. Thiagarajan, M. J. Reeves, M. Ritchey, C. J. Rodriguez, G. A. Roth, W. D. Rosamond, C. Sasson, A. Towfighi, C. W. Tsao, M. B. Turner, S. S. Virani, J. H. Voeks, J. Z. Willey, J. T. Wilkins, J. H. Wu, H. M. Alger, S. S. Wong, and P. Muntner. Heart disease and stroke statistics-2017 update: A report from the american heart association. *Circulation*, 135(10):e146–e603, 2017. doi: 10.1161/CIR.0000000000000485.

A. Benussi, V. Cantoni, M. S. Cotelli, M. Cotelli, C. Brattini, A. Datta, C. Thomas, E. Santarnecchi, A. Pascual-Leone, and B. Borroni. Exposure to gamma tacs in alzheimer's disease: a randomized, double-blind, sham-controlled, crossover, pilot study. *Brain Stimulation*, 2021.

L. J. Bindman, O. C. Lippold, and J. W. Redfearn. The action of brief polarizing currents on the cerebral cortex of the rat (1) during current flow and (2) in the production of long-lasting after-effects. *The Journal of Physiology*, 172(3):369–382, 1964.

N. S. Bland and M. V. Sale. Current challenges: The ups and downs of tacs. *Experimental Brain Research*, 237(12):3071–3088, 2019.

M. Bola and B. A. Sabel. Dynamic reorganization of brain functional networks during cognition. *NeuroImage*, 114:398–413, 2015. ISSN 1095-9572. doi: 10.1016/j.neuroimage.2015.03.057.

M. Bola, C. Gall, and B. A. Sabel. The second face of blindness: processing speed deficits in the intact visual field after pre- and post-chiasmatic lesions. *PloS one*, 8(5):e63700, 2013. ISSN 1932-6203. doi: 10.1371/journal.pone.0063700.

M. Bola, C. Gall, C. Moewes, A. Fedorov, H. Hinrichs, and B. A. Sabel. Brain functional connectivity network breakdown and restoration in blindness. *Neurology*, 83(6):542–551, 2014. doi: 10.1212/WNL.0000000000000672.

M. Bönstrup, R. Schulz, G. Schön, B. Cheng, J. Feldheim, G. Thomalla, and C. Gerloff. Parietofrontal network upregulation after motor stroke. *NeuroImage. Clinical*, 18:720–729, 2018. doi: 10.1016/j.nicl.2018.03.006.

U. Brandes. A faster algorithm for betweenness centrality*. *The Journal of Mathematical Sociology*, 25(2):163–177, 2001. doi: 10.1080/0022250X.2001.9990249.

T. Brandt, S. F. Bucher, K. C. Seelos, and M. Dieterich. Bilateral functional mri activation of the basal ganglia and middle temporal/medial superior temporal motion-sensitive areas. *Archives of Neurology*, 55(8):1126, 1998. ISSN 0003-9942. doi: 10.1001/archneur.55.8.1126.

S. Breit, J. B. Schulz, and A.-L. Benabid. Deep brain stimulation. *Cell and Tissue Research*, 318(1):275–288, 2004.

C. Brevet-Aeby, M. Mondino, E. Poulet, and J. Brunelin. Three repeated sessions of transcranial random noise stimulation (trns) leads to long-term effects on reaction time in the go/no go task. *Neurophysiologie Clinique/Clinical Neurophysiology*, 49(1):27–32, 2019. doi: 10.1016/j.neucli.2018.10.066.

J. Bruna, W. Zaremba, A. Szlam, and Y. LeCun. Spectral networks and locally connected networks on graphs. *arXiv preprint arXiv:1312.6203*, 2013.

R. L. Buckner, J. Sepulcre, T. Talukdar, F. M. Krienen, H. Liu, T. Hedden, J. R. Andrews-Hanna, R. A. Sperling, and K. A. Johnson. Cortical hubs revealed by intrinsic functional connectivity: mapping, assessment of stability, and relation to alzheimer's disease. *The Journal of Neuroscience : the official journal of the Society for Neuroscience*, 29(6):1860–1873, 2009. ISSN 0270-6474. doi: 10.1523/JNEUROSCI.5062-08.2009.

S. S. Buss, P. J. Fried, and A. Pascual-Leone. Therapeutic noninvasive brain stimulation in alzheimer's disease and related dementias. *Current opinion in Neurology*, 32(2):292, 2019.

C. R. Butson, S. E. Cooper, J. M. Henderson, and C. C. McIntyre. Predicting the effects of deep brain stimulation with diffusion tensor based electric field models. *Medical image computing and computer-assisted intervention*, 9(Pt 2):429–437, 2006. doi: 10.1007/11866763{\textunderscore}53.

M. Bystad, O. Grønli, I. D. Rasmussen, N. Gundersen, L. Nordvang, H. Wang-Iversen, and P. M. Aslaksen. Transcranial direct current stimulation as a memory enhancer in patients with alzheimer's disease: a randomized, placebo-controlled trial. *Alzheimer's research & therapy*, 8(1):1–7, 2016.

G. A. Campbell, Bruce C. V. Ischaemic stroke. *Nature reviews. Disease primers*, 5(1):70, 2019. doi: 10.1038/s41572-019-0118-8.

M. Cappelletti, E. Gessaroli, R. Hithersay, M. Mitolo, D. Didino, R. Kanai, R. Cohen Kadosh, and V. Walsh. Transfer of cognitive training across magnitude dimensions achieved with concurrent brain stimulation of the parietal lobe. *The Journal of Neuroscience : the official journal of the Society for Neuroscience*, 33(37):14899–14907, 2013. ISSN 0270-6474. doi: 10.1523/JNEUROSCI.1692-13.2013.

S. T. Carmichael, L. Wei, C. M. Rovainen, and T. A. Woolsey. New patterns of intracortical projections after focal cortical stroke. *Neurobiology of Disease*, 8(5):910–922, 2001. ISSN 0969-9961. doi: 10.1006/nbdi.2001.0425.

M. Catani, F. Dell'acqua, F. Vergani, F. Malik, H. Hodge, P. Roy, R. Valabregue, and M. Thiebaut de Schotten. Short frontal lobe connections of the human brain. *Cortex;*

a journal devoted to the study of the nervous system and behavior, 48(2):273–291, 2012. doi: 10.1016/j.cortex.2011.12.001.

M. R. Cavanaugh and K. R. Huxlin. Visual discrimination training improves humphrey perimetry in chronic cortically induced blindness. *Neurology*, 88(19):1856–1864, 2017.

C. Cavézian, I. Gaudry, C. Perez, O. Coubard, G. Doucet, C. Peyrin, C. Marendaz, M. Obadia, O. Gout, and S. Chokron. Specific impairments in visual processing following lesion side in hemianopic patients. *Cortex*, 46(9):1123–1131, 2010.

C. Cavézian, C. Perez, C. Peyrin, I. Gaudry, M. Obadia, O. Gout, and S. Chokron. Hemisphere-dependent ipsilesional deficits in hemianopia: Sightblindness in the 'intact' visual field. *Cortex; a journal devoted to the study of the nervous system and behavior*, 69:166–174, 2015. doi: 10.1016/j.cortex.2015.05.010.

A. Chail, R. K. Saini, P. Bhat, K. Srivastava, and V. Chauhan. Transcranial magnetic stimulation: a review of its evolution and current applications. *Industrial Psychiatry Journal*, 27(2):172, 2018.

C.-H. Chang, H.-Y. Lane, and C.-H. Lin. Brain stimulation in alzheimer's disease. *Frontiers in psychiatry*, 9:201, 2018.

A. Chaturvedi, C. R. Butson, S. E. Cooper, and C. C. McIntyre. Subthalamic nucleus deep brain stimulation: accurate axonal threshold prediction with diffusion tensor based electric field models. *the IEEE Engineering in Medicine and Biology Society*, 2006:1240–1243, 2006. ISSN 1557-170X. doi: 10.1109/IEMBS.2006.260502.

Y. Choi and J.-H. Kwon. Ensemble of deep convolutional neural networks for prognosis of ischemic stroke. In *Brainlesion*, volume 10154 of *LNCS sublibrary. SL 6, Image processing, computer vision, pattern recognition, and graphics*, pages 231–243. Springer, Cham, Switzerland, 2016. ISBN 978-3-319-55523-2. doi: 10.1007/978-3-319-55524-9{\textunderscore}22.

S. Chokron, C. Perez, M. Obadia, I. Gaudry, L. Laloum, and O. Gout. From blindsight to sight: cognitive rehabilitation of visual field defects. *Restorative Neurology and Neuroscience*, 26(4, 5):305–320, 2008.

M. Christopher, Bowd, and L. M. Zangwill. Deep learning approaches predict glaucomatous visual field damage from oct optic nerve head en face images and retinal nerve fiber layer thickness maps. *Ophthalmology*, 127(3):346–356, 2020. doi: 10.1016/j.ophtha.2019.09.036.

P. Ciechanski and A. Kirton. Transcranial direct-current stimulation can enhance motor learning in children. *Cerebral Cortex (New York, N.Y. : 1991)*, 27(5):2758–2767, 2017. doi: 10.1093/cercor/bhw114.

K. J. Clancy, S. K. Baisley, A. Albizu, N. Kartvelishvili, M. Ding, and W. Li. Lasting connectivity increase and anxiety reduction via transcranial alternating current stimulation. *Social Cognitive and Affective Neuroscience*, 13(12):1305–1316, 2018.

Cohen. Understanding lstm networks. 2015. URL `https://colah.github.io/posts/2015-08-Understanding-LSTMs/`.

D. L. Collins, A. P. Zijdenbos, V. Kollokian, J. G. Sled, N. J. Kabani, C. J. Holmes, and A. C. Evans. Design and construction of a realistic digital brain phantom. *IEEE transactions on medical imaging*, 17(3):463–468, 1998. ISSN 0278-0062. doi: 10.1109/42.712135.

V. Conde, L. Tomasevic, I. Akopian, K. Stanek, G. B. Saturnino, A. Thielscher, T. O. Bergmann, and H. R. Siebner. The non-transcranial tms-evoked potential is an inherent source of ambiguity in tms-eeg studies. *Neuroimage*, 185:300–312, 2019.

G. Contemori, Y. Trotter, B. R. Cottereau, and M. Maniglia. trns boosts perceptual learning in peripheral vision. *Neuropsychologia*, 125:129–136, 2019. ISSN 1873-3514. doi: 10.1016/j.neuropsychologia.2019.02.001.

M. Corbetta, M. J. Kincade, C. Lewis, A. Z. Snyder, and A. Sapir. Neural basis and recovery of spatial attention deficits in spatial neglect. *Nature Neuroscience*, 8(11):1603–1610, 2005. doi: 10.1038/nn1574.

A. Cowey and P. Stoerig. The neurobiology of blindsight. *Trends in Neurosciences*, 14(4):140–145, 1991.

J. J. Crofts, D. J. Higham, R. Bosnell, S. Jbabdi, P. M. Matthews, T. E. J. Behrens, and H. Johansen-Berg. Network analysis detects changes in the contralesional hemisphere following stroke. *NeuroImage*, 54(1):161–169, 2011. ISSN 1095-9572. doi: 10.1016/j.neuroimage.2010.08.032.

S. Dalise, F. Ambrosio, and M. Modo. Brain plasticity and recovery in preclinical models of stroke. *Archives italiennes de biologie*, 152(4):190–215, 2014. ISSN 0003-9829. doi: 10.12871/00039829201442.

E. Dayan, N. Censor, E. R. Buch, M. Sandrini, and L. G. Cohen. Noninvasive brain stimulation: from physiology to network dynamics and back. *Nature Neuroscience*, 16(7):838–844, 2013.

M. Defferrard, X. Bresson, and P. Vandergheynst. Convolutional neural networks on graphs with fast localized spectral filtering. *arXiv preprint arXiv:1606.09375*, 2016.

A. Del Felice, L. Castiglia, E. Formaggio, M. Cattelan, B. Scarpa, P. Manganotti, E. Tenconi, and S. Masiero. Personalized transcranial alternating current stimulation (tacs) and physical therapy to treat motor and cognitive symptoms in parkinson's disease: a randomized cross-over trial. *NeuroImage: Clinical*, 22:101768, 2019.

E. L. Dennis and P. M. Thompson. Functional brain connectivity using fmri in aging and alzheimer's disease. *Neuropsychology Review*, 24(1):49–62, 2014.

J. Devlin, M.-W. Chang, K. Lee, and K. Toutanova. Bert: Pre-training of deep bidirectional transformers for language understanding. *arXiv preprint arXiv:1810.04805*, 2018.

L. di Biase, E. Falato, and V. Di Lazzaro. Transcranial focused ultrasound (tfus) and transcranial unfocused ultrasound (tus) neuromodulation: from theoretical principles to stimulation practices. *Frontiers in Neurology*, 10:549, 2019.

B. C. Dickerson and R. A. Sperling. Large-scale functional brain network abnormalities in alzheimer's disease: insights from functional neuroimaging. *Behavioural Neurology*, 21(1):63–75, 2009. doi: 10.3233/BEN-2009-0227.

A. Dosovitskiy, L. Beyer, A. Kolesnikov, D. Weissenborn, X. Zhai, T. Unterthiner, M. Dehghani, M. Minderer, G. Heigold, S. Gelly, et al. An image is worth 16x16 words: Transformers for image recognition at scale. *arXiv preprint arXiv:2010.11929*, 2020.

L. Douw, M. Schoonheim, D. Landi, M. Van der Meer, J. Geurts, J. Reijneveld, M. Klein, and C. Stam. Cognition is related to resting-state small-world network topology: an magnetoencephalographic study. *Neuroscience*, 175:169–177, 2011.

J. Dundas, G. Thickbroom, and F. Mastaglia. Perception of comfort during transcranial dc stimulation: effect of nacl solution concentration applied to sponge electrodes. *Clinical Neurophysiology*, 118(5):1166–1170, 2007.

N. M. Dundon, C. Bertini, E. Làdavas, B. A. Sabel, and C. Gall. Visual rehabilitation: Visual scanning, multisensory stimulation and vision restoration trainings. *Frontiers in behavioral Neuroscience*, 9:192, 2015. ISSN 1662-5153. doi: 10.3389/fnbeh.2015.00192.

N. Dusi, S. Barlati, A. Vita, and P. Brambilla. Brain structural effects of antidepressant treatment in major depression. *Current Neuropharmacology*, 13(4):458–465, 2015.

B. Elsner, G. Kwakkel, J. Kugler, and J. Mehrholz. Transcranial direct current stimulation (tdcs) for improving capacity in activities and arm function after stroke: a network meta-analysis of randomised controlled trials. *Journal of Neuroengineering and Rehabilitation*, 14(1):1–12, 2017.

A. Fedorov, S. Jobke, V. Bersnev, A. Chibisova, Y. Chibisova, C. Gall, and B. A. Sabel. Restoration of vision after optic nerve lesions with noninvasive transorbital alternating current stimulation: A clinical observational study. *Brain Stimulation*, 4(4):189–201, 2011. ISSN 1876-4754. doi: 10.1016/j.brs.2011.07.007.

V. L. Feigin, B. Norrving, and G. A. Mensah. Global burden of stroke. *Circulation Research*, 120(3):439–448, 2017. doi: 10.1161/CIRCRESAHA.116.308413.

D. J. Felleman and D. C. Van Essen. Distributed hierarchical processing in the primate cerebral cortex. *Cerebral Cortex (New York, NY: 1991)*, 1(1):1–47, 1991.

R. Ferrucci, F. Mameli, I. Guidi, S. Mrakic-Sposta, M. Vergari, S. Marceglia, F. Cogiamanian, S. Barbieri, E. Scarpini, and A. Priori. Transcranial direct current stimulation improves recognition memory in alzheimer disease. *Neurology*, 71(7):493–498, 2008.

R. Ferrucci, F. Cortese, M. Bianchi, D. Pittera, R. Turrone, T. Bocci, B. Borroni, M. Vergari, F. Cogiamanian, G. Ardolino, et al. Cerebellar and motor cortical transcranial stimulation decrease levodopa-induced dyskinesias in parkinson's disease. *The Cerebellum*, 15(1):43–47, 2016.

A. Fertonani and C. Miniussi. Transcranial electrical stimulation: What we know and do not know about mechanisms. *The Neuroscientist : a review journal bringing neurobiology, neurology and psychiatry*, 23(2):109–123, 2017. ISSN 1073-8584. doi: 10.1177/1073858416631966.

A. Fornito, A. Zalesky, and E. T. Bullmore. Network scaling effects in graph analytic studies of human resting-state fmri data. *Frontiers in Systems Neuroscience*, 4:22, 2010. ISSN 1662-5137. doi: 10.3389/fnsys.2010.00022.

N. Forss, M. Hietanen, O. Salonen, and R. Hari. Modified activation of somatosensory cortical network in patients with right-hemisphere stroke. *Brain*, 122(10):1889–1899, 1999. ISSN 0006-8950. doi: 10.1093/brain/122.10.1889.

L. C. Freeman. Centrality in social networks conceptual clarification. *Social Networks*, 1 (3):215–239, 1978. ISSN 03788733. doi: 10.1016/0378-8733(78)90021-7.

F. Fregni, S. Thome-Souza, M. A. Nitsche, S. D. Freedman, K. D. Valente, and A. Pascual-Leone. A controlled clinical trial of cathodal dc polarization in patients with refractory epilepsy. *Epilepsia*, 47(2):335–342, 2006.

M. Fuchs, M. Wagner, and J. Kastner. Boundary element method volume conductor models for eeg source reconstruction. *Clinical Neurophysiology*, 112(8):1400–1407, 2001. ISSN 1388-2457.

H. Fujimoto, M. Mihara, N. Hattori, M. Hatakenaka, T. Kawano, H. Yagura, I. Miyai, and H. Mochizuki. Cortical changes underlying balance recovery in patients with hemiplegic stroke. *NeuroImage*, 85 Pt 1:547–554, 2014. ISSN 1095-9572. doi: 10.1016/j.neuroimage.2013.05.014.

C. Gall, A. B. Fedorov, L. Ernst, A. Borrmann, and B. A. Sabel. Repetitive transorbital alternating current stimulation in optic neuropathy. *NeuroRehabilitation*, 27(4):335–341, 2010a. ISSN 1878-6448. doi: 10.3233/NRE-2010-0617.

C. Gall, G. H. Franke, and B. A. Sabel. Vision-related quality of life in first stroke patients with homonymous visual field defects. *Health and quality of life outcomes*, 8:33, 2010b. doi: 10.1186/1477-7525-8-33.

C. Gall, S. Sgorzaly, S. Schmidt, S. Brandt, A. Fedorov, and B. A. Sabel. Noninvasive transorbital alternating current stimulation improves subjective visual functioning and vision-related quality of life in optic neuropathy. *Brain Stimulation*, 4(4):175–188, 2011. ISSN 1876-4754. doi: 10.1016/j.brs.2011.07.003.

C. Gall, B. Steger, J. Koehler, and B. A. Sabel. Evaluation of two treatment outcome prediction models for restoration of visual fields in patients with postchiasmatic visual pathway lesions. *Neuropsychologia*, 51(11):2271–2280, 2013. ISSN 1873-3514. doi: 10.1016/j.neuropsychologia.2013.06.028.

C. Gall, K. Silvennoinen, and B. A. Sabel. Non-invasive electric current stimulation for restoration of vision after unilateral occipital stroke. *Contemporary clinical trials*, 43: 231–236, 2015. ISSN 1559-2030. doi: 10.1016/j.cct.2015.06.005.

C. Gall, S. Schmidt, M. P. Schittkowski, A. Antal, G. G. Ambrus, W. Paulus, M. Dannhauer, R. Michalik, A. Mante, M. Bola, A. Lux, S. Kropf, S. A. Brandt, and B. A. Sabel. Alternating current stimulation for vision restoration after optic nerve damage: A randomized clinical trial. *PloS one*, 11(6):e0156134, 2016. ISSN 1932-6203. doi: 10.1371/journal.pone.0156134.

Y. Gao, C. Huber, and B. A. Sabel. Stable microsaccades and microsaccade-induced global alpha band phase reset across the life span. *Investigative Ophthalmology & Visual Science*, 59(5):2032–2041, 2018.

N. Gilbert, R. A. Bernier, V. D. Calhoun, E. Brenner, E. Grossner, S. M. Rajtmajer, and F. G. Hillary. Diminished neural network dynamics after moderate and severe traumatic brain injury. *PloS one*, 13(6):e0197419, 2018. ISSN 1932-6203. doi: 10.1371/journal.pone.0197419.

Q. Gong and Y. He. Depression, neuroimaging and connectomics: a selective overview. *Biological psychiatry*, 77(3):223–235, 2015. doi: 10.1016/j.biopsych.2014.08.009.

P. Goodin, G. Lamp, R. Vidyasagar, D. McArdle, R. J. Seitz, and L. M. Carey. Altered functional connectivity differs in stroke survivors with impaired touch sensation following left and right hemisphere lesions. *NeuroImage. Clinical*, 18:342–355, 2018. doi: 10.1016/j.nicl.2018.02.012.

D. Goodwin. Homonymous hemianopia: challenges and solutions. *Clinical Ophthalmology (Auckland, N.Z.)*, 8:1919–1927, 2014. ISSN 1177-5467. doi: 10.2147/OPTH.S59452.

M. Gori, G. Monfardini, and F. Scarselli. A new model for learning in graph domains. In *Proceedings. 2005 IEEE International Joint Conference on Neural Networks, 2005.*, volume 2, pages 729–734. IEEE, 2005.

A. t. Gorman. Differential patterns of activation of the pyramidal system elicited by surface anodal and cathodal cortical stimulation. *Journal of Neurophysiology*, 29(4): 547–564, 1966.

A. Graves and J. Schmidhuber. Framewise phoneme classification with bidirectional lstm and other neural network architectures. *Neural Networks*, 18(5-6):602–610, 2005.

C. Grefkes and N. S. Ward. Cortical reorganization after stroke: how much and how functional? *The Neuroscientist : a review journal bringing neurobiology, neurology and psychiatry*, 20(1):56–70, 2014. ISSN 1073-8584. doi: 10.1177/1073858413491147.

K. Grill-Spector and R. Malach. The human visual cortex. *Annu. Rev. Neurosci.*, 27: 649–677, 2004.

J. Gross, J. Kujala, and Hamalainen.etc. Dynamic imaging of coherent sources: Studying neural interactions in the human brain. *Proceedings of the National Academy of Sciences of the United States of America*, 98(2):694–699, 2001. ISSN 0027-8424. doi: 10.1073/pnas.98.2.694.

X. Guo, Z. Jin, X. Feng, and S. Tong. Enhanced effective connectivity in mild occipital stroke patients with hemianopia. *IEEE transactions on Neural Systems and Rehabilitation Engineering : a publication of the IEEE Engineering in Medicine and Biology Society*, 22(6):1210–1217, 2014. doi: 10.1109/TNSRE.2014.2325601.

P. Hagmann, L. Cammoun, X. Gigandet, R. Meuli, C. J. Honey, J. van Wedeen, and O. Sporns. Mapping the structural core of human cerebral cortex. *PLoS Biology*, 6(7): e159, 2008. ISSN 1545-7885.

Y. Hashimoto, R. Asaoka, M. Kiwaki, and K. Yamanishi. Deep learning model to predict visual field in central 10° from optical coherence tomography measurement in glaucoma. *The British journal of Ophthalmology*, 2020. doi: 10.1136/bjophthalmol-2019-315600.

K. He, X. Zhang, S. Ren, and J. Sun. Deep residual learning for image recognition. In *Proceedings of the IEEE conference on computer vision and pattern recognition*, pages 770–778, 2016.

R. F. Helfrich, T. R. Schneider, S. Rach, S. A. Trautmann-Lengsfeld, A. K. Engel, and C. S. Herrmann. Entrainment of brain oscillations by transcranial alternating current stimulation. *Current Biology : CB*, 24(3):333–339, 2014. ISSN 1879-0445. doi: 10.1016/j.cub.2013.12.041.

L. Henriksson, A. Raninen, R. Näsänen, L. Hyvärinen, and S. Vanni. Training-induced cortical representation of a hemianopic hemifield. *Journal of Neurology, Neurosurgery & Psychiatry*, 78(1):74–81, 2007.

C. S. Herrmann, S. Rach, T. Neuling, and D. Strüber. Transcranial alternating current stimulation: A review of the underlying mechanisms and modulation of cognitive processes. *Frontiers in Human Neuroscience*, 7:279, 2013. ISSN 1662-5161. doi: 10.3389/fnhum.2013.00279.

S. Hochreiter and J. Schmidhuber. Long short-term memory. *Neural Computation*, 9(8): 1735–1780, 1997.

C. J. Holmes and Hoge.etc. Enhancement of mr images using registration for signal averaging. *Journal of Computer Assisted Tomography*, 22(2):324–333, 1998. ISSN 0363-8715. doi: 10.1097/00004728-199803000-00032.

P. E. Holtzheimer, M. M. Husain, S. H. Lisanby, S. F. Taylor, L. A. Whitworth, S. McClintock, K. V. Slavin, J. Berman, G. M. McKhann, P. G. Patil, et al. Subcallosal cingulate deep brain stimulation for treatment-resistant depression: a multisite, randomised, sham-controlled trial. *The Lancet Psychiatry*, 4(11):839–849, 2017.

W. Hou, C. Sours Rhodes, L. Jiang, S. Roys, J. Zhuo, J. JaJa, and R. P. Gullapalli. Dynamic functional network analysis in mild traumatic brain injury. *Brain Connectivity*, 9(6):475–487, 2019. doi: 10.1089/brain.2018.0629.

Y.-Z. Huang, M.-K. Lu, A. Antal, J. Classen, M. Nitsche, U. Ziemann, M. Ridding, M. Hamada, Y. Ugawa, S. Jaberzadeh, A. Suppa, W. Paulus, and J. Rothwell. Plasticity induced by non-invasive transcranial brain stimulation: A position paper. *Clinical Neurophysiology*, 128(11):2318–2329, 2017. ISSN 1388-2457. doi: 10.1016/j.clinph.2017.09.007.

Z. Huang, W. Xu, and K. Yu. Bidirectional lstm-crf models for sequence tagging. *arXiv preprint arXiv:1508.01991*, 2015.

T. Huff, N. Mahabadi, and P. Tadi. Neuroanatomy, visual cortex. *StatPearls [Internet]*, 2020.

C. Huo, G. Xu, Z. Li, Z. Lv, Q. Liu, W. Li, H. Ma, D. Wang, and Y. Fan. Limb linkage rehabilitation training-related changes in cortical activation and effective connectivity

after stroke: A functional near-infrared spectroscopy study. *Scientific Reports*, 9(1): 6226, 2019. ISSN 2045-2322. doi: 10.1038/s41598-019-42674-0.

F. T. Husain and S. A. Schmidt. Using resting state functional connectivity to unravel networks of tinnitus. *Hearing Research*, 307:153–162, 2014. doi: 10.1016/j.heares.2013.07.010.

K. R. Huxlin, T. Martin, K. Kelly, M. Riley, D. I. Friedman, W. S. Burgin, and M. Hayhoe. Perceptual relearning of complex visual motion after v1 damage in humans. *Journal of Neuroscience*, 29(13):3981–3991, 2009.

F. Iandola, M. Moskewicz, S. Karayev, R. Girshick, T. Darrell, and K. Keutzer. Densenet: Implementing efficient convnet descriptor pyramids. *arXiv preprint arXiv:1404.1869*, 2014.

C. Im, H. Seo, and S. C. Jun. Stimulation effect of inter-subject variability in tdcs–multi-scale modeling study. In *2018 40th Annual International Conference of the IEEE Engineering in Medicine and Biology Society (EMBC)*, pages 3092–3095. IEEE, 2018.

M. B. Iyer, U. Mattu, J. Grafman, M. Lomarev, S. Sato, and E. M. Wassermann. Safety and cognitive effect of frontal dc brain polarization in healthy individuals. *Neurology*, 64(5):872–875, 2005. doi: 10.1212/01.WNL.0000152986.07469.E9.

L. Jiang, H. Xu, and C. Yu. Brain connectivity plasticity in the motor network after ischemic stroke. *Neural Plasticity*, 2013, 2013.

G. C. Jickling and F. R. Sharp. Biomarker panels in ischemic stroke. *Stroke*, 46(3): 915–920, 2015.

S. Jobke, E. Kasten, and B. A. Sabel. Vision restoration through extrastriate stimulation in patients with visual field defects: a double-blind and randomized experimental study. *Neurorehabilitation and Neural Repair*, 23(3):246–255, 2009. ISSN 1552-6844. doi: 10.1177/1545968308324221.

S. A. Jones and R. A. Shinton. Improving outcome in stroke patients with visual problems. *Age and ageing*, 35(6):560–565, 2006. doi: 10.1093/ageing/afl074.

H. J. Kaiser, J. Flammer, P. J. Bucher, R. De Natale, D. Stümpfig, and P. Hendrickson. High-resolution perimetry of the central visual field. *Ophthalmologica*, 208(1):10–14, 1994.

S. Kalénine, L. J. Buxbaum, and H. B. Coslett. Critical brain regions for action recognition: lesion symptom mapping in left hemisphere stroke. *Brain*, 133(11):3269–3280, 2010. ISSN 0006-8950. doi: 10.1093/brain/awq210.

H.-O. Karnath, J. Rüter, A. Mandler, and M. Himmelbach. The anatomy of object recognition—visual form agnosia caused by medial occipitotemporal stroke. *Journal of Neuroscience*, 29(18):5854–5862, 2009.

D. Kaski, R. Dominguez, J. Allum, A. Islam, and A. Bronstein. Combining physical training with transcranial direct current stimulation to improve gait in parkinson's disease: a pilot randomized controlled study. *Clinical Rehabilitation*, 28(11):1115–1124, 2014.

E. Kasten, H. Strasburger, and B. A. Sabel. Programs for diagnosis and therapy of visual field deficits in vision rehabilitation. *Spatial Vision*, 10:499–503, 1997.

E. Kasten, S. Wüst, W. Behrens-Baumann, and B. A. Sabel. Computer-based training for the treatment of partial blindness. *Nature Medicine*, 4(9):1083–1087, 1998. ISSN 1078-8956. doi: 10.1038/2079.

F. H. Kasten, K. Duecker, M. C. Maack, A. Meiser, and C. S. Herrmann. Integrating electric field modeling and neuroimaging to explain inter-individual variability of tacs effects. *Nature Communications*, 10(1):1–11, 2019.

G. Kerkhoff, U. Münßinger, E. Haaf, G. Eberle-Strauss, and E. Stögerer. Rehabilitation of homonymous scotomata in patients with postgeniculate damage of the visual system: saccadic compensation training. *Restorative Neurology and Neuroscience*, 4(4):245–254, 1992.

S. J. Kim, G. J. Moon, and O. Y. Bang. Biomarkers for stroke. *Journal of Stroke*, 15(1): 27, 2013.

D. P. Kingma and J. Ba. Adam: A method for stochastic optimization. *arXiv preprint arXiv:1412.6980*, 2014.

M. M. Klein, R. Treister, T. Raij, A. Pascual-Leone, L. Park, T. Nurmikko, F. Lenz, J.-P. Lefaucheur, M. Lang, M. Hallett, et al. Transcranial magnetic stimulation of the brain: guidelines for pain treatment research. *Pain*, 156(9):1601, 2015.

H. Kolster, R. Peeters, and G. A. Orban. The retinotopic organization of the human middle temporal area mt/v5 and its cortical neighbors. *Journal of Neuroscience*, 30 (29):9801–9820, 2010.

K. Kostoglou, K. P. Michmizos, P. Stathis, D. Sakas, K. S. Nikita, and G. D. Mitsis. Classification and prediction of clinical improvement in deep brain stimulation from intraoperative microelectrode recordings. *IEEE transactions on bio-medical engineering*, 64(5):1123–1130, 2017. doi: 10.1109/TBME.2016.2591827.

B. Krasovitski, V. Frenkel, S. Shoham, and E. Kimmel. Intramembrane cavitation as a unifying mechanism for ultrasound-induced bioeffects. *Proceedings of the National Academy of Sciences*, 108(8):3258–3263, 2011.

V. Krause, C. Wach, M. Südmeyer, S. Ferrea, A. Schnitzler, and B. Pollok. Cortico-muscular coupling and motor performance are modulated by 20 hz transcranial alternating current stimulation (tacs) in parkinson's disease. *Frontiers in Human Neuroscience*, 7:928, 2014.

M. L. Kringelbach, N. Jenkinson, S. L. Owen, and T. Z. Aziz. Translational principles of deep brain stimulation. *Nature Reviews Neuroscience*, 8(8):623–635, 2007.

A. Krizhevsky, I. Sutskever, and G. E. Hinton. Imagenet classification with deep convolutional neural networks. *Advances in neural information processing systems*, 25: 1097–1105, 2012.

I. Laakso, S. Tanaka, S. Koyama, V. De Santis, and A. Hirata. Inter-subject variability in electric fields of motor cortical tdcs. *Brain Stimulation*, 8(5):906–913, 2015.

Y. LeCun, Y. Bengio, and G. Hinton. Deep learning. *nature*, 521(7553):436–444, 2015.

A. Lee, E. Schoonderwaldt, M. Chadde, and E. Altenmüller. Movement induced tremor in musicians and non-musicians reflects adaptive brain plasticity. *Frontiers in Psychology*, 5:824, 2014. ISSN 1664-1078. doi: 10.3389/fpsyg.2014.00824.

J.-P. Lefaucheur, A. Antal, S. S. Ayache, D. H. Benninger, J. Brunelin, F. Cogiamanian, M. Cotelli, D. de Ridder, R. Ferrucci, B. Langguth, P. Marangolo, V. Mylius, M. A. Nitsche, F. Padberg, U. Palm, E. Poulet, A. Priori, S. Rossi, M. Schecklmann, S. Vanneste, U. Ziemann, L. Garcia-Larrea, and W. Paulus. Evidence-based guidelines on the therapeutic use of transcranial direct current stimulation (tdcs). *Clinical Neurophysiology*, 128(1):56–92, 2017. ISSN 1388-2457. doi: 10.1016/j.clinph.2016.10.087.

T. Li. Brain electrophysiological oscillations and vision loss in occipital stroke patients. 2016.

X.-Y. Li, Y. Wan, S.-J. Tang, Y. Guan, F. Wei, and D. Ma. Maladaptive plasticity and neuropathic pain. *Neural Plasticity*, 2016:4842159, 2016. doi: 10.1155/2016/4842159.

Y. Li, Y. Qin, X. Chen, and W. Li. Exploring the functional brain network of alzheimer's disease: based on the computational experiment. *PloS one*, 8(9):e73186, 2013. ISSN 1932-6203. doi: 10.1371/journal.pone.0073186.

Z. Li. A saliency map in primary visual cortex. *Trends in Cognitive Sciences*, 6(1):9–16, 2002.

J. Liepert, K. Haevernick, C. Weiller, and A. Barzel. The surround inhibition determines therapy-induced cortical reorganization. *NeuroImage*, 32(3):1216–1220, 2006. ISSN 1095-9572. doi: 10.1016/j.neuroimage.2006.05.028.

R. Lindenberg, V. Renga, L. Zhu, D. Nair, and G. Schlaug. Bihemispheric brain stimulation facilitates motor recovery in chronic stroke patients. *Neurology*, 75(24):2176–2184, 2010.

J. Lindow, M. Domin, M. Grothe, U. Horn, S. B. Eickhoff, and M. Lotze. Connectivity-based predictions of hand motor outcome for patients at the subacute stage after stroke. *Frontiers in Human Neuroscience*, 10:101, 2016.

M. Lobier, J. M. Palva, and S. Palva. High-alpha band synchronization across frontal, parietal and visual cortex mediates behavioral and neuronal effects of visuospatial attention. *Neuroimage*, 165:222–237, 2018.

A. M. Lozano, N. Lipsman, H. Bergman, P. Brown, S. Chabardes, J. W. Chang, K. Matthews, C. C. McIntyre, T. E. Schlaepfer, M. Schulder, et al. Deep brain stimulation: current challenges and future directions. *Nature Reviews Neurology*, 15(3): 148–160, 2019.

S. J. Luck, L. Chelazzi, S. A. Hillyard, and R. Desimone. Neural mechanisms of spatial selective attention in areas v1, v2, and v4 of macaque visual cortex. *Journal of Neurophysiology*, 77(1):24–42, 1997.

MATLAB. *version 7.10.0 (R2017a)*. The MathWorks Inc, Natick, Massachusetts, 2017.

J. D. Medaglia. Functional neuroimaging in traumatic brain injury: From nodes to networks. *Frontiers in Neurology*, 8:407, 2017. ISSN 1664-2295. doi: 10.3389/fneur.2017.00407.

A. Micheli. Neural network for graphs: A contextual constructive approach. *IEEE transactions on Neural Networks*, 20(3):498–511, 2009.

A. Mohammed, M. Zamani, R. Bayford, and A. Demosthenous. Toward on-demand deep brain stimulation using online parkinson's disease prediction driven by dynamic detection. *IEEE transactions on Neural Systems and Rehabilitation Engineering*, 25(12): 2441–2452, 2017. doi: 10.1109/TNSRE.2017.2722986.

V. Moliadze, A. Antal, and W. Paulus. Boosting brain excitability by transcranial high frequency stimulation in the ripple range. *The Journal of Physiology*, 588(24):4891–4904, 2010.

F. Monti, D. Boscaini, J. Masci, E. Rodola, J. Svoboda, and M. M. Bronstein. Geometric deep learning on graphs and manifolds using mixture model cnns. In *Proceedings of the IEEE conference on computer vision and pattern recognition*, pages 5115–5124, 2017.

B. Moret, R. Donato, M. Nucci, G. Cona, and G. Campana. Transcranial random noise stimulation (trns): a wide range of frequencies is needed for increasing cortical excitability. *Scientific Reports*, 9(1):1–8, 2019.

A. Naro, D. Milardi, M. Russo, C. Terranova, V. Rizzo, A. Cacciola, S. Marino, R. S. Calabro, and A. Quartarone. Non-invasive brain stimulation, a tool to revert maladaptive plasticity in neuropathic pain. *Frontiers in Human Neuroscience*, 10:376, 2016. ISSN 1662-5161. doi: 10.3389/fnhum.2016.00376.

E. Nava and B. Röder. Adaptation and maladaptation insights from brain plasticity. *Progress in Brain Research*, 191:177–194, 2011. doi: 10.1016/B978-0-444-53752-2.00005-9.

G. Nelles, G. Widman, A. de Greiff, A. Meistrowitz, A. Dimitrova, J. Weber, M. Forsting, J. Esser, and H. C. Diener. Brain representation of hemifield stimulation in poststroke visual field defects. *Stroke*, 33(5):1286–1293, 2002.

G. Nelles, A. de Greiff, A. Pscherer, M. Forsting, H. Gerhard, J. Esser, and H. C. Diener. Cortical activation in hemianopia after stroke. *Neuroscience Letters*, 426(1):34–38, 2007. ISSN 0304-3940. doi: 10.1016/j.neulet.2007.08.028.

T. Neuling, S. Rach, and C. S. Herrmann. Orchestrating neuronal networks: sustained after-effects of transcranial alternating current stimulation depend upon brain states. *Frontiers in Human Neuroscience*, 7:161, 2013a. ISSN 1662-5161. doi: 10.3389/fnhum.2013.00161.

T. Neuling, S. Rach, and C. S. Herrmann. Orchestrating neuronal networks: sustained after-effects of transcranial alternating current stimulation depend upon brain states. *Frontiers in Human Neuroscience*, 7:161, 2013b.

M. E. J. Newman. Fast algorithm for detecting community structure in networks. *Physical Review. E, Statistical, nonlinear, and soft matter physics*, 69(6 Pt 2):066133, 2004. ISSN 1539-3755. doi: 10.1103/PhysRevE.69.066133.

Z. Nissa, S. A. Siddiqi, and S. A. M. Abdool. Occipital seizures and persistent homonymous hemianopia with t2 hypointensity on mri in nonketotic hyperglycemia. *Epilepsy & behavior case reports*, 6:3–5, 2016. ISSN 2213-3232. doi: 10.1016/j.ebcr.2016.04.008.

M. A. Nitsche and W. Paulus. Excitability changes induced in the human motor cortex by weak transcranial direct current stimulation. *The Journal of Physiology*, 527(Pt 3): 633–639, 2000. doi: 10.1111/j.1469-7793.2000.t01-1-00633.x.

M. A. Nitsche, D. Liebetanz, N. Lang, A. Antal, F. Tergau, and W. Paulus. Safety criteria for transcranial direct current stimulation (tdcs) in humans. *Clinical Neurophysiology*, 114(11):2220–2222, 2003. ISSN 1388-2457. doi: 10.1016/S1388-2457(03)00235-9.

G. Nolte. The magnetic lead field theorem in the quasi-static approximation and its use for magnetoencephalography forward calculation in realistic volume conductors. *Physics in Medicine and Biology*, 48(22):3637–3652, 2003. ISSN 0031-9155.

G. Nolte, O. Bai, and Wheaton. Identifying true brain interaction from eeg data using the imaginary part of coherency. *Clinical Neurophysiology*, 115(10):2292–2307, 2004a. ISSN 1388-2457. doi: 10.1016/j.clinph.2004.04.029.

G. Nolte, O. Bai, L. Wheaton, Z. Mari, S. Vorbach, and M. Hallett. Identifying true brain interaction from eeg data using the imaginary part of coherency. *Clinical Neurophysiology*, 115(10):2292–2307, 2004b.

N. E. O'Connell, L. Marston, S. Spencer, L. H. DeSouza, and B. M. Wand. Non-invasive brain stimulation techniques for chronic pain. *Cochrane database of systematic reviews*, (3), 2018.

M. Oliveri, P. M. Rossini, R. Traversa, P. Cicinelli, M. M. Filippi, P. Pasqualetti, F. Tomaiuolo, and C. Caltagirone. Left frontal transcranial magnetic stimulation reduces contralesional extinction in patients with unilateral right brain damage. *Brain*, 122(9):1731–1739, 1999. ISSN 0006-8950. doi: 10.1093/brain/122.9.1731.

R. Oostenveld, P. Fries, E. Maris, and J.-M. Schoffelen. Fieldtrip: open source software for advanced analysis of meg, eeg, and invasive electrophysiological data. *Computational Intelligence and Neuroscience*, 2011.

R. Oostenveld, D. F. Stegeman, P. Praamstra, and A. van Oosterom. Brain symmetry and topographic analysis of lateralized event-related potentials. *Clinical Neurophysiology*, 114(7):1194–1202, 2003. ISSN 1388-2457. doi: 10.1016/S1388-2457(03)00059-2.

R. Oostenveld, P. Fries, E. Maris, and J.-M. Schoffelen. Fieldtrip: Open source software for advanced analysis of meg, eeg, and invasive electrophysiological data. *Computational Intelligence and Neuroscience*, 2011:156869, 2011. doi: 10.1155/2011/156869.

U. Palm, M. A. Chalah, F. Padberg, T. Al-Ani, M. Abdellaoui, M. Sorel, D. Dimitri, A. Créange, J.-P. Lefaucheur, and S. S. Ayache. Effects of transcranial random noise stimulation (trns) on affect, pain and attention in multiple sclerosis. *Restorative Neurology and Neuroscience*, 34(2):189–199, 2016a.

U. Palm, F. M. Segmiller, A. N. Epple, F.-J. Freisleder, N. Koutsouleris, G. Schulte-Körne, and F. Padberg. Transcranial direct current stimulation in children and adolescents: a

comprehensive review. *Journal of Neural Transmission (Vienna, Austria : 1996)*, 123 (10):1219–1234, 2016b. doi: 10.1007/s00702-016-1572-z.

A. L. Pambakian and C. Kennard. Can visual function be restored in patients with homonymous hemianopia? *The British journal of Ophthalmology*, 81(4):324–328, 1997. ISSN 0007-1161.

A. L. Pambakian, D. S. Wooding, N. Patel, A. B. Morland, C. Kennard, and S. K. Mannan. Scanning the visual world: a study of patients with homonymous hemianopia. *Journal of Neurology, Neurosurgery, and Psychiatry*, 69(6):751–759, 2000. ISSN 0022-3050.

G. V. Paramei and B. A. Sabel. Contour-integration deficits on the intact side of the visual field in hemianopia patients. *Behavioural brain research*, 188(1):109–124, 2008.

G. V. Paramei, O. Favrod, B. A. Sabel, and M. H. Herzog. Pathological completion in the intact visual field of hemianopia patients. *Visual Cognition*, 25(1-3):169–183, 2017.

K. Park, J. Kim, and J. Lee. Visual field prediction using recurrent neural network. *Scientific Reports*, 9(1):8385, 2019. doi: 10.1038/s41598-019-44852-6.

K. H. Park, S. Sun, Y. H. Lim, H. R. Park, J. M. Lee, K. Park, B. Jeon, H.-P. Park, H. C. Kim, and S. H. Paek. Clinical outcome prediction from analysis of microelectrode recordings using deep learning in subthalamic deep brain stimulation for parkinson‘s disease. *PloS one*, 16(1):e0244133, 2021. doi: 10.1371/journal.pone.0244133.

A. Pascual-Leone, A. Amedi, F. Fregni, and L. B. Merabet. The plastic human brain cortex. *Annual review of Neuroscience*, 28:377–401, 2005. ISSN 0147-006X. doi: 10.1146/annurev.neuro.27.070203.144216.

C. A. Pedersini, J. Guàrdia-Olmos, M. Montalà-Flaquer, N. Cardobi, J. Sanchez-Lopez, G. Parisi, S. Savazzi, and C. A. Marzi. Functional interactions in patients with hemianopia: A graph theory-based connectivity study of resting fmri signal. *PloS one*, 15 (1):e0226816, 2020.

E. Pereda, R. Q. Quiroga, and J. Bhattacharya. Nonlinear multivariate analysis of neurophysiological signals. *Progress in neurobiology*, 77(1-2):1–37, 2005. ISSN 0301-0082. doi: 10.1016/j.pneurobio.2005.10.003.

J. S. Perlmutter and J. W. Mink. Deep brain stimulation. *Annu. Rev. Neurosci.*, 29: 229–257, 2006.

J. C. Peters, J. Reithler, T. A. de Graaf, T. Schuhmann, R. Goebel, and A. T. Sack. Concurrent human tms-eeg-fmri enables monitoring of oscillatory brain state-dependent gating of cortico-subcortical network activity. *Communications Biology*, 3(1):1–11, 2020.

R. Pineiro, S. Pendlebury, H. Johansen-Berg, and P. M. Matthews. Functional mri detects posterior shifts in primary sensorimotor cortex activation after stroke: evidence of local adaptive reorganization? *Stroke*, 32(5):1134–1139, 2001. doi: 10.1161/01.str.32.5.1134.

E. B. Plow, S. N. Obretenova, F. Fregni, A. Pascual-Leone, and L. B. Merabet. Comparison of visual field training for hemianopia with active versus sham transcranial direct cortical stimulation. *Neurorehabilitation and Neural Repair*, 26(6):616–626, 2012. ISSN 1552-6844. doi: 10.1177/1545968311431963.

D. A. Poggel, E. Kasten, and B. A. Sabel. Attentional cueing improves vision restoration therapy in patients with visual field defects. *Neurology*, 63(11):2069–2076, 2004. doi: 10.1212/01.WNL.0000145773.26378.E5.

R. Polanía, M. Moisa, A. Opitz, M. Grueschow, and C. C. Ruff. The precision of value-based choices depends causally on fronto-parietal phase coupling. *Nature Communications*, 6(1):1–10, 2015.

A. Priori. Brain polarization in humans: a reappraisal of an old tool for prolonged non-invasive modulation of brain excitability. *Clinical Neurophysiology*, 114(4):589–595, 2003.

A. Priori, A. Berardelli, S. Rona, N. Accornero, and M. Manfredi. Polarization of the human motor cortex through the scalp. *NeuroReport*, 9(10):2257–2260, 1998. ISSN 0959-4965.

D. P. Purpura and J. G. McMurtry. Intracellular activities and evoked potential changes during polarization of motor cortex. *Journal of neurophysiology*, 28(1):166–185, 1965.

A. Quartarone, H. R. Siebner, and J. C. Rothwell. Task-specific hand dystonia: can too much plasticity be bad for you? *Trends in Neurosciences*, 29(4):192–199, 2006. ISSN 01662236. doi: 10.1016/j.tins.2006.02.007.

R. S. Ramrattan, R. C. Wolfs, S. Panda-Jonas, J. B. Jonas, D. Bakker, H. A. Pols, A. Hofman, and P. T. de Jong. Prevalence and causes of visual field loss in the elderly and associations with impairment in daily functioning: the rotterdam study. *Archives of ophthalmology (Chicago, Ill. : 1960)*, 119(12):1788–1794, 2001. ISSN 0003-9950.

B. R. Rao. Partial canonical correlations. *Trabajos de estadistica y de investigación operativa*, 20(2-3):211–219, 1969.

J. Redmon, S. Divvala, R. Girshick, and A. Farhadi. You only look once: Unified, real-time object detection. In *Proceedings of the IEEE conference on computer vision and pattern recognition*, pages 779–788, 2016.

R. M. Reinhart and J. A. Nguyen. Working memory revived in older adults by synchronizing rhythmic brain circuits. *Nature Neuroscience*, 22(5):820–827, 2019.

L. Remedios, P. Mabil, J. Flores-Hernández, O. Torres-Ramírez, N. Huidobro, G. Castro, L. Cervantes, J. A. Tapia, B. De la Torre Valdovinos, and E. Manjarrez. Effects of short-term random noise electrical stimulation on dissociated pyramidal neurons from the cerebral cortex. *Neuroscience*, 404:371–386, 2019.

S. Ren, K. He, R. Girshick, and J. Sun. Faster r-cnn: Towards real-time object detection with region proposal networks. *arXiv preprint arXiv:1506.01497*, 2015.

S. Ren, K. He, R. Girshick, and J. Sun. Faster r-cnn: towards real-time object detection with region proposal networks. *IEEE transactions on pattern analysis and machine intelligence*, 39(6):1137–1149, 2016.

M. V. M. R. Ribeiro, H. N. Hasten-Reiter Júnior, E. A. N. Ribeiro, M. J. Jucá, F. T. Barbosa, and C. F. d. Sousa-Rodrigues. Association between visual impairment and

depression in the elderly: a systematic review. *Arquivos brasileiros de oftalmologia*, 78 (3):197–201, 2015a. doi: 10.5935/0004-2749.20150051.

M. V. M. R. Ribeiro, H. N. Hasten-Reiter Júnior, E. A. N. Ribeiro, M. J. Jucá, F. T. Barbosa, and C. F. d. Sousa-Rodrigues. Association between visual impairment and depression in the elderly: a systematic review. *Arquivos brasileiros de oftalmologia*, 78 (3):197–201, 2015b.

O. Ronneberger, P. Fischer, and T. Brox. U-net: Convolutional networks for biomedical image segmentation. In *International Conference on Medical image computing and computer-assisted intervention*, pages 234–241. Springer, 2015.

C. Rossi, F. Sallustio, S. Di Legge, P. Stanzione, and G. Koch. Transcranial direct current stimulation of the affected hemisphere does not accelerate recovery of acute stroke patients. *European Journal of Neurology*, 20(1):202–204, 2013.

P. M. Rossini, C. Calautti, F. Pauri, and J.-C. Baron. Post-stroke plastic reorganisation in the adult brain. *The Lancet. Neurology*, 2(8):493–502, 2003. ISSN 1474-4422. doi: 10.1016/s1474-4422(03)00485-x.

P. M. Rossini, R. Di Iorio, M. Bentivoglio, G. Bertini, F. Ferreri, C. Gerloff, R. J. Ilmoniemi, F. Miraglia, M. A. Nitsche, F. Pestilli, M. Rosanova, Y. Shirota, C. Tesoriero, Y. Ugawa, F. Vecchio, U. Ziemann, and M. Hallett. Methods for analysis of brain connectivity: An ifcn-sponsored review. *Clinical Neurophysiology*, 130(10):1833–1858, 2019. ISSN 1388-2457. doi: 10.1016/j.clinph.2019.06.006.

F. Rowe, D. Brand, C. A. Jackson, A. Price, L. Walker, S. Harrison, C. Eccleston, C. Scott, N. Akerman, C. Dodridge, C. Howard, T. Shipman, U. Sperring, S. Macdiarmid, and C. Freeman. Visual impairment following stroke: do stroke patients require vision assessment? *Age and ageing*, 38(2):188–193, 2009. doi: 10.1093/ageing/afn230.

F. J. Rowe. Stroke survivors' views and experiences on impact of visual impairment. *Brain and behavior*, 7(9):e00778, 2017. doi: 10.1002/brb3.778.

F. J. Rowe, D. Wright, and Brand. A prospective profile of visual field loss following stroke: prevalence, type, rehabilitation, and outcome. *BioMed Research International*, 2013:719096, 2013. ISSN 2314-6141. doi: 10.1155/2013/719096.

M. Rubin. Do p values lose their meaning in exploratory analyses? it depends how you define the familywise error rate. *Review of General Psychology*, 21(3):269–275, 2017.

M. Rubinov and O. Sporns. Complex network measures of brain connectivity: Uses and interpretations. *NeuroImage*, 52(3):1059–1069, 2010. ISSN 1095-9572. doi: 10.1016/j.neuroimage.2009.10.003.

M. Rubinov, S. A. Knock, C. J. Stam, S. Micheloyannis, A. W. F. Harris, L. M. Williams, and M. Breakspear. Small-world properties of nonlinear brain activity in schizophrenia. *Human Brain Mapping*, 30(2):403–416, 2009. ISSN 1097-0193.

B. A. Sabel. Non-invasive current stimulation for restoration of vision. *ClinicalTrials.gov*, (NCT04008589), 2019.

B. A. Sabel and J. Gudlin. Vision restoration training for glaucoma: a randomized clinical trial. *JAMA Ophthalmology*, 132(4):381–389, 2014.

B. A. Sabel and E. Kasten. Restoration of vision by training of residual functions. *Current opinion in ophthalmology*, 11(6):430–436, 2000a.

B. A. Sabel and E. Kasten. Restoration of vision by training of residual functions. *Current opinion in ophthalmology*, 11(6):430–436, 2000b.

B. A. Sabel, H. Strasburger, and E. Kasten. Programs for diagnosis and therapy of visual field deficits in vision rehabilitation. *Spatial Vision*, 10(4):499–503, 1997.

B. A. Sabel, S. Kenkel, and E. Kasten. Vision restoration therapy (vrt) efficacy as assessed by comparative perimetric analysis and subjective questionnaires. *Restorative Neurology and Neuroscience*, 22(6):399–420, 2004. ISSN 1878-3627.

B. A. Sabel, A. B. Fedorov, N. Naue, A. Borrmann, C. Herrmann, and C. Gall. Non-invasive alternating current stimulation improves vision in optic neuropathy. *Restorative Neurology and Neuroscience*, 29(6):493–505, 2011a. ISSN 1878-3627. doi: 10.3233/RNN-2011-0624.

B. A. Sabel, P. Henrich-Noack, A. Fedorov, and C. Gall. Vision restoration after brain and retina damage: the residual vision activation theory. *Progress in brain research*, 192:199–262, 2011b. doi: 10.1016/B978-0-444-53355-5.00013-0.

B. A. Sabel, J. Wang, L. Cárdenas-Morales, M. Faiq, and C. Heim. Mental stress as consequence and cause of vision loss: the dawn of psychosomatic ophthalmology for preventive and personalized medicine. *The EPMA journal*, 9(2):133–160, 2018. ISSN 1878-5077. doi: 10.1007/s13167-018-0136-8.

B. A. Sabel, Y. Gao, and A. Antal. Reversibility of visual field defects through induction of brain plasticity: vision restoration, recovery and rehabilitation using alternating current stimulation. *Neural regeneration research*, 15(10):1799, 2020a.

B. A. Sabel, G. Thut, J. Haueisen, P. Henrich-Noack, C. S. Herrmann, A. Hunold, T. Kammer, B. Matteo, E. G. Sergeeva, W. Waleszczyk, et al. Vision modulation, plasticity and restoration using non-invasive brain stimulation-an ifcn-sponsored review. *Clinical Neurophysiology: official journal of the International Federation of Clinical Neurophysiology*, 131(4):887–911, 2020b.

A. Sahraie, C. T. Trevethan, M. J. MacLeod, A. D. Murray, J. A. Olson, and L. Weiskrantz. Increased sensitivity after repeated stimulation of residual spatial channels in blindsight. *Proceedings of the National Academy of Sciences of the United States of America*, 103 (40):14971–14976, 2006. ISSN 0027-8424. doi: 10.1073/pnas.0607073103.

F. A. San Lucas, J. Redell, D. Pramod, and Y. Liu. Classifying mild traumatic brain injuries with functional network analysis. *BMC Systems Biology*, 12(Suppl 8), 2018. doi: 10.1186/s12918-018-0645-z.

R. Sawaya, W. Radwan, R. Alameddine, and S. Hammoud. Reversible homonymous hemianopia secondary to occipital lobe seizures. *Seizure*, 23(10):915–917, 2014. doi: 10.1016/j.seizure.2014.07.001.

F. Scarselli, M. Gori, A. C. Tsoi, M. Hagenbuchner, and G. Monfardini. The graph neural network model. *IEEE transactions on Neural Networks*, 20(1):61–80, 2008.

J. Schadow, N. Dettler, G. V. Paramei, D. Lenz, I. Fründ, B. A. Sabel, and C. S. Herrmann. Impairments of gestalt perception in the intact hemifield of hemianopic patients are reflected in gamma-band eeg activity. *Neuropsychologia*, 47(2):556–568, 2009.

C. J. Schankin, F. H. Maniyar, D. E. Chou, M. Eller, T. Sprenger, and P. J. Goadsby. Structural and functional footprint of visual snow syndrome. *Brain*, 143(4):1106–1113, 2020.

I. M. Schepers, J. F. Hipp, T. R. Schneider, B. Röder, and A. K. Engel. Functionally specific oscillatory activity correlates between visual and auditory cortex in the blind. *Brain*, 135(Pt 3):922–934, 2012. ISSN 0006-8950. doi: 10.1093/brain/aws014.

D. J. L. G. Schutter and R. Hortensius. Retinal origin of phosphenes to transcranial alternating current stimulation. *Clinical Neurophysiology*, 121(7):1080–1084, 2010. ISSN 1388-2457. doi: 10.1016/j.clinph.2009.10.038.

M. A. Serrano, M. Boguñá, and A. Vespignani. Extracting the multiscale backbone of complex weighted networks. *Proceedings of the National Academy of Sciences of the United States of America*, 106(16):6483–6488, 2009. ISSN 0027-8424. doi: 10.1073/pnas.0808904106.

D. J. Sharp, G. Scott, and R. Leech. Network dysfunction after traumatic brain injury. *Nature Reviews Neurology*, 10(3):156, 2014.

H. R. Siebner, G. Hartwigsen, T. Kassuba, and J. C. Rothwell. How does transcranial magnetic stimulation modify neuronal activity in the brain? implications for studies of cognition. *Cortex*, 45(9):1035–1042, 2009.

J. S. Siegel, L. E. Ramsey, A. Z. Snyder, N. V. Metcalf, R. V. Chacko, K. Weinberger, A. Baldassarre, C. D. Hacker, G. L. Shulman, and M. Corbetta. Disruptions of network connectivity predict impairment in multiple behavioral domains after stroke. *Proceedings of the National Academy of Sciences*, 113(30):E4367–E4376, 2016.

A. Snowball, I. Tachtsidis, T. Popescu, J. Thompson, M. Delazer, L. Zamarian, T. Zhu, and R. Cohen Kadosh. Long-term enhancement of brain function and cognition using cognitive training and brain stimulation. *Current Biology : CB*, 23(11):987–992, 2013. ISSN 1879-0445. doi: 10.1016/j.cub.2013.04.045.

S. Sourav, D. Bottari, R. Kekunnaya, and B. Röder. Evidence of a retinotopic organization of early visual cortex but impaired extrastriate processing in sight recovery individuals. *Journal of Vision*, 18(3):22, 2018. doi: 10.1167/18.3.22.

A. Sperduti and A. Starita. Supervised neural networks for the classification of structures. *IEEE transactions on Neural Networks*, 8(3):714–735, 1997.

D. P. Spiegel, B. C. Hansen, W. D. Byblow, and B. Thompson. Anodal transcranial direct current stimulation reduces psychophysically measured surround suppression in the human visual cortex. *PloS one*, 7(5):e36220, 2012. ISSN 1932-6203. doi: 10.1371/journal.pone.0036220.

C. J. Stam, W. de Haan, A. Daffertshofer, B. F. Jones, I. Manshanden, van Cappellen van Walsum, Anne-Marie, T. Montez, J. P. Verbunt, J. C. de Munck, B. W. van Dijk, et al. Graph theoretical analysis of magnetoencephalographic functional connectivity in alzheimer's disease. *Brain*, 132(1):213–224, 2008. ISSN 0006-8950.

A. Stayman, B. W. Abou-Khalil, P. Lavin, and N. J. Azar. Homonymous hemianopia in nonketotic hyperglycemia is an ictal phenomenon. *Neurology. Clinical Practice*, 3(5): 392–397, 2013. ISSN 2163-0402. doi: 10.1212/CPJ.0b013e3182a7bb76.

C. Stephani, M. A. Nitsche, M. Sommer, and W. Paulus. Impairment of motor cortex plasticity in parkinson's disease, as revealed by theta-burst-transcranial magnetic stimulation and transcranial random noise stimulation. *Parkinsonism & Related Disorders*, 17(4):297–298, 2011.

P. Stoerig and A. Cowey. Blindsight in man and monkey. *Brain: a journal of Neurology*, 120(3):535–559, 1997.

A. P. Strafella and T. Paus. Modulation of cortical excitability during action observation: a transcranial magnetic stimulation study. *Neuroreport*, 11(10):2289–2292, 2000.

D. Strbian, N. Ahmed, N. Wahlgren, M. Kaste, and T. Tatlisumak. Intravenous thrombolysis in ischemic stroke patients with isolated homonymous hemianopia: analysis of safe implementation of thrombolysis in stroke-international stroke thrombolysis register (sits-istr). *Stroke*, 43(10):2695–2698, 2012a. doi: 10.1161/STROKEAHA.112.658435.

D. Strbian, L. Soinne, T. Sairanen, F. Scheperjans, O. Salonen, M. Palomäki, M. Kaste, and T. Tatlisumak. Intravenous thrombolysis in ischemic stroke patients with isolated homonymous hemianopia. *Acta neurologica Scandinavica*, 126(4):e17–9, 2012b. ISSN 1600-0404. doi: 10.1111/j.1600-0404.2012.01646.x.

E. Striem-Amit, S. Ovadia-Caro, A. Caramazza, D. S. Margulies, A. Villringer, and A. Amedi. Functional connectivity of visual cortex in the blind follows retinotopic organization principles. *Brain*, 138(Pt 6):1679–1695, 2015. ISSN 0006-8950. doi: 10.1093/brain/awv083.

S. Sulaimany, M. Khansari, P. Zarrineh, M. Daianu, N. Jahanshad, P. M. Thompson, and A. Masoudi-Nejad*. Predicting brain network changes in alzheimer's disease with link prediction algorithms†‡. *Molecular BioSystems*, 13(4):725–735, 2017. ISSN 1742-206X. doi: 10.1039/c6mb00815a.

H. Sunwoo, Y.-H. Kim, W. H. Chang, S. Noh, E.-J. Kim, and M.-H. Ko. Effects of dual transcranial direct current stimulation on post-stroke unilateral visuospatial neglect. *Neuroscience Letters*, 554:94–98, 2013. ISSN 0304-3940. doi: 10.1016/j.neulet.2013.08.064.

F. Tecchio, A. Cancelli, C. Cottone, R. Ferrucci, M. Vergari, G. Zito, P. Pasqualetti, M. M. Filippi, A. Ghazaryan, D. Lupoi, et al. Brain plasticity effects of neuromodulation against multiple sclerosis fatigue. *Frontiers in Neurology*, 6:141, 2015.

P. Tekturk, E. T. Erdogan, A. Kurt, E. N. Vanli-Yavuz, E. Ekizoglu, E. Kocagoncu, Z. Kucuk, S. Aksu, N. Bebek, Z. Yapici, et al. The effect of transcranial direct current

stimulation on seizure frequency of patients with mesial temporal lobe epilepsy with hippocampal sclerosis. *Clinical Neurology and Neurosurgery*, 149:27–32, 2016.

Q. K. Telesford, S. L. Simpson, J. H. Burdette, S. Hayasaka, and P. J. Laurienti. The brain as a complex system: using network science as a tool for understanding the brain. *Brain Connectivity*, 1(4):295–308, 2011. doi: 10.1089/brain.2011.0055.

D. Terney, L. Chaieb, V. Moliadze, A. Antal, and W. Paulus. Increasing human brain excitability by transcranial high-frequency random noise stimulation. *The Journal of Neuroscience : the official journal of the Society for Neuroscience*, 28(52):14147–14155, 2008. ISSN 0270-6474. doi: 10.1523/JNEUROSCI.4248-08.2008.

A. R. Tharaldsen, K. M. Sand, I. Dalen, G. Wilhelmsen, H. Næss, A. Midelfart, E. Rødahl, L. Thomassen, J. M. Hoff, N.-O. R. Group, et al. Vision-related quality of life in patients with occipital stroke. *Acta Neurologica Scandinavica*, 141(6):509–518, 2020.

G. Tinkhauser, A. Pogosyan, S. Little, M. Beudel, D. M. Herz, H. Tan, and P. Brown. The modulatory effect of adaptive deep brain stimulation on beta bursts in parkinson's disease. *Brain*, 140(4):1053–1067, 2017.

Y. Tufail, A. Matyushov, N. Baldwin, M. L. Tauchmann, J. Georges, A. Yoshihiro, S. I. H. Tillery, and W. J. Tyler. Transcranial pulsed ultrasound stimulates intact brain circuits. *Neuron*, 66(5):681–694, 2010.

Y. Tufail, A. Yoshihiro, S. Pati, M. M. Li, and W. J. Tyler. Ultrasonic neuromodulation by brain stimulation with transcranial ultrasound. *Nature Protocols*, 6(9):1453–1470, 2011.

N. Tzourio-Mazoyer and Landeau. Automated anatomical labeling of activations in spm using a macroscopic anatomical parcellation of the mni mri single-subject brain. *NeuroImage*, 15(1):273–289, 2002. ISSN 1095-9572. doi: 10.1006/nimg.2001.0978.

G. Vallar and D. Perani. The anatomy of unilateral neglect after right-hemisphere stroke lesions. a clinical/ct-scan correlation study in man. *Neuropsychologia*, 24(5):609–622, 1986. ISSN 1873-3514. doi: 10.1016/0028-3932(86)90001-1.

M. P. van den Heuvel and H. E. Hulshoff Pol. Exploring the brain network: A review on resting-state fmri functional connectivity. *European Neuropsychopharmacology*, 20(8): 519–534, 2010. ISSN 1873-7862. doi: 10.1016/j.euroneuro.2010.03.008.

M. P. van den Heuvel, C. J. Stam, R. S. Kahn, and H. E. Hulshoff Pol. Efficiency of functional brain networks and intellectual performance. *The Journal of Neuroscience : the official journal of the Society for Neuroscience*, 29(23):7619–7624, 2009. ISSN 0270-6474. doi: 10.1523/JNEUROSCI.1443-09.2009.

B. C. M. Van Wijk, C. J. Stam, and A. Daffertshofer. Comparing brain networks of different size and connectivity density using graph theory. *PloS one*, 5(10):e13701, 2010. ISSN 1932-6203. doi: 10.1371/journal.pone.0013701.

S. Vanni, A. Raninen, R. Näsänen, T. Tanskanen, and L. Hyvärinen. Dynamics of cortical activation in a hemianopic patient. *NeuroReport*, 12(4):861–865, 2001. ISSN 0959-4965. doi: 10.1097/00001756-200103260-00047.

R. VanRullen. Perceptual cycles. *Trends in Cognitive Sciences*, 20(10):723–735, 2016. doi: 10.1016/j.tics.2016.07.006.

A. Vaswani, N. Shazeer, N. Parmar, J. Uszkoreit, L. Jones, A. N. Gomez, Ł. Kaiser, and I. Polosukhin. Attention is all you need. pages 5998–6008, 2017.

F. Vecchio, C. Tomino, F. Miraglia, F. Iodice, C. Erra, R. Di Iorio, E. Judica, F. Alù, M. Fini, and P. M. Rossini. Cortical connectivity from eeg data in acute stroke: A study via graph theory as a potential biomarker for functional recovery. *International Journal of Psychophysiology : official journal of the International Organization of Psychophysiology*, 146:133–138, 2019. doi: 10.1016/j.ijpsycho.2019.09.012.

A. Vossen, J. Gross, and G. Thut. Alpha power increase after transcranial alternating current stimulation at alpha frequency (a-tacs) reflects plastic changes rather than entrainment. *Brain Stimulation*, 8(3):499–508, 2015a. ISSN 1876-4754. doi: 10.1016/j.brs.2014.12.004.

A. Vossen, J. Gross, and G. Thut. Alpha power increase after transcranial alternating current stimulation at alpha frequency (\alpha-tacs) reflects plastic changes rather than entrainment. *Brain Stimulation*, 8(3):499–508, 2015b. ISSN 1876-4754.

D. Wang, P. Cui, and W. Zhu. Structural deep network embedding. In *Proceedings of the 22nd ACM SIGKDD international conference on Knowledge discovery and data mining*, pages 1225–1234, 2016a.

J. Wang, X. Zuo, and Y. He. Graph-based network analysis of resting-state functional mri. *Frontiers in Systems Neuroscience*, 4:16, 2010. ISSN 1662-5137. doi: 10.3389/fnsys.2010.00016.

J. Wang, T. Li, B. A. Sabel, Z. Chen, H. Wen, J. Li, X. Xie, D. Yang, W. Chen, N. Wang, J. Xian, and H. He. Structural brain alterations in primary open angle glaucoma: a 3t mri study. *Scientific Reports*, 6:18969, 2016b. ISSN 2045-2322. doi: 10.1038/srep18969.

L. Wang, X. Guo, J. Sun, Z. Jin, and S. Tong. Cortical networks of hemianopia stroke patients: A graph theoretical analysis of eeg signals at resting state. *Conference proceedings : ... Annual International Conference of the IEEE Engineering in Medicine and Biology Society. IEEE Engineering in Medicine and Biology Society. Annual Conference*, 2012: 49–52, 2012. doi: 10.1109/EMBC.2012.6345868.

D. J. Watts and S. H. Strogatz. Collective dynamics of 'small-world' networks. *Nature*, 393(6684):440–442, 1998. ISSN 0028-0836. doi: 10.1038/30918.

J. C. Wen, C. S. Lee, P. A. Keane, S. Xiao, A. S. Rokem, P. P. Chen, Y. Wu, and A. Y. Lee. Forecasting future humphrey visual fields using deep learning. *PloS one*, 14(4): e0214875, 2019. doi: 10.1371/journal.pone.0214875.

S. Wiethoff, M. Hamada, and J. C. Rothwell. Variability in response to transcranial direct current stimulation of the motor cortex. *Brain Stimulation*, 7(3):468–475, 2014.

M. Wischnewski, M. Engelhardt, M. Salehinejad, D. Schutter, M.-F. Kuo, and M. Nitsche. Nmda receptor-mediated motor cortex plasticity after 20 hz transcranial alternating current stimulation. *Cerebral Cortex*, 29(7):2924–2931, 2019.

A. J. Woods, A. Antal, M. Bikson, P. S. Boggio, A. R. Brunoni, P. Celnik, L. G. Cohen, F. Fregni, C. S. Herrmann, E. S. Kappenman, H. Knotkova, D. Liebetanz, C. Miniussi, P. C. Miranda, W. Paulus, A. Priori, D. Reato, C. Stagg, N. Wenderoth, and M. A. Nitsche. A technical guide to tdcs, and related non-invasive brain stimulation tools. *Clinical Neurophysiology*, 127(2):1031–1048, 2016. ISSN 1388-2457. doi: 10.1016/j.clinph.2015.11.012.

C. J. Woolf. Recent advances in the pathophysiology of acute pain. *British Journal of Anaesthesia*, 63(2):139–146, 1989. ISSN 0007-0912. doi: 10.1093/bja/63.2.139.

X.-J. Wu, L.-L. Zeng, H. Shen, L. Yuan, J. Qin, P. Zhang, and D. Hu. Functional network connectivity alterations in schizophrenia and depression. *Psychiatry Research. Neuroimaging*, 263:113–120, 2017. doi: 10.1016/j.pscychresns.2017.03.012.

Z. Wu, S. Pan, F. Chen, G. Long, C. Zhang, and S. Y. Philip. A comprehensive survey on graph neural networks. *IEEE transactions on Neural Networks and Learning Systems*, 2020.

S. Wüst, E. Kasten, and B. A. Sabel. Blindsight after optic nerve injury indicates functionality of spared fibers. *Journal of Cognitive Neuroscience*, 14(2):243–253, 2002.

M. Xia, J. Wang, and Y. He. Brainnet viewer: a network visualization tool for human brain connectomics. *PloS one*, 8(7):e68910, 2013. ISSN 1932-6203. doi: 10.1371/journal.pone.0068910.

J. Xu, Z. Wu, A. Nürnberger, and B. A. Sabel. Decoding resting-state eeg to predict visual field defect with convolutional neural network in stroke. In *2021 10th International IEEE/EMBS Conference on Neural Engineering (NER)*, pages 807–810. IEEE, 2021.

Y. Xu, Q.-h. Hou, S. D. Russell, B. C. Bennett, A. J. Sellers, Q. Lin, and D.-f. Huang. Neuroplasticity in post-stroke gait recovery and noninvasive brain stimulation. *Neural Regeneration Research*, 10(12):2072–2080, 2015. ISSN 1673-5374. doi: 10.4103/1673-5374.172329.

N. Yadati, M. Nimishakavi, P. Yadav, V. Nitin, A. Louis, and P. Talukdar. Hypergcn: A new method of training graph convolutional networks on hypergraphs. *arXiv preprint arXiv:1809.02589*, 2018.

Y. Yan, L. Zhaoping, and W. Li. Bottom-up saliency and top-down learning in the primary visual cortex of monkeys. *Proceedings of the National Academy of Sciences*, 115(41): 10499–10504, 2018.

R. Ying, J. You, C. Morris, X. Ren, W. L. Hamilton, and J. Leskovec. Hierarchical graph representation learning with differentiable pooling. *arXiv preprint arXiv:1806.08804*, 2018.

R. Ying, J. You, C. Morris, X. Ren, W. L. Hamilton, and J. Leskovec. *Hierarchical Graph Representation Learning with Differentiable Pooling*. 2019.

T. Zaehle, S. Rach, and C. S. Herrmann. Transcranial alternating current stimulation enhances individual alpha activity in human eeg. *PloS one*, 5(11):e13766, 2010. ISSN 1932-6203. doi: 10.1371/journal.pone.0013766.

X. Zhang, S. Kedar, M. J. Lynn, N. J. Newman, and V. Biousse. Natural history of homonymous hemianopia. *Neurology*, 66(6):901–905, 2006a. doi: 10.1212/01.wnl.0000203338.54323.22.

X. Zhang, S. Kedar, M. J. Lynn, N. J. Newman, and V. Biousse. Homonymous hemianopias: clinical-anatomic correlations in 904 cases. *Neurology*, 66(6):906–910, 2006b. doi: 10.1212/01.wnl.0000203913.12088.93.

L. Zhaoping and J. Ackermann. Reversed depth in anticorrelated random-dot stereograms and the central-peripheral difference in visual inference. *Perception*, 47(5):531–539, 2018.

C. Zhou, L. Zemanová, G. Zamora, C. C. Hilgetag, and J. Kurths. Hierarchical organization unveiled by functional connectivity in complex brain networks. *Physical Review letters*, 97(23):238103, 2006. ISSN 0031-9007. doi: 10.1103/PhysRevLett.97.238103.

J. Zhou, G. Cui, S. Hu, Z. Zhang, C. Yang, Z. Liu, L. Wang, C. Li, and M. Sun. Graph neural networks: A review of methods and applications. *AI Open*, 1:57–81, 2020.

U. Ziemann. Transcranial magnetic stimulation at the interface with other techniques: a powerful tool for studying the human cortex. *The Neuroscientist*, 17(4):368–381, 2011.

A Resume

Jiahua Xu Email: jiahua.xu@ieee.org

- Education

  PHD candidate, Faculty of Computer Science, Otto-von-Guericke-Universität Magdeburg, Magdeburg, Germany, 2016–Current

  Master degree, Computer information science, Faculty of Computer Science, University Macau, Macau, China, 2010–2013

  Bachelor degree, Electronic engineering, Macau university of Science and Technology, 2005–2009

- Research area

  Noninvasive brain stimulation, EEG/MEG, Medical imaging, Machine Learning

- Publication

  Decoding Resting-state EEG to Predict Visual Field Defect with Convolutional Neural Network. 10th International IEEE EMBS Conference on Neural Engineering 4-6 May 2021.

  Interhemispheric Cortical Network Connectivity Reorganization Predicts Vision Impairment in Stroke. 43rd Annual International Conference of the IEEE Engineering in Medicine and Biology Society (EMBC), October 31 – November 4, 2021, In press.

  Predicting Brain Electrical Stimulation Outcome in Stroke by Clinical-inspired Hybrid Graph Convolutional Autoencoder 2nd IEEE International Conference on Human-Machine Systems, Germany, 8-10 September 2021.

  Reorganization of brain functional connectivity network and vision restoration following combined tDCS-tACS treatment after occipital stroke, Frontier of Neurology.

  Adaptive and maladaptive brain functional network reorganization after stroke, Brain connectivity.

- Events

  Doktorandentag, Otto-von-Guericke-Universität Magdeburg, 21 Feb 2021

- Languages

  Chinese : fluent (native language)

  English: fluent

  German: basic

B Ehrenerklärung

Ich versichere hiermit, dass ich die vorliegende Arbeit ohne unzulässige Hilfe Dritter und ohne Benutzung anderer als der angegebenen Hilfsmittel angefertigt habe; verwendete fremde und eigene Quellen sind als solche kenntlich gemacht. Insbesondere habe ich nicht die Hilfe eines kommerziellen Promotionsberaters in Anspruch genommen. Dritte haben von mir weder unmittelbar noch mittelbar geldwerte Leistungen für Arbeiten erhalten, die im Zusammenhang mit dem Inhalt der vorgelegten Dissertation stehen. Ich habe insbesondere nicht wissentlich:

- Ergebnisse erfunden oder widersprüchliche Ergebnisse verschwiegen.
- Statistische Verfahren absichtlich missbraucht, um Daten in ungerechtfertigter Weise zu interpretieren.
- Fremde Ergebnisse oder Veröffentlichungen plagiiert.
- Fremde Forschungsergebnisse verzerrt wiedergegeben.

Mir ist bekannt, dass Verstöße gegen das Urheberrecht Unterlassungs- und Schadensersatzansprüche des Urhebers sowie eine strafrechtliche Ahndung durch die Strafverfolgungsbehörden begründen kann. Die Arbeit wurde bisher weder im Inland noch im Ausland in gleicher oder ähnlicher Form als Dissertation eingereicht und ist als ganzs auch noch nicht verofftilivht.

Magdeburg, den February 4, 2022